Self-Organisation and Dissipation in Real and Synthetic Earthquake Populations

Fahad H. Y. Al-Kindy

BSc (Hons), Dunelm, 1998

MRes, Edinburgh, 1999

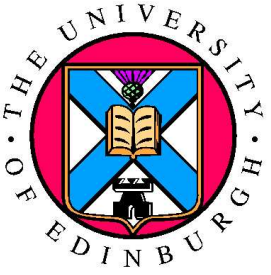

Thesis submitted in fulfilment of

the requirements for the degree of

Doctor of Philosophy

University of Edinburgh

Submitted: September 2003

Viva: January 2004

Abstract

Energy released from the Earth's crust in the form of earthquakes commonly follows a power-law gamma type probability distribution. This spontaneous organisation is in apparent contradiction to the second law of thermodynamics that states that a system should naturally evolve to a state of maximum disorder or entropy. However, developments in the field of modern thermodynamics suggest that some systems can undergo organisation locally, at the expense of increasing disorganisation (or entropy) globally through a process of entropy production. The primary aim of this thesis is to investigate self-organisation in the Earth's seismogenic lithosphere as a driven, far-from-equilibrium, self-organising 'dissipative structure' in a very near critical steady-state and the underlying general mechanisms involved. The secondary aim is to test in more detail the applicability of the Bak, Tang and Wiesenfeld (BTW) model of *Self-Organised Criticality* (SOC) in describing Earth's seismicity. This is done by: 1. Mathematical derivation of analytical solutions for system energy and entropy using the tools of equilibrium statistical mechanics; 2. The study of conservative and non-conservative versions of the BTW numerical model and 3. Analysis of temporal and spatial properties of earthquake data from the Harvard Centroid Moment Tensor catalogue and the Global Heat Flow Database. The modified gamma distribution predicts analytically that entropy S is related to the energy probability distribution scaling exponent B and the expectation of the logarithm of seismic energy $\langle \ln E \rangle$ in the form of the *gamma entropy equation* $S \sim B\langle \ln E \rangle$. This solution is confirmed for both numerical model results and real earthquake data. Phase diagrams of B vs. $\langle \ln E \rangle$ suggest that the universality in B need not be maintained for a system to remain critical provided there is a corresponding change in $\langle \ln E \rangle$ and S. The power-law systems examined are different from equilibrium systems since the critical points do not occur at global maximum entropy. For the dissipative BTW model at a steady-state, the externally radiated energy follows out-of-equilibrium power-law gamma type statistics, but, the internal energy has two

characteristics that are indicative of equilibrium systems; a Gaussian type energy probability distribution and a Brownian noise power-spectrum for the internal energy fluctuations. This suggests an observer dependency in assessing criticality. The internal and external entropies calculated for the model are negatively correlated suggesting that driven systems self-organise at the expense of increasing entropy globally through a process of dissipation. A power-law dependency of mean radiated energy $\langle E \rangle$ on dissipation $1 - \alpha$ is confirmed for a locally driven dissipative system in the form $\langle E \rangle \sim (1-\alpha)^{-0.975}$. The BTW model shows spatial heterogeneity whilst maintaining universality in contradiction to previous assumptions. The quantitative analysis of real data reveals that earthquakes are more predictable spatially then temporally. Regionalisation using the Flinn-Engdahl classification shows that mid-ocean ridges are more organised (lower entropy) than subduction zones. A regional study of three different scaling exponents suggests that universality in earthquake scaling is violated, in contradiction to the original model of SOC. A model of self-organised sub-criticality (SOSC) is proposed as an alternative model for Earth seismicity. Overall, the results suggest that the tools of equilibrium thermodynamics can be applied to a steady-state far-from-equilibrium system such as the Earth's seismogenic lithosphere, and that the resulting self-organisation occurs at the expense of maximising dissipation and hence entropy production.

Declaration

I declare that this thesis has been composed solely by myself and, except where otherwise acknowledged, the work presented is entirely my own. Any deviation from this declaration is purely unintentional.

Fahad Al-Kindy

September, 2003.

Acknowledgements

It is with privilege and gratitude that I thank my supervisor Prof. Ian Main for his guidance, enthusiasm and being a great pleasure to work with. Throughout he has lent stimulating and inspiring discussions for which I am grateful. The guitar playing and excellent choice of restaurants in Edinburgh will be remembered. Second supervisor Wyn Williams is also thanked.

Constructive discussions were appreciated in Edinburgh and various conferences over the last few years with: R. Blythe, M. Chapman, S. Chastin, P. Cowie, S. Crampin, R. Dewar, C. Goltz, J-R Grasso, P. Leary, R. Lorenz, C. Narteau, H. Ozawa and S. Zatsepin.

On the computing side I am grateful to M. Hagdorn for setting me up with Linux and LaTeX, C. McKernon for help with GMT and computing officers S. Voss and J. McNiel. Also thanks to Dave and Allan for helpful bit and bobs.

I would like to thank my friends and family in Oman and friends/flatmates in Britain for their love and support: Everyone I met in Oxford. The friends I can never forget from my degree years in Durham. In Edinburgh, all friends from the MRes course, the Untapped Talent Society, the ‘student’ newspaper and the wonderful team of editors and writers I worked with at ‘fest’ during the Edinburgh Festival. Enormous thanks also to all other friends I met in Edinburgh during my PhD and PhD colleagues for support and making it such an enjoyable time; the meals, trips, emails, lunch breaks, CD swaps, cups of tea, gigs, txts and late nights will always be cherished. Sorry I can’t mention you all by name (you know who you are). The lovely staff at KB union are also thanked despite the undrinkable coffee there. Comedians Simon Munnery and Dan Antopolski are also thanked for their mind bending humour.

I truly thank my friends Abigail B. and Sonja M. for the gruesome task of proof reading the main parts of this thesis.

This research would not be possible without the financial sponsorship of Petroleum Development of Oman (PDO) and all their committed staff. I thank them for fully supporting me to study in Britain for the last ten years (Scholarship PGS4223).

Finally I would like to thank my family from the bottom of my heart: My mother Fawzia for inspiring me to dream, my father Hamed for encouraging me think, my sisters Nada and Nahla for giving me love and strength and my brother-in-law Shabib and nephews Hatim and Ibrahim for their loving support. My former step father Ali is also thanked for his support and interest in my work.

During the course of this thesis, the scientific community lost three great minds that were a great inspiration to me: Claude Shannon (1916-2001) with his pioneering work on information theory, Per Bak (1947-2002) who gave us self-organised criticality and Ilya Prigogine (1917-2003) who enlightened us on self-organisation with his entropy production theorem. This work is dedicated to their memory.

Fahad Al-Kindy

Edinburgh 2003.

Contents

List of Tables

List of Figures

Chapter 1

Introduction

> *"It is clearly seen that near the critical point we have long-range chemical correlations. Again the system acts as a whole in spite of the short-range character of the chemical interactions. Chaos gives rise to order."*[1]

The quote above is an excerpt of the Nobel Lecture given by Ilya Prigogine at the prestigious award ceremony in Stockholm on the 8th of December 1977. Prigogine was awarded the Nobel Prize in chemistry for his work on organisation in 'non-equilibrium thermodynamics and dissipative structures'. Along with his colleagues at the 'Brussels school', Prigogine predicted that under certain conditions, some chemical reactions that are not at equilibrium can show correlations or 'patterns' that span length scales that far exceed the distances at which the individual molecules interact with each other. From a thermodynamics point of view, this is somewhat peculiar since the Second Law of thermodynamics states that a system should naturally evolve to a state of maximum disorder. In other words, the entropy, which is a measure of disorder, should increase (Kondepudi and Prigogine, 1998). This is why we can make an omelette from an egg but never an egg from an omelette.

However, Prigogine and his colleagues have shown that certain systems can organise themselves locally at the expense of increasing disorganisation of their surroundings globally through

[1] Speech documented at the Nobel Prize e-museum: http://www.nobel.se/

a process of maximising their *entropy production*[2] (Nicolis and Prigogine, 1977). This can seem counter intuitive since it implies the spontaneous emergence of order or pattern through local processes, which may be random, or chaotic. Self-organisation however can conceptually be thought of as a ball rolling up a small hill in order to get to the other side to roll down a bigger hill. Such systems are referred to as driven *'dissipative structures'* since they are away-from-equilibrium and are interacting with their surroundings through the process of energy (and/or matter) dissipation (in or out) (Cross and Hohenberg, 1993). Such systems are different from traditional 'equilibrium' thermodynamic systems since they are not at the same *temperature* (see chapter 2) as their surroundings. The work on dissipative structures was seen as a big step closer to explaining the emergence of spatial and/or temporal order or patterns in certain chemical reactions and complex natural systems. These include biological processes that lead to intricate structures such as DNA (Kondepudi and Prigogine, 1998; Cavanagh and Akke, 2000).

Precisely a decade later in 1987, Bak, Tang and Wiesenfeld published a seminal paper in the journal Physical Review Letters titled *'Self-Organized Criticality: an explanation of 1/f noise'* (Bak et al., 1987). Just as with Prigogine's chemical experiments, Bak et al. produced a simple 'driven' far-from-equilibrium numerical cellular-automata (computer) model where the individual components, or 'cells', only interact with their closest neighbours. Yet the model as a whole was found to exhibit a pattern or order that spans the size of the entire system. They called this observation *Self-Organised Criticality* or 'SOC'. In the literature, their model is generally referred to as the BTW (from the names of the three authors) model of SOC. The term 'self-organized' highlights the fact that the system evolves to a pattern spontaneously without any external tuning. The term 'critical' refers to this pattern being a 'power-law' of 'fractal' (see below) similar to what is observed in other 'critical' systems. More precise definitions of the terms used here will be given in chapter 2.

Two years after their initial publication, Bak and Tang wrote a follow-up paper entitled *'Earthquakes as a Self-Organized Critical Phenomenon'* (Bak and Tang, 1989). But what does their somewhat abstract model have to do with earthquakes? The fractal or power-law pattern that

[2]Defined with example in chapter 2.

evolves in the BTW model, without any tuning of parameters is in the form (Main, 1995):

$$p(E) \sim E^{-B-1} \tag{1.1}$$

where $p(E)$ is the probability of having an energy state E and B is a scaling exponent. The radiated energy dissipated by the Earth through the process of earthquakes follows this distribution to a first approximation. This power-law empirically observed for earthquake energy release is also represented in the form of the famous Gutenberg-Richter law (Gutenberg and Richter, 1954)

$$N(m) = a - bm \tag{1.2}$$

where $N(m)$ is the number of earthquakes that exceed a magnitude m, a and b are constants with b found globally to be ~ 1, and the magnitude m is related to the logarithm of the radiated seismic energy through $m \sim \frac{2}{3} \ln E$. This relation is maintained globally despite the complex details of the fault-fault interactions, variations in rock type, differences in tectonic plate settings and the effectively infinite degrees of freedom inherent. It is enchanting that the complex dynamics of the Earth's seismicity can be reduced to a single universal scaling law of two simple variables; frequency and magnitude. These power-law statistics and inherent complexities suggest that the Earth's crust is a dynamic self-organising dissipative structure, similar to the chemical interactions of Prigogine and the BTW model of SOC.

The power-law observed for earthquakes is of great interest since this statistical relation is shared with other systems found in the fields of statistical physics and thermodynamics and *critical point* phenomena undergoing a *phase-transition* (Main 1996). But what is a critical system? This is a very wide question that will be addressed in chapters 2 and 3. However, a simple example of a thermodynamic process at the critical point is a water liquid-gas phase transition at a very specific 'critical' pressure and temperature where the density contrast between the liquid and gas phases disappears. At this *critical point*, the water-gas molecules cluster at all length scales, showing power-law statistics (Bruce and Wallace, 1989). These statistics are similar to the Gutenberg-Richter law mentioned above. The way in which thermodynamics or statistical physics address such systems of many components (such as say a gas) is by reducing them to just a few global parameters without the need to explicitly solve for minor-scale details. In other words, we are interested in the average or probabilistic attributes of the system such as its mean energy, pressure or temperature (Mandl, 1988).

Although the application of statistical physics or thermodynamics to earthquakes statistics is not new (e.g. Main and Burton, 1984), the work of Prigogine has not been formally applied to better understanding, assessing or explaining self-organisation and criticality in the Earth's crust. Also, many of the approaches used to assess criticality in the crust from a thermodynamic point of view have done so by assuming equilibrium critical point thermodynamics (e.g. Bowmann et al., 1998; Robinson, 2000; Zöller and Hainzl, 2001). As I will clarify, although critical systems in equilibrium and out of equilibrium thermodynamics do have common characteristics such as power-law statistics, they are fundamentally different both in their dynamics and predictability. Caution must therefore be taken when applying tools of equilibrium thermodynamics to away-from equilibrium-systems. Nonetheless, the application of equilibrium statistical mechanics and thermodynamics to self-organising far-from-equilibrium systems is a new and emerging field of physics (Ruelle, 2001).

In this thesis, I examine two main points:

1. Firstly I address Earth's seismicity from a thermodynamic point of view treating the seismogenic lithosphere as a slowly driven, dissipative structure undergoing self-organisation. This enables me to formally examine and understand the underlying processes that govern self-organisation in the crust. More importantly, this is a way to assess the applicability of equilibrium thermodynamics to a far-from-equilibrium system such as the Earth. Although such an approach has only been emerging recently, the application of equilibrium thermodynamics to non-equilibrium systems under certain conditions has been successfully demonstrated since the work on this thesis began. These works include and application to a chaotic magnetic model (Egolf, 2000) and for laboratory experiments on granular matter (D'Anna et al., 2003) and will be shown in this thesis for crustal seismicity.

2. Secondly, I question the concept of self-organised criticality (SOC) and its applicability as a null hypothesis in describing the Earth's crust. There are two rationales for addressing this issue:

   a) Despite its application and acceptance in the scientific community, SOC is not precisely defined in the literature (Jensen, 1998). It is therefore important to first refine

what is meant by SOC and outline the criteria associated with it, then to find a formal and quantitative way to establish if these criteria are in harmony with observations of real earthquake statistics.

b) It is a prediction of the BTW model that a purely SOC system would be virtually unpredictable in space and time. Questioning the commonly accepted SOC description of the crust will have an impact on the way we approach the seismicity of the Earth and seismic hazard analysis in general.

I attempt to address the issues outlined above as follows:

Chapter 2: Here I review three areas of the literature that aid in addressing the goals of this thesis. Firstly, literature associated with statistical physics, thermodynamics, entropy, the concept of self-organisation and critical point phenomena. This will include illustrations from the often cited Bénard cell convection experiment (Kondepudi and Prigogine, 1998) and the percolation model. Secondly, I define power-laws and fractals and their common link to equilibrium critical point phenomena (CP) and SOC. I explicitly clarify the differences between CP and SOC systems. Finally, I cover some earthquake phenomenology such as the observed power-law distributions relating earthquake frequencies to their magnitudes (or energy release) and temporal observations such as foreshocks and aftershocks.

Chapter 3: I look at the power-law *gamma distribution* from a theoretical perspective and its relation to criticality and the *three criticality regimes*. I then use these tools to derive an analytical model that links the entropy S (level of self-organisation) of a gamma power-law probability distribution with its expectation logarithmic energy $\langle \ln E \rangle$ and its power-law scaling exponent B. Then, I use the analytical solutions to predict the entropy-energy phase-space for a power-law system at and away from criticality. I propose this as an analytical thermodynamic method of assessing criticality in the crust.

Chapter 4: I carry out numerical cellular automata modelling to test and verify some of the aspects of self-organisation and predictions of chapter 3. I formally reintroduce a non-conservative BTW earthquake model of SOC. I use the model to measure internal and external thermodynamic properties of a driven self-organising dissipative structure. The rationale for

using the model is that only external properties such as the radiated seismic energy can be measured for the earth. More specifically, I look at the effect of dissipation on the internal and external properties of the system and its influence on the entropies measured and self-organisation. SOC and its properties are also formally examined in the BTW model.

Chapter 5: I compare the analytical and numerical predictions of chapters 3 and 4 with the results of analysing earthquake data from the Harvard Centriod Moment Tensor (CMT) catalogue. By comparing the theoretical, modelling and 'real' results, I assess the proximity of the Earth to criticality. The analysis is on both temporal and spatial earthquake ensembles. I also investigate the seismic scaling exponents in some detail and their relevance as an indicator for the degree of self-organisation and their 'universality'.

Chapter 6: I discuss the results of this thesis in the wider context of self-organising systems and criticality in general. I also make some suggestions on how the work presented in this thesis could be built upon and possible directions for further research.

Chapter 7: I give a summary of the main conclusions of this thesis.

In summary, the primary aim of this thesis is to study the Earth's crust as self-organising dissipative structure in order to better understand and verify its proximity to criticality and any underlying mechanisms that govern self-organisation. This is carried out using a thermodynamic approach by reference to analytical statistical mechanics and thermodynamics, numerical modelling and the analysis of global earthquake data temporally and spatially. The secondary aim is to examine self-organised criticality formally in the original BTW model and then assess its applicability as a model to describe the Earth's seismicity.

Chapter 2

Background: From thermodynamics to earthquakes

2.1 Introduction

The main disciplines that shall be used in addressing the issues outlined in this thesis are statistical physics and thermodynamics of dissipative systems, self-organisation, power-laws in critical systems and earthquake statistics. I therefore conduct a literature review of some of the relevant background and terminology used within these disciplines that will assist in the understanding of this thesis. First I give a general introduction to statistical physics, thermodynamics and the concept of entropy. I also look at critical point phenomena with an example from percolation theory and their association with fractals and self-organisation. These will be accompanied with examples found in the laboratory and nature. Then, I introduce the concept of Self-Organised Criticality (SOC) and clarify its association and differences with critical point phenomena. Finally, I cover earthquake phenomenology observed both in time and space and their currently understood association with SOC.

2.2 Overview

Broadly speaking, statistical physics/mechanics and thermodynamics are the branches of physics that describe the macroscopic state of systems consisting of a large number of particles or molecules such as a gas. Their power stems from their ability to describe such 'many body' systems in terms of just a few parameters such as temperature and pressure (Mandl, 1988). For example, it would be impossible to describe the motion and interaction of Avogadro's number ($\sim 6 \times 10^{23}$) of particles for a gas analytically in the same way one would use Newtonian mechanics to describe the trajectory of say, a ball falling off a table. Although the latter scenario would only require the solution of one or two equations to describe it, the former would require solving at least $\sim 6 \times 10^{23}$ equations! This 'microscopic' approach that requires a complete description of the system at an atomic scale is usually impossible. The strategy is to address a problem statistically i.e. what on average will particles be doing and what does this average tell us about the system as a whole. The key is the prediction of macroscopic properties of the system when the probability distribution of its energetic micro-states is known.

In statistical physics, for example, the probability that a system is in a given state is often expressed through its probability distribution (Mandl, 1988) as follows:

$$p(E_r) = \frac{1}{Z} g(E_r) e^{-\beta E_r} \tag{2.1}$$

Expression 2.1 is commonly known as the Bolzmann Distribution applied for example to the kinetic theory of gases where $p(E_r)$ is the probability of having a state of energy E_r, $g(E_r)$ is known as the *degeneracy* which is the number of different states with the same energy E_r, β is a *temperature parameter* and Z is a normalizing constant know as the *partition function* where

$$Z = \sum_{E_r} g(E_r) e^{-\beta E_r} \tag{2.2}$$

The partition function ensures unit sum of probabilities in the Boltzmann distribution. Once p and Z are known for a system, it is possible for example to calculate other external parameters such as the mean energy $\overline{E}$ where

$$\overline{E} = \sum_{r} p_r E_r = -\frac{\partial \ln Z}{\partial \beta} \tag{2.3}$$

It will be shown that such statistical descriptions are useful in describing earthquake populations (Chapter 3) given the complexities involved and the large number of degrees of freedom associated with earthquakes ensembles (Rundle, 1993; Kagan, 1994).

2.3 Systems

Thermodynamic or statistical systems tend to be described based on direct measurements of macroscopic properties, phenomenological observation and physical experimentation. These descriptions are of their interaction with the 'outside world' or their surroundings. Therefore, thermodynamic systems can be broadly divided in to three types: *Isolated systems* that do not exchange energy or matter with their exterior, *closed systems* that exchange energy but not matter with their exterior and finally, *open systems* that exchange both energy and matter with their exterior (Mandl, 1988; Kondepudi and Prigogine, 1998). A thermodynamic description is in tune with the statistical approach when addressing Earth seismicity. This is because we gain our general insight from a statistical description based on our macroscopic observations of earthquake ensembles rather than on individual seismic events. The seismogenic crust to a first approximation is best described as 'closed' as it predominately exchanges seismic energy with its surroundings but no matter. However, we can generalise the description as 'open' to account for exchange of matter from the crust in the form of gases, magma etc. although matter exchange is beyond the scope of this thesis and is only mentioned here for completeness.

2.4 Proximity to equilibrium

The applicability of aspects of statistical physics and thermodynamics can depend on the state of the system, particularly for evolving or driven systems such as the Earth or systems whose properties may vary with time. Here I give a summary of the states statistical or *stochastic* systems can be in.

2.4.1 Equilibrium systems

An equilibrium system is one that through irreversible processes (section 2.5.1) evolves to a time invariant state where these processes vanish and its physical and chemical properties do not evolve with time (Kondepudi and Prigogine, 1998; Perrot, 1998). That is, the system has a uniform "temperature" throughout. Equilibrium is best described by the Zero'th Law of Thermodynamics which states that if a body A is in equilibrium with body B and body B is in equilibrium with body C, then body C is in equilibrium with body A (Mandl, 1988).

2.4.2 Non-equilibrium systems

Following from the definition of equilibrium systems, a non-equilibrium or far-from-equilibrium system therefore can be described as one undergoing an irreversible process and not of uniform temperature. An example of this is an ice cube in a glass of warm water. There will be heterogeneity in the temperature of the system (the water) and through an irreversible process of the ice melting and the water losing heat, the system will eventually reach a state of equilibrium. Non-equilibrium systems cannot therefore be defined by a global temperature but rather by local or mean temperatures (Kondepudi and Prigogine, 1998). Under certain conditions for both reversible and irreversible processes, the rate at which the processes occur will be an important factor since a non-equilibrium system evolving at an effectively infinitely slow rate can resemble an equilibrium system if observed over short time scales. In relation to self-organisation Alan Turing concluded that ordered patterns usually only occur in driven far-from-equilibrium open systems (in Ben-Jacob and Levine, 2001). The Earth's crust fits in to this category of systems since it is driven and dissipative.

2.4.3 Stationary and steady state

It is sometimes easy to confuse 'equilibrium' with 'steady' or 'stationary' states. *Equilibrium* as defined above will depend on the thermodynamic state of the system and its temperature distribution. Stationary or steady state systems however are those whose statistical properties or more specifically, probability density distributions do not alter with time regardless of proxim-

ity to equilibrium. What mainly distinguishes a stationary system from an equilibrium system is that stationary systems will have a non-zero entropy production (defined in section 2.5.5), whereas the entropy production in equilibrium systems is zero since they have a homogonous temperature distribution.

2.5 Entropy

Entropy is generally defined in the literature as *a measure of disorder*. Since we are interested in self-organising systems where there can be an evolution towards a more ordered state, it can be seen why entropy will play an important role in our understanding of such systems. Here I introduce thermodynamic and statistical type entropies.

2.5.1 Thermodynamic entropy

In 1865, the term entropy (Greek for transformation) was coined by Rudolf Clausius (1822-1888) who was extending the work of French engineer Sadi Carnot (1796-1832) (Perrot, 1998). Carnot showed that no real heat engine could be 100% efficient since work would be needed to transform energy or heat from one state to another. Carnot's theorem is expressed as

$$\frac{Q_1}{T_1} < \frac{Q_2}{T_2} \tag{2.4}$$

for a heat engine that absorbs heat Q_1 from a hot reservoir at absolute temperature T_1 and discards heat Q_2 to a reservoir at absolute temperature T_2 (Kondepudi and Prigogine, 1998). The '$<$' sign in equation 2.4 is indicative of an *irreversible* process or cycle. A *reversible* process on the other hand is defined as one in which the '$<$' sign in equation 2.4 is replaced with a '$=$' sign. However, such systems in reality may not exist, as they would have to be 100% efficient; irreversible processes existing in nature is debated (Bridgman, 1950).

It was Carnot's work that would lead the way for Clausius to develop the first two laws of

thermodynamics for a *closed* system. The first law states that

$$dE = dQ + dW \tag{2.5}$$

where dE is the change in energy of the system, dQ and dW are the heat exchange or transfer, and work (through say a mechanical process) exchanged between the system and its surroundings (Perrot,1998; Kondepudi and Prigogine, 1998). The seminal 'Second Law' states that the entropies of a reversible and irreversible process are respectively

$$dS = \frac{dQ}{T} \tag{2.6}$$

$$dS \geq \frac{dQ}{T} \tag{2.7}$$

where S is the *thermodynamic entropy* of the system and dQ is the heat exchange with the exterior at *thermodynamic temperature* T. In words the Second Law is often stated as: 'The sum of entropy of a system and its surrounding can never decrease' (Dugdale, 1996). The statement that the entropy of a system can only increase can be thought of as a system trying to minimise its *Helmholtz's free energy* F, that is, energy available to do work. This is expressed as

$$F = E - TS \tag{2.8}$$

Note that when the entropy $S = 0$, the amount of available energy to do work is a maximum.

2.5.2 Statistical entropy

In addition to thermodynamic entropy, there is what is known as *statistical* entropy. Boltzmann proposed an expression for statistical entropy to reconcile the reversibility predicted from the laws of statistical mechanics and the irreversibility constrained by the Second Law (Kondepudi and Prigogine, 1998). To clarify this, the following example is given: A container is partitioned with N_1 molecules in side A and N_2 in side B with $N_1 > N_2$ (figure 2.1)

Although there is no mechanical reason prohibiting molecules from side B to move to side A once the partition is removed, the more probable state (that of higher entropy) will be one where more particles from side A will move to side B. This will continue until the molecules

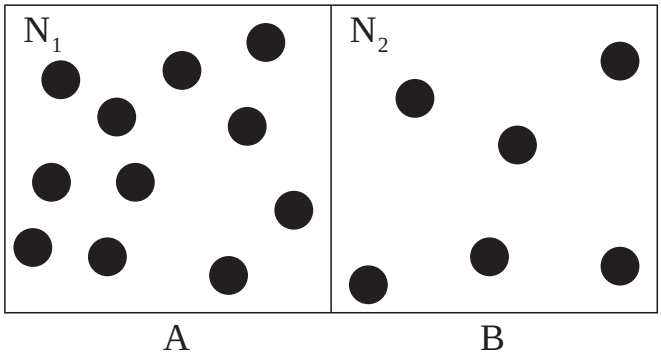

Figure 2.1: Binary system with a heterogeneous distribution of molecules.

are spread homogenously in the container and an equilibrium state reached (just like in the ice cube in glass example).

Mathematically, Boltzmann expressed the entropy S of such a system as

$$S = k_b \ln W \tag{2.9}$$

where W is the number of microstates corresponding to the macrostate with entropy S and k_b is Boltzmann's constant ($k_b = 1.381 \times 10^{-23} JK^{-1}$). For the binary system outlined above, the laws of probability theory will dictate that the number of microstates W with N_1 molecules in one half and N_2 in the other is

$$W = \frac{(N_1 + N_2)!}{N_1! N_2!} \tag{2.10}$$

As predicted, W and therefore S will be an absolute maximum when N_1=N_2. For a more general system where we do not necessarily know all the microstates p_r, if we have

$$\sum_r p_r = 1 \tag{2.11}$$

then the statistical entropy[1] (Mandl, 1988) is defined as

$$S = -k \sum_r p_r \ln p_r \tag{2.12}$$

For the example given above we can calculate the variation of S with p. Let us simplify the example as follows: If the probability of having a particle in one half of the container is $p_1 = p$,

[1]The derivation of statistical or shannon entropy can be found in the appendix of this thesis and in Shannon (1948) and Jaynes (1957).

then the probability of having it in the other half of the container will be $p_2 = 1 - p$. Using equation 2.12 and ignoring k, I calculate the phase space of S verses p_1 (figure 2.2). It can

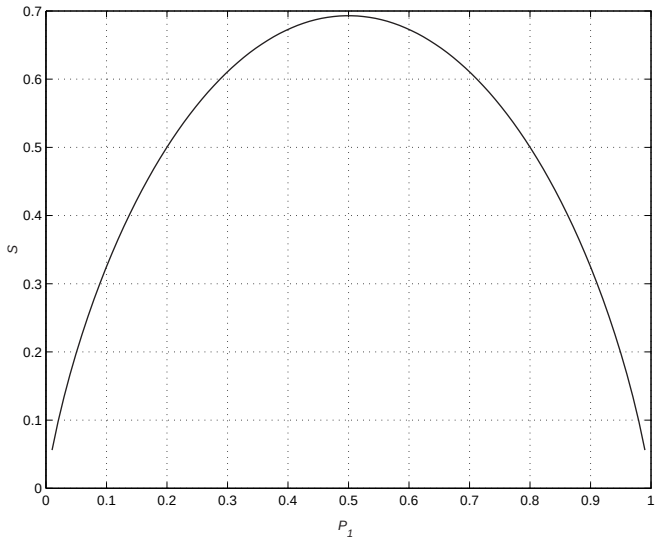

Figure 2.2: Plot of S against P_1 for a binary system with maximum S where $p_1 = p_2$.

be seen from the figure that as $p_1 \rightarrow 0.5$ i.e. $p_1 = p_2$, the entropy is a maximum. The figure reflects what equation 2.10 is telling us without having to refer to the equation. Statistical entropy has been shown to be applicable to both equilibrium and non-equilibrium systems (see section 2.5.3). Statistical entropy is also referred to as 'generalised', 'Gibbs' or 'Shannon' entropy in the literature.

2.5.3 Shannon entropy

In 1948, Claude Shannon published a prolific paper with the title *A Mathematical Theory of Communication* (Shannon, 1948). The publication deals with a variety of topics related to information theory including filtering, encryption and the transfer of information. It is said that when Shannon derived the equation to assess information gain and loss through a transmission channel, he was told by mathematician Van-Neumann to call it entropy since it had the same

format as 2.12 above. Shannon's[2] derivation gave the following result:

$$H = -K \sum_{i=1}^{i=n} p_i \log p_i \tag{2.13}$$

Here K is a positive constant that depends on the units of measure. This form of information entropy was obtained from the constraints that the function should be positive, increase with increasing uncertainty and additive for independent sources of uncertainty. Equations 2.12 and 2.13 refer to two different types of systems. The first gives our certainty in the state of a physical statistical system, and the latter refers to our certainty in the non-physical and perhaps more abstract concept of information transfer based on partial knowledge of the system, but are the two entropies analogous? Jaynes (1957) addresses this question elegantly. By freeing the statistical entropy from any physical constraints and looking at it as a method of statistical inference -which is essentially what it is as outlined in the container example above- he shows mathematically that the information and statistical entropies can be regarded as fundamentally the same. This is based on the simple fact that for both cases, the entropy is maximised as our uncertainty in the system reaches a maximum (as in figure 2.2). More importantly, Jaynes showed that following from this idea of maximizing entropy, the statistical / Shannon entropy concept may also be applied to systems out of equilibrium, a result recently further verified by Dewar (2003) (see section 2.5.5).

2.5.4 Configurational entropy

Somewhat related to information entropy is configurational or spatial entropy which takes into account the actual positioning of particles or bodies in a system. Following the description of Goltz and Böse (2002), this entropy is used as a form of box counting as follows: For a system divided to $L \times L$ square grids, we choose an area of size $l \times l$ and count the number of active cells[3] $N_k(l)$ out of a total of $N(l)$ cells (active + inactive) within the $l \times l$ grid. The probability of finding an active cell within the grid is then

$$p_k(l) = \frac{N_k(l)}{N(l)} \tag{2.14}$$

[2] Shannon used the notation H for entropy rather than the commonly used S.

[3] In Goltz (2002), the number of active cells are those containing earthquakes.

so the configurational entropy[4] H is given by

$$H(l) = -\sum_{k=0}^{l^2} p_i(l) \log p_i(l) \tag{2.15}$$

Configurational entropy has been widely used in the study of spatial organisation in various systems including cellular automaton models (Wolfram, 1986), earthquake clustering (Nicholson et al., 2000; Goltz and Böse, 2002), and in rock fracture experiments (Nanjo et al., 2000). This form of entropy will not be measured in this thesis but is mentioned here for completeness.

2.5.5 Entropy production and self-organisation

Work on entropy production had begun as a means of understanding irreversible processes in driven systems (Onsager et al., 1953) and self-organisation (Nicolis and Prigogine, 1977). Here, entropy production is explained through a classic experiment. The often cited example of self-organisation is that of Bénard cell convection given here in accordance with the description of Nicolis (1989). The experiment is set up such that there is a thin layer of fluid between two horizontal plates. Left to itself, the fluid is in a state of equilibrium in the thermodynamic sense i.e., of homogonous temperature. A temperature gradient, which acts as a driving force, is then introduced by applying heat to the lower plate. This gradient ΔT is increased to some critical temperature gradient ΔT_C precisely at which the fluid undergoes convection and organises its self into convection or Bénard cells (figure 2.3). Above the critical temperature, the patterns disappear and more chaotic fluctuations occur. Below the critical temperature, there is not enough energy for convection to occur and heat is dissipated by conduction through the fluid. It can be seen from figure 2.3 that the patterns of organisation are at length scales that far exceed the scales at which the individual molecules interact. Nicolis (1989) describes this emergence of patterns as *symmetry-breaking* since the patterns create a notion of space. One can imagine moving through a homogenous medium (say inside a black box) and not notice the movement whereby moving in the fluid with the cells there, one can feel the motion since there will be reference points (the edges of cells) present. Although this experiment is somewhat basic, it depicts the notion of self-organisation well.

[4] H is also used rather than S and is sometimes also given as I 'information' in the literature.

Figure 2.3: The spontaneous emergence of pattern in the Bénard cell convection experiment (from Kondepudi and Prigogine, 1998. No scale is given with the original reference).

However, it follows from the Second Law of thermodynamics that a system undergoing an irreversible process should reach a maximum state of entropy or disorder and relax to an equilibrium state. In nature, however, most systems are neither in equilibrium nor in a state of maximum disorder i.e. they show organised structures and patterns (e.g. Bak, 1997; Ball, 1999). The work of Prigogine shows however that a system can lower its entropy locally at the expense of increasing it globally. This is expressed as follows:

$$dS = d_e S + d_i S; \qquad dS > 0 \tag{2.16}$$

Here dS is the total change in entropy of the system, $d_i S$ is the internal change due to irreversible processes and $d_e S$ is the change in external entropy due to exchange of energy and/or matter with the surroundings. This is depicted in figure 2.4.

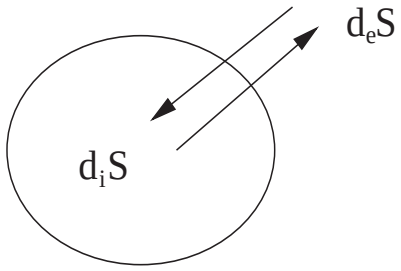

Figure 2.4: Internal entropy change $d_i S$ and external change $d_e S$ with $d_i S \geq 0$, (redrawn from Kondepudi and Prigogine, 1998)

In accordance with the Second Law we must always have $d_i S > 0$ regardless of whether the system is open or closed. $d_e S$ on the other hand is only non-zero for a dissipative structure and can decrease (implying a decrease in that component of entropy) provided relation 2.16 is maintained; this is the essence of self-organisation. Note that the system must be driven far from equilibrium otherwise $d_i S$ and $d_e S$ would be zero (Nicolis and Prigogine, 1977). However, one could ask why $d_e S$ should be driven to become negative? The property that has recently been receiving more attention is that of *entropy production*. This, for an open thermodynamic system, is generally defined as (Kondepudi and Prigogine, 1998)

$$d_i S = \sum_k F_k dX_k \geq 0 \tag{2.17}$$

and

$$d_e S = \frac{dQ}{T} + dS_{matter} \tag{2.18}$$

dX is a flow term such as dQ for heat or dN for say moles flowing in a time dt. F_k here is the thermodynamic force[5] such as a function of temperature. To show the relation between entropy and entropy production due to heat flow, we look at a simple example of an isolated container ($d_e S = 0$) divided in to two halves of temperature T_1 and T_2 (figure 2.5)

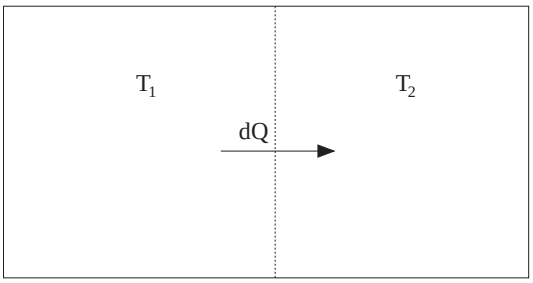

Figure 2.5: Entropy production due to the transfer of heat between two components. The entropy production $\frac{dS}{dT}$ is zero when $T_1 = T_2$ and the entropy S is a maximum.

with $T_1 > T_2$. Putting $dX = dQ$ and $F_k = (1/T_2 - 1/T_1)$ we have for time dt that

$$\frac{d_i S}{dt} = (\frac{1}{T_2} - \frac{1}{T_1})\frac{dQ}{dt} \tag{2.19}$$

From equation 2.19 we can see that the entropy production is greatest when the temperature difference between the two sides of the container is largest (further away from equilibrium) i.e. a state of *maximum entropy production* or MEP. On the other hand, when the system reaches an equilibrium state ($T_1 = T_2$), the entropy production is zero and the entropy is a maximum. This competition between entropy and entropy production is shown in figure 2.6.

It can be seen from figure 2.6 that if one assumes that slowly driven systems away from equilibrium approach a state of maximum entropy production, this will occur at the expense of decreasing absolute entropy. In the Bénard cell convection example, the cells emerge at the

[5]Not to be confused with the free energy F given in equation 2.8 above

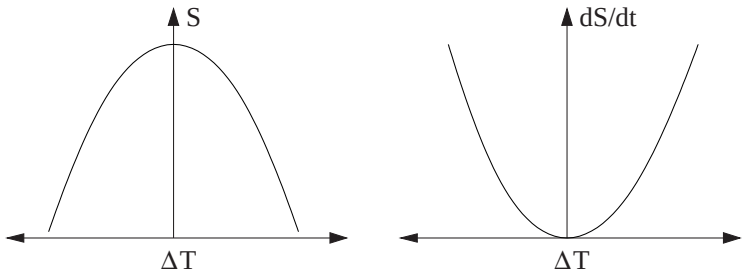

Figure 2.6: Change of entropy S and entropy production $\frac{dS}{dt}$ with temperature difference ΔT (redrawn from Kondepudi and Prigogine, 1998).

expense of increasing the dissipation of heat away from the system and hence increasing the entropy globally.

A similar definition of entropy production given by equation 2.19 is used by Lorenz et al (2001) to address a climate problem. Using a simple model, they show that a state of MEP explains the observed temperature variations with latitude on Mars and Titan that could not be explained by more traditional climate models. It seems that these gradients self-organise to a state where the heat flow (and accordingly the entropy production) is maximized (figure 2.7).

Similar approaches of applying MEP to climate models have been proposed by Ohmura and Ozuma (1997) and Wyant et al. (1988). To my best of knowledge, no such approach has been applied to better understanding self-organisation in earthquakes, real or synthetic[6].

2.6 Fractals

2.6.1 Introduction

I have spoken about *patterns* and *order* in systems with the example of Bénard cells but is there a formal definition to what is meant by 'pattern'? In a beautifully illustrated book on self-organised structures in nature *'The Self-made Tapestry'*, Ball (1999) gives examples of

[6]After the initial submission of this thesis, a good review of maximum entropy production and climate was published by Ozawa et al., (2003).

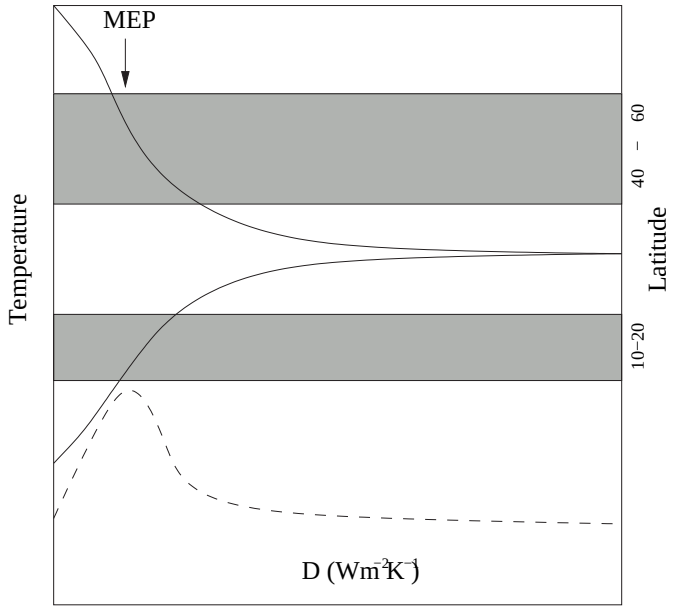

Figure 2.7: Figure shows model results of Lorenz et al. (2001). The y-axis normalised temperature and latitude, and the x-axis denotes D which is a term proportional to the ease at which the system radiates heat. The model temperatures (solid curves) fit observed average temperatures values on Titan for latitude $10 - 20$ and $40 - 60$ degrees (shaded areas) at the state of maximum entropy production or MEP (dashed line). Redrawn from Lorenz et al., 2001.

self-organisation from the forms of desert sand dunes, to patterns on sea molluscs. However, in a book that spans over 250 pages, only the following insight is given in his introduction to what is meant by 'patterns' or 'form':

> *"This book is about the development of pattern and form, and so it is well to have an indication of what I mean when I use these words. I cannot give either term a definition of mathematical rigour, however, nor can I always maintain a clear distinction between the two... Form is more an individual affair."*

Fortunately for the purpose of this thesis, the 'pattern' or 'form' seen in earthquakes, is well defined and known as 'fractals' or 'power-laws', as referred to in my introduction and are defined below in more detail.

2.6.2 What is a *fractal*?

Fractals are ubiquitous in nature. Natural examples of fractals include snowflakes (figure 2.8), coastlines, various branch structures and faults in rocks (Feder, 1988; Bak, 1997; Turcotte, 1997). The term *fractal* was coined by Mandelbrot in 1967 to describe geometries or systems that were self-similar and had no characteristic scale. Mandelbrot defined a fractal as *' ...a shape made of parts similar to the whole in some way'* , a more formal definition also given by Mandelbrot was *'... a set for which the Hausdorff-Besicovitch dimension strictly exceeds the topological dimension'* (Feder, 1988). Terms usually associated with fractals are 'power-law' (see below), 'scale-invariant' and 'self-similar' (Turcotte, 1997). Mathematically, these are defined by the power-law

$$N(r) = \frac{C}{r^D} \tag{2.20}$$

where $N(r)$ is the number of objects with linear dimension r, C is a proportionality constant and D is a non-integer 'power' or scaling exponent known as the *fractal dimension* usually found to have values $E - 1 < D < E$ where E here is the Euclidian dimension. For a two dimensional space ($E = 2$), typically $1 < D < 2$ (Dubois, 1998). In reality, D is

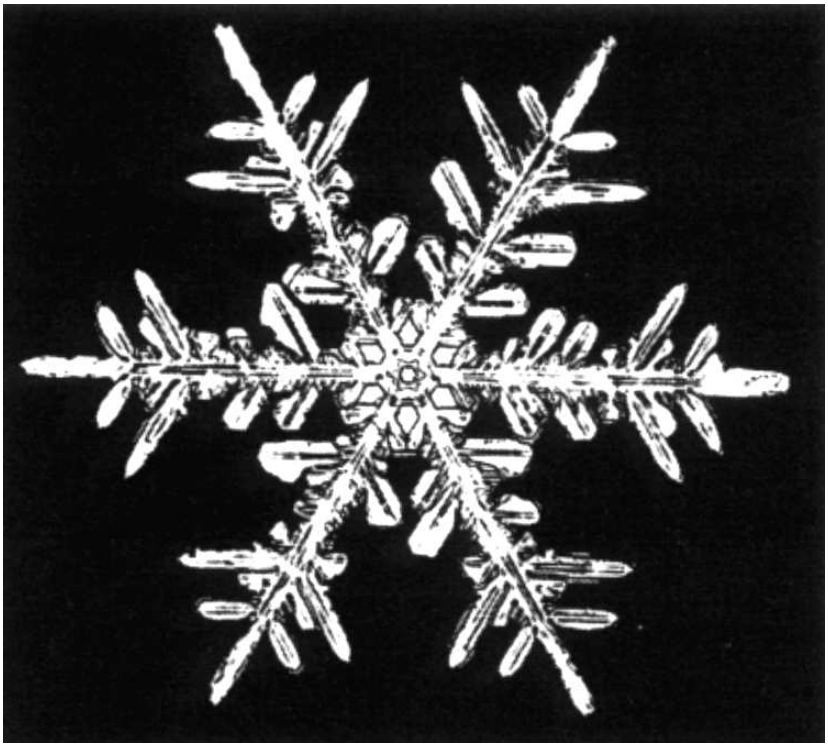

Figure 2.8: The snowflake; an example of a fractal geometry occurring in nature (from Ball, 1999).

usually measured using a box counting technique[7] where a geometry is divided in to square grids of size r and the number of grids $N(r)$ intersecting the geometry are counted and then r is varied and the counting process is repeated for that scale and so on (see descriptions by Feder, 1988 and Turcotte, 1997). Figure 2.9 shows a 'text book' example of a geometrical fractal representing the fragmentation of a block into smaller replicas (from Turcotte, 1997). Notice from the figure how the 'parts are similar to the whole' at the different scales. In this

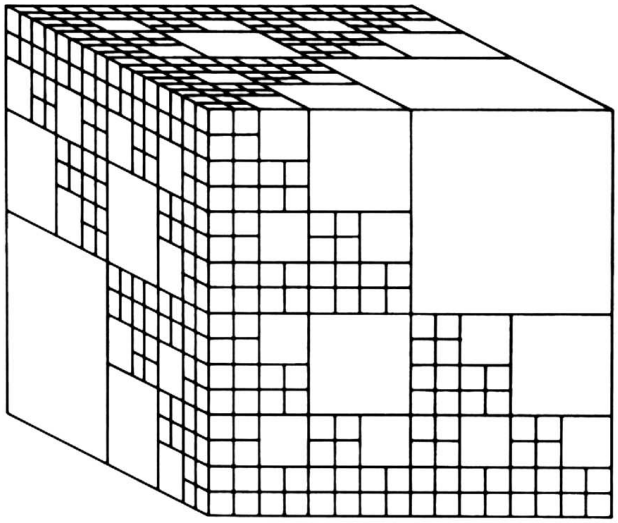

Figure 2.9: Example of a three-dimensional geometric fractal. From Turcotte, 1997.

example of a fractal, the size r of the squares scales as a power-law with their relative numbers N (figure 2.10), consistent with equation 2.20. Such power-laws are used to describe several scale-invariant geometries in nature including the fault size distributions in the Earth's crust (Bonnet et al., 2001) (also see section 2.8.3), climate variations (Bak, 1997), various aspects of biology (e.g. Ben-Jacob and Levine, 2001; Ball, 1999) and observations as far diverse as hospital waiting lists (Smethurst and Williams, 2001). It should be noted here that although the expression 2.20 above is boundless (r can be infinite), this is usually only true for conceptual or computer generated fractal geometries. In nature however, r will be limited by the smallest component of the system as a lower bound and by the system size as an upper bound. Such size limitations may give rise to *band-limited* fractals. Also, in some cases, the clustering in

[7] Other methods used to measure D include the *mass dimension* and *multi-fractal analysis*. See review by Bonnet et al., (2001).

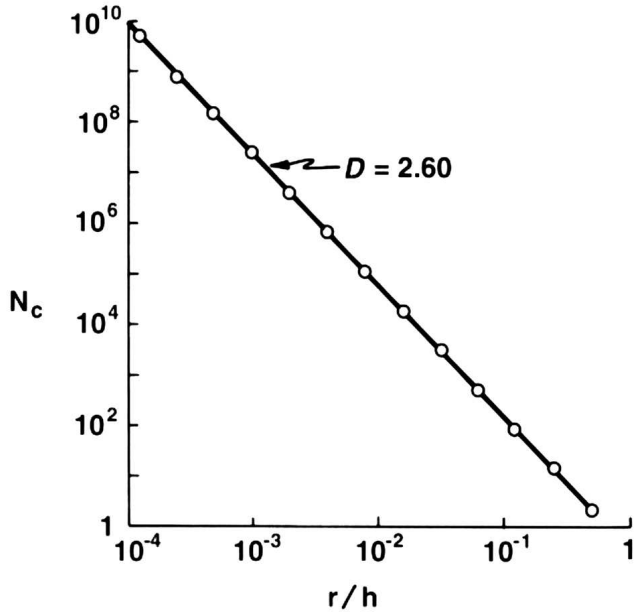

Figure 2.10: Corresponding log-log plot with slope (fractal dimension) D=2.60. From Turcotte, 1997

different vicinities of a fractal can show variation, an example of which is the process of crystal growth by diffusion-limited aggregation (Feder, 1988; Schroeder, 1991).

2.6.3 Fractals and the critical-point

Now that fractals or power-laws have been defined (referred to just as power-laws hereon), I return to statistical systems and their association with power-law distributions. A good example of this is the percolation model. The model is described by Staufer and Aharnoy (1998) and, in relation to earthquakes, by Main et al. (2000). Here, the model is described as follows: I run a computational percolation model on a $N \times N$ square grid with $N = 100$. A site is picked at random on the grid and is then defined as being 'broken'. The number of broken sites n divided by the total number of sites N^2 gives us the probability p of finding a broken cell so $p = n/N^2$. A *cluster* is then defined as the number of connected neighbouring broken cells. This is shown in figure 2.11.

As n is gradually increased, and therefore p, the number of clusters also increases forming

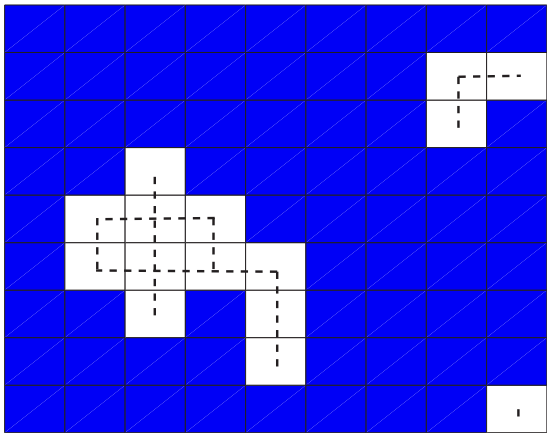

Figure 2.11: Clusters in the percolation model. The cluster area A is defined as the number of neighbouring broken cells. The dashed line indicates the percolation flow path network. The size of the largest cluster determines the correlation length ξ.

clusters of different sizes (figure 2.12). However, at some *critical point* (CP) where $p = p_C$ two interesting things occur. Firstly we very suddenly get what is called an *infinite cluster*, that is, one that connects one side of the system to the other allowing *percolation* to occur. The second thing that occurs precisely at p_C is that the distribution of cluster sizes (or area) A follow

$$N(A) \sim A^{-D} \tag{2.21}$$

with the number of clusters $N(A)$ is related by a power-law to the cluster size A with fractal dimension D. Note that this power-law distribution is similar to that seen in other statistical systems at the critical point such as the magnetic Ising model where there is a sudden change in magnetization at the Curie Temperature (Bruce and Wallace, 1989), or water at the critical temperature (T_C) as outlined in the introduction. The critical point p_C [8] for this example is referred to as the *percolation threshold* since there will be a rapid transition in the size of the largest cluster or correlation length[9] ξ where as $p \to p_C$,

$$\xi \propto |p - p_C|^{-\nu} \tag{2.22}$$

[8]The actual value of p_C will depend on the various parameters such as the dimensions of the system and the shape of the cells but for the example given is ~ 0.5927 (see Stauffer and Aharony (1998), pg. 17).

[9]The correlation length can be defined in different ways depending the system examined. Generally speaking however, ξ can be regarded as being a measure of the size of the largest cluster A_{max} in the system with $\xi \propto \sqrt{A_{max}}$.

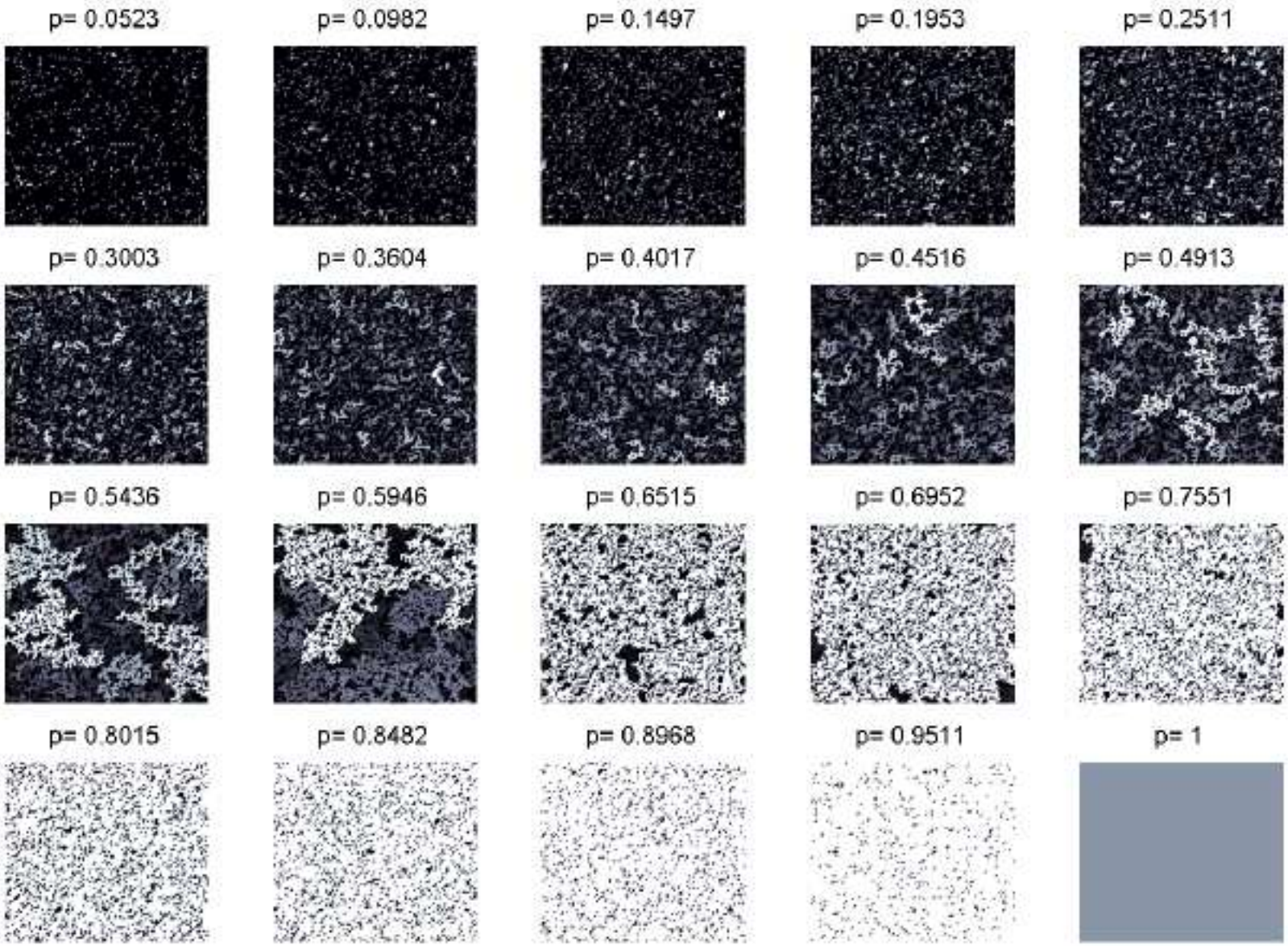

Figure 2.12: Plots of percolation model with p varying from 0 to 1. The brightness of a cluster in the figures is proportional to the cluster size.

where ν is a critical exponent. This rapid increase in ξ or A_{max} is demonstrated for a single run in figure 2.13. Note that when $p > p_C$, $\xi = \infty$ by definition since the entire system is

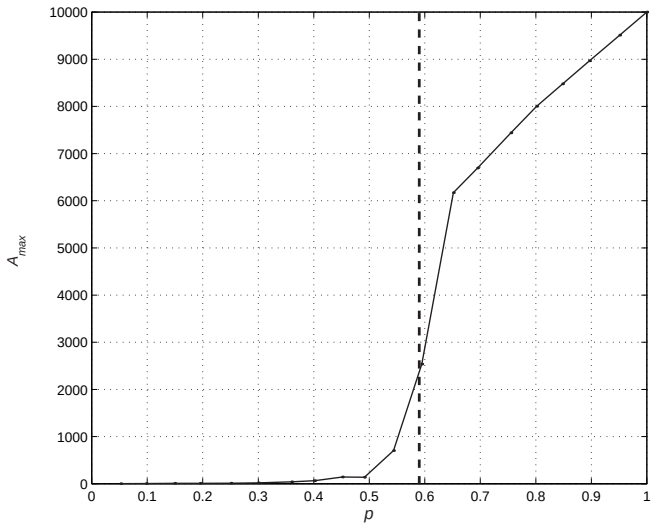

Figure 2.13: Plot of non-linear increase of maximum cluster size A_{max} with p for a single run of the percolation model with grid size $N = 100 \times 100$. The dashed line indicates the percolation threshold $p = p_C = 0.5927$. The size of the 'infinite' cluster (A_{max} is restricted by the system size at $p = 1$.

considered broken by the 'infinite' percolation cluster. The rapid acceleration in maximum cluster size as demonstrated by equation 2.22 is also found in the Ising model as the Curie temperature is approached (Nicolis, 1989) and has been reported in seismicity for earthquakes prior to some large events (e.g. Bowman et al., 1998) (see section 2.8.4 below). The critical point is associated with the process of *phase transitions* due to the rapid change in properties of the system such as the size of the largest cluster. In the case of a liquid-gas phase transition, the critical point (CP) corresponds to T_C (or a critical preasure) where there is a change of phase from liquid to gas with no change in density. The percolation model is therefore interesting since it resembles other statistical systems in its statistical properties prior to and at the critical point regardless of the detailed physics of the system, a property usually associated with *universality* (Main, 1996). This has encouraged the application of critical point statistical-physics or thermodynamics to stochastic systems such as the Earth's crust (Main, 1986; Zöller et al, 2001). This application must however be done with caution (see section 2.7.2).

2.7 Self-Organised Criticality (SOC)

2.7.1 Definition?

> *"There does not exist a clear cut and generally accepted definition of what SOC is. Nor does a very clear picture exist of the necessary conditions under which SOC behaviour arises"* -from the book *Self-Organised Criticality*, Jensen (1998).

Despite SOC having been cited in various literature over 2000 times since its publication, (Hergardten, 2002) the above quote from Jensen (1998) remains true. So far, I have discussed self-organisation in the light of thermodynamics of 'dynamic' dissipative structures and 'static' power-laws at the critical point in equilibrium thermodynamics and statistical physics (static). The great interest in SOC is because it is believed to be a link between critical point systems and driven dissipative systems. It is proposed as an explanation of the spontaneous emergence of power-law statistics in driven complex systems such as the Earth (Jensen, 1998; Ball, 1999).

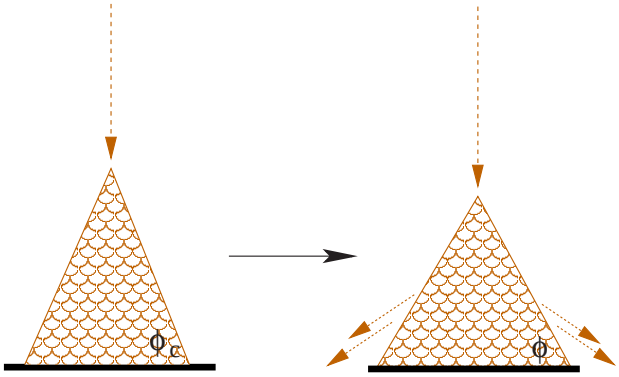

Figure 2.14: The avalanche process in the sand pile model with critical angle ϕ_C.

Bak et al. (1987) use the paradigm of sand piles to explain SOC. Sand is added to a pile grain by grain at a constant rate until the slope of the pile reaches some critical angle of repose ϕ_C when an avalanche is triggered as seen in figure 2.14. Any surplus sand is allowed to escape from the edge of the pile. The avalanches frequency-size distribution follows a power law[10]

[10]It was found later in laboratory experiments that not all sand piles produce power-law statistics although experiments showed that power-law avalanches were produced by rice grains with an elongated shape (Frette et al.,

distribution. The current accepted criteria of SOC as suggested from the BTW sand pile model are as follows:

1. A slowly driven system far from equilibrium that self-organises to a critical steady-state showing power-law statistics with fluctuations about the critical point of no characteristic size.

2. Sensitivity to minor perturbations that could trigger large events (avalanches) that can span the length scale of the system, i.e. one grain of sand could trigger a very large avalanche.

3. The power-law nature is global and independent of local dynamics (Bak et al., 1987).

Note from figure 2.14 that the sand leaves or dissipates from the system at the edges when an avalanche occurs. Dissipation[11] in SOC systems is required, otherwise, an infinite event may be triggered that would go on indefinitely (such as an infinitely large sand pile collapsing). The interesting point about SOC is the way 'energy' enters and leaves the system. The input driving force or energy is uniform or linear, whereas the output is punctuated in the form of avalanches of various size that follow a power-law (figure 2.15). An SOC system can be seen as a self-regulating power-law generator. The criteria associated with SOC given above can, to a first approximation, be used to examine if the crust is strictly SOC (see e.g. Main, 1996). SOC will be discussed in more detail in chapter 4.

2.7.2 Critical differences

I have mentioned the word 'critical' in relation to thermodynamic systems at the critical point (CP) (section 2.6.3), and in relation to SOC (section 2.7). There are important yet subtle differences between the two systems. Firstly, the CP systems away from the critical point are generally considered to be at equilibrium since there is no dissipation of energy and no

1996).

[11] Dissipation as cited in the SOC model literature can refer to two things, dissipation out of the system (at the edges) and dissipation within the system itself. Models with only dissipation at the edges are sometimes referred to as *conservative*. This is explained in detail in chapter 4.

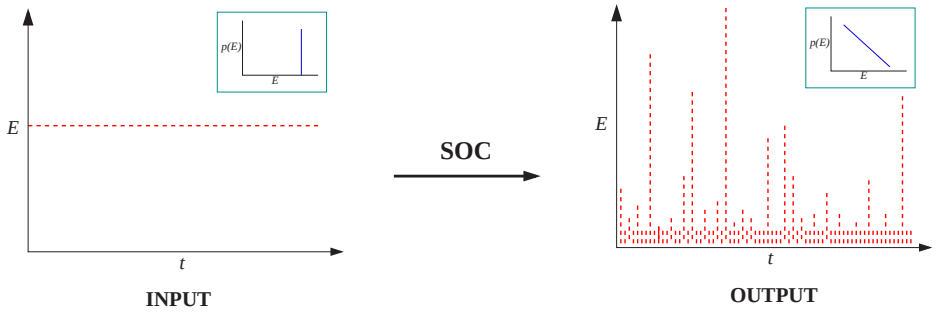

Figure 2.15: Figure shows the SOC process with a 'linear' input of energy and the punctuated power-law output. The inset boxes show the corresponding energy probability distributions on a log-log scale.

power-law features. However, the SOC systems are usually driven away from equilibrium by a driving force such as sand entering and dissipating in and out of the sand pile model. Also, the CP systems only show power-law structures at the critical point. Any perturbations to the equilibrium systems whilst away from the critical point will not drastically alter their statistics. It is only at the critical point that a perturbation -say a breaking of a cell in the percolation model- can alter the system significantly in the form of a phase transition. An example of this is changing the temperature of a fluid at the critical temperature; a slight increase would cause an evaporation whereby a slight decrease would cause condensation.

Conversely, in an SOC system, the system sensitivity to a perturbation is in the sense that a small perturbation may trigger a large event that spans the entire system but the power-law statistics overall remain resilient to noise (perturbations) provided the amplitude of the perturbations do not overshadow the intrinsic system fluctuations (Ceva, 1995; Mousseau, 1996; Main et al., 2000). Finally, CP systems must be 'tuned' to the critical point at which the patterns occur, that is, they will not naturally evolve towards the critical point (T_C, p_C, etc.). SOC systems will naturally evolve to the critical point as it is an attractor state. This usually can occur regardless of the starting conditions (Jensen, 1998). The differences between SOC and CP systems outlined are summarised in table 2.7.2.

Property	**CP**	**SOC**
Dynamics	Static	Driven & dissipative
State	At equilibrium when away from the critical point	Away from equilibrium
Power-law	Only at critical point	Always (within limits)
Dissipation	Not required	Essential
Sensitivity to perturbations	Sensitive close to and at critical point	Robust to perturbations over time although a small perturbation can trigger a large event
Criticality	Tuned	Attractor state

Table 2.1: Table of qualitative differences between equilibrium systems at the critical point (CP) and systems showing SOC.

2.8 Earthquakes

2.8.1 General introduction

Earthquakes mainly occur in the Earth's brittle crust in the proximity of active fault margins where tectonic plates converge, diverge or slide with one another (figure 2.16). The crust and the upper mantle broadly consist of the rigid lithosphere, which 'floats' over the more ductile (plastic) asthenosphere. In accordance with *elastic rebound theory*, tectonic forces drive the plates (usually at a slow rate of a few centimetres a year) and energy accumulates in the elastic-brittle upper crust as they deform and/or rub against one another until a threshold frictional force is overcome (this is analogous to ϕ_C in the SOC model above). When this occurs, the stored energy is released in the form of heat and radiated seismic energy.

Statistically, earthquakes belong to a class of systems which are very non-linear and away-from-equilibrium, so much so that their statistics have been likened to those of fluid turbulence (Kagan, 1994). This non-linearity is evident two fold; firstly in the power-law avalanche type behaviour observed in their energy release and their spatial and temporal statistics (see section 2.8.3), and on a more practical level in our inability to accurately predict large earthquakes despite over a century of research into prediction (Geller, 1997). It seems that earthquake

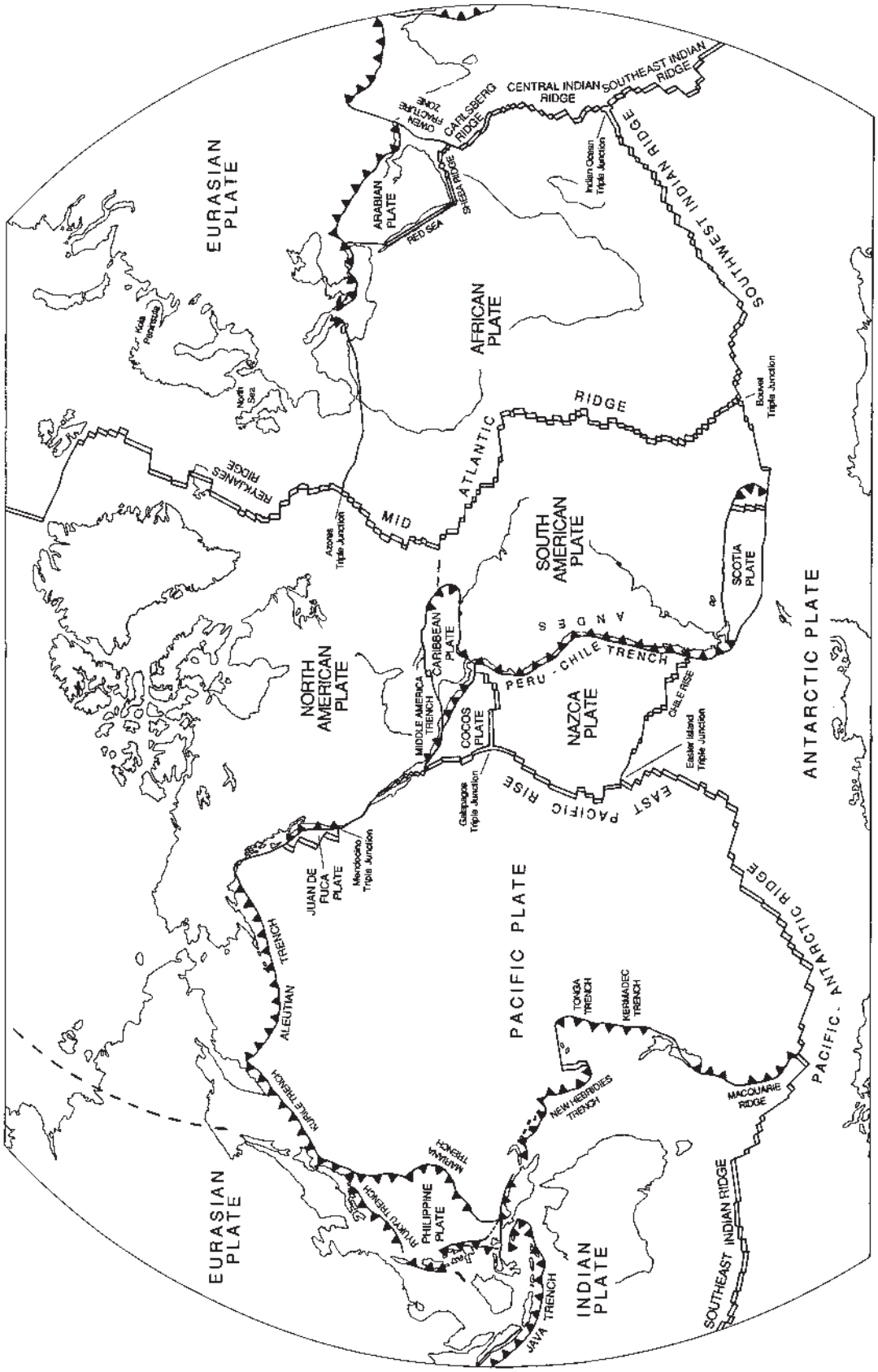

Figure 2.16: The major tectonic plates where plates showing convergent (triangles), divergent (double solid line), and transform (solid line) fault boundaries, (from Fowler, 1990).

prediction remains a 'holy grail' of geophysics (Main, 1996). It is this predicament that is thought to have divided the geophysical community into those who use a 'holistic' approach of data gathering and analysis, and those who concentrate on earthquake physics (Kagan, 1999). But, it is also these observed non-linearities that have encouraged a more integrated statistical approach to our understanding of earthquake phenomenology (Kagan, 1994; Main, 1996; Malamud and Turcotte, 1998; Bird et al., 2002).

2.8.2 Earthquake energy state

A simple 'thermodynamic' energy balance equation for seismic energy release can to a first approximation be written as (Scholz, 2002)

$$W_f = Q + E_S + U_S \tag{2.23}$$

where W_f is the mechanical work done in faulting (friction + deformation), Q is heat, E_S is the seismic energy release due to earthquakes, and U_S is the *surface energy* which is negligible. The seismic energy release E_S can be more specifically defined as

$$E_S = \frac{1}{2}\Delta\sigma\overline{\Delta u}A \tag{2.24}$$

where $\Delta\sigma$ is the stress change (drop) due to a seismic event, A is the fault area, and $\overline{\Delta u}$ is the mean slip or displacement along the fault. Referring to the laws of thermodynamics (see equation 2.4), one cannot expect all the work W_f to be converted in to seismic energy and heat alone as some will be expended through deformation, fluid circulation and so on (Scholz, 2002) . In the case of seismicity, the efficiency of this energy transformation η is referred to as the *seismic efficiency* (e.g. Dobrovol'skiy, 1994) and is defined as

$$\eta = 100\frac{E_S}{W_f}. \tag{2.25}$$

Note that E_S depends on the stress drop due to an earthquake and W_f will depend on the total stress in the crust. W_f is in practical terms difficult to calculate (Main et al., 2000). Nonetheless, It is known that stress drops due to seismic events are in the order of a few MPa compared to total stresses in the crust that are in the range of $10 - 100MPa$ (Abercrombie and Leary, 1993; Scholz, 2002). This is in agreement with the Second Law since no 'engine'

can be 100% efficient. However, the seismic efficiency is sometimes reported as being equal to unity (e.g. Kagan, 1999) in apparent contradiction to the Second Law. This is due to the great uncertainties in its calculation (Scholz, 2002). A 100% efficiency would require a lack of any deformation or heat flow in a seismic region and cause an earthquake whose radiated energy would resonate about the globe indefinitely, both requirements of which contradict general observations. In the light of self-organisation and dissipation, a form of seismic efficiency may play an important role in self-organisation in the crust since it is related to dissipation of energy. However, as can be seen from equation 2.25, realistically calculating η for earthquakes may be in practice impossible (Scholz, 2002) and therefore, the effects of dissipation are best examined in theoretical and numerical models of seismicity (chapters 3 and 4).

2.8.3 Earthquakes and power-laws

As mentioned in the introduction of this thesis, earthquakes follow power-law distribution in the form of the Gutenberg-Richter (GR) relation (Gutenberg and Richter, 1957) over several orders of magnitude where

$$\log(N) = a - bm \tag{2.26}$$

m is the *scalar magnitude* of the seismic event size and b is the seismic b-value generally ~ 1 worldwide (Kagan, 1999). It is this power-law nature of seismicity that leads us to suggest that the Earth is an SOC system in line with criterion 1 in section 2.7. The GR relation ensures that while small events are very numerous (several thousand a day for $m < 3$, larger events are very infrequent (one $m > 8$ annually on average). Why this distribution should organise its self to a power-law as opposed to any other distribution is elusive. This question is addressed by Kanamori and Anderson (1975) in terms of simple geometry. The magnitude of an earthquake is proportional to the area of its corresponding fault (equation 2.29 below). The problem is then reduced to a question of accommodation; you can fit many small faults within an active seismic region but only a few larger ones and accordingly, more smaller earthquakes than large ones. This explanation does not, however, account for the power-law being robust over several orders of magnitude despite the complexities involved in the Earth that lead to the SOC hypothesis as an explanation (section 2.7). It is also this robustness of the power-law observed for over a century that validates us addressing the Earth's seismicity as a 'stationary' process (as defined

in section 2.4.3).

As an alternative to the measurement of m, a more rigorous measure of earthquake energy release is known as the *moment magnitude* M_O. This magnitude is calculated from solving the *moment tensors* of an event which are the fault orientation and displacements in three dimensions as measured by multi-component seismograms. This measure of energy (Kanamori and Anderson, 1975; Fowler, 1990) is given by

$$M_O = \mu \Delta u A \tag{2.27}$$

where μ is the shear modulus, Δu is the slip and M_O is in units of Nm. M_O scales directly with source rupture area A (Kanamori and Anderson, 1975). For a scale invariant source, $\frac{\Delta u}{\sqrt{A}} \sim constant$ (Kanamori and Anderson, 1975; Abercrombie, 1995) so with reference to equation 2.27 it is found that

$$M_O \sim A^{3/2} \tag{2.28}$$

The moment magnitude has been empirically related to the surface wave magnitude M_S (analogous to m above) by

$$\log M_O = \frac{3}{2} M_S + 9.1 \tag{2.29}$$

M_S is measured from the logarithm of the amplitude of the surface wave at a period of 20 sec whereby the scalar magnitude M_O is in effect calculated at infinite periods (Kanamori and Anderson, 1975). Therefore, there will be an apparent attenuation or saturation at higher magnitudes of M_S so events of high M_O will be measured at only marginally high M_S where $M_S \sim 8$ (Reiter, 1991). Finally, given that $E_S = \frac{\Delta\sigma}{2\mu} M_O$ (Kanamori and Anderson, 1975; Scholz, 2002), we can deduce by substituting into 2.26 that the energy release radiated by an earthquake is empirically given by

$$\log E_S = \frac{3}{2} M_S + 4.8 \tag{2.30}$$

where E_S is in Joules.

In relation to fractals, it can be noted from equation 2.26 above that the b-value is a scaling exponent similar to the fractal dimension D in equation 2.20 above. The exponents b and D can be related as follows: Substituting 2.28 into 2.29, we have

$$M_S \sim \log A \tag{2.31}$$

Given that $m = M_S$ and substituting into 2.26 we have

$$N \sim A^{-b} \tag{2.32}$$

Since we are dealing with an area ($A \sim r^2$), we can rewrite 2.20 as

$$N \sim A^{-D/2} \tag{2.33}$$

So comparing the powers of 2.32 and 2.33 we have (Henderson, 1992; Turcotte, 1997)

$$D = 2b \tag{2.34}$$

This is essentially identical to the result of Kanamori and Anderson (1975) except that here, D need not be an integer. This result gives a mathematical link between the power-law observed for earthquakes and observations of fractal fault scaling found in the crust (e.g. Turcotte, 1997; Scholz, 1997; Bonnet et al., 2001). However, studies on real data have shown that relation 2.34 doesn't always hold for field data (e.g. Henderson et al., 1994; Öncel et al., 2001)

The Gutenberg-Richter relation can be written in terms of a true power-law in the form of an energy probability distribution. Putting $m \sim M_S$ we have $\log E \sim \frac{3}{2}m$ from 2.30 and $\log(N(m)) \sim m$ from 2.26. The $N(m)$ term can be written as a probability by simply dividing $N(m)$ by the total number of events for a sample. This gives the incremental energy probability distribution

$$p(E)dE \sim E^{-B-1}dE \tag{2.35}$$

where B is a scaling exponent. From 2.26 and 2.30 we can deduce that

$$B \sim \frac{2}{3}b \tag{2.36}$$

Note that 2.35 is a power-law at all scales. However, it has been found that earthquake energy probability distributions deviate from a straight line at higher magnitudes (e.g. Kagan, 1997; Burroughs and Tebbens, 2002). To take in to account any finite size effects such as the limited size and/or thickness of tectonic plates and finite rate of energy released seismically per unit time, a modification of 2.35 is therefore used in the literature and is known as the *modified gamma distribution* (Shen and Manshina, 1983; Main and Burton, 1984; Kagan, 1993) in the form

$$p(E) \sim E^{-B-1}e^{-E/\theta} \tag{2.37}$$

where $p(E)$ is the probability of having an earthquake of energy E and θ is a measure of the size of the largest possible event (analogous to the correlation length mentioned above). The gamma distribution will be discussed in detail and derived in chapter 3 (see section 3.2). Note that 2.37 has energy to the power $B+1$ as is sometimes quoted as having power B which can be a source of some confusion. However, the two scaling exponents are the same in the sense that this will depend on if a probability is incremental, cumulative or a density. Bonnet et al. (2001) give a good review of the different cases and are also defined by Sornette (2000, p.7-9).

2.8.4 Foreshocks and aftershocks

The GR law however is not the only power-law to be observed from earthquake dynamics. The second observation is that of the power-law time to/from failure given as Bufe and Varnes, (1993) and Zöller et al., (2001) as

$$\xi \sim (t_C - t)^{-k} \tag{2.38}$$

where ξ here is the correlation length (size of the largest seismic event within a region), t is time, t_C is time of failure, and k is the power-law scaling exponent. ξ here is often replaced by the cumulative Benioff 'strain' or $\sum[M_O]^{1/2}$ before a large event (Robinson, 2000; Bowman et al., 1998) where ξ is replaced by $\Sigma M_O(t)$ Note that although the term 'strain' is used in the literature in this context (e.g. Vere-Jones et al., 2001; Zöller and Hainzl, 2001), this is not a strain but a function of the stress drop or seismic energy release.

Looking at 2.38, one can instantly note the similarities with equation 2.22 as a critical point is approached. Therefore, this observation -when made- is suggested as supporting evidence that the Earth is a 'critical point' system and being in a state of SOC (e.g. Zöller et al., 2001). However, as I have outlined in section 2.7.2, 'critical point' and SOC are not the same thing.

A reverse of equation 2.38 above is the famous Omori law. If we swap t_C and t in 2.38 we retrieve the modified Omori Law which is generally give as

$$n(t) = K(t - t_C + c)^{-p} \tag{2.39}$$

where $n(t)$ is the number of aftershocks per unit time at time t; K, p and c are constants, t_C is the time of the main shock and t is the time following the main shock. Although 2.38 above is

not always observed prior to large events, the Omori Law has been well documented for real data for over 100 years (see Utsu et al., 1995).

2.8.5 Earthquakes *and* SOC?

Where do we currently stand in our assessment of earthquakes as an SOC system? There appear to be four approaches in addressing SOC in the crust:

1. **Observation:** With reference to the criteria outlined in section 2.7, the Earth's crust is a very slowly driven system with plate motions of only a few cm. a year (Fowler, 1990). Also, power-law statistics are found globally both spatially for the geometric distribution of Earth's tectonic plates (Sornette and Pisarenko, 2003) and for earthquake frequency-size distributions (e.g. Kagan, 1997). Furthermore, the process of small perturbations manifesting themselves into large events is also sometimes observed such as small changes in ground pressure that can trigger seismic events (Grasso and Sornette, 1998).

2. **Numerical models:** Several computer models of seismicity show power-law behaviour in their energy-frequency distribution (e.g. Burridge and Knopoff, 1979; Olami et al., 1992; Kumagai et al., 1999) despite having somewhat different underlying rules (heterogeneity, noise, dissipation, etc.). However, one must be cautious when making any conclusions as to what is occurring in the Earth based on what is being observed in a simple model. Models will be discussed in detail in Chapter 4.

3. **Critical point (CP):** As I discussed in section 2.8.4 above, although the observation of precursors in the form of a power-law increase in correlation length or cumulative seismic moment release may be a sign of the Earth acting as a critical point phenomena, this concept should not be confused with SOC. Temporal changes in the statistics of avalanche behaviour are not observed in the original BTW model of Bak et al. (1987). Equilibrium CP phenomena are fundamentally different from the far-from-equilibrium state of SOC.

4. **Theory:** There have been attempts at showing that SOC applies to the crust from a the-

oretical perspective. For example, these have been done using a mean field approach in deriving the power-law seen in the crust (Sornette et al., 1990). Other attempts have been made in analytically solving models of seismicity; Helander et al. (1999) analytically solve a one-dimensional sand pile model and retrieve power-law avalanches in both space and time. A similar approach is carried out by Lauritsen et al. (1996) using a generalised mean-field approach with the addition of a dissipation factor. They also predict power-law statistics in the locally conservative case, consistent with what is seen in numerical models. The success of an analytical approach indicates that a statistical mechanics can be useful in determining stationary solutions for systems out of equilibrium.

In addition to the second point outlined above, there are also other statistical observations that are seen in earthquakes that are not seen in the original BTW model such as anomalous stress diffusion in earthquake transient locations (Marsan et al., 2000). Therefore, if SOC is to be rejected as null hypothesis for crustal dynamics, one would require a description that: 1. does not contradict what is observed for real data, 2. is theoretically tractable and 3. can be verifiable though the use of numerical models. Therefore, an integrated approach using observation, theory and models is perhaps the best approach to address the question of SOC in the crust.

2.9 Summary

In this chapter I have covered some of the basics of statistical physics and thermodynamics to assist in the understanding of the lesser known branches of thermodynamics of dissipative structures and non-equilibrium systems. I then, in light of the thermodynamics, introduced definitions of entropy including statistical entropy, the important process of maximum entropy production (MEP) and its role in self-organisation. Although MEP has been used to better understand climate models, for example, it has not been formally applied to seismicity.

Power-law or fractal organisation in statistical systems was then examined and their link with the critical point and SOC described. The differences between a thermodynamic system at the

critical point and SOC systems was also highlighted. Although the general aspects of SOC are agreed upon amongst the scientific community, a formal definition of SOC remains elusive as pointed out by Jensen (1998). Finally, I gave a broad description of earthquake statistics and their current understood association with the concept of SOC and fractals. The GR law has been found to hold over time worldwide giving a rationale in addressing Earth's seismicity as a stationary steady-state process. Recent work on MEP (Dewer, 2003) that extends the work of Jaynes (1957) confirms that the tools of equilibrium statistical physics and thermodynamics can be applied to far-from equilibrium systems and systems undergoing SOC. This thesis addresses the question of self-organisation and criticality directly using analytical theory (chapter 3), numerical modelling (chapter 4) and analysis on earthquake populations (chapter 5).

Chapter 3

Entropy and the gamma distribution

> *"Statistical mechanics can describe not only the world of the very small and complex but also the very large and complex. It is likely that the application of statistical mechanical problems in the earth sciences will only continue to increase in the future"* -Rundle (1993)

3.1 Introduction

Earthquake populations are observed to be best described by a modified gamma distribution (a power-law with an exponential tail) in their frequency-energy statistics (section 2.8.3). In the previous two chapters I have covered aspects of thermodynamics, statistical physics and some of the observed phenomenology associated with earthquakes and self-organisation. Equilibrium systems can be tuned through an external variable (e.g. pressure or temperature) to undergo a phase transition via a critical point. In contrast, self-organising critical systems are spontaneously attracted to a critical attractor state under conditions that are far from equilibrium. The term 'critical' therefore takes on a different meaning when being applied to equilibrium and far-from-equilibrium systems (section 2.7.2).

In this chapter I address the term 'critical' theoretically using the tools of thermodynamics and statistical physics/mechanics described in chapter 2. I concentrate on analytical solutions associated with the energy probability distribution observed for SOC systems or more specifically, earthquakes. I recall the derivation of the modified gamma distribution in accordance with Shen and Manshina (1983) and Main and Burton (1984) using statistical (Shannon) entropy and how it varies in the sub-critical, critical and super-critical regimes. The three regimes are addressed individually in section 3.3. I then put forward a theoretical derivation of generalised entropy for the gamma distribution and the thermodynamic variables associated with it. A continuous version (non-discrete) of this result was derived in collaboration with Ian Main and has been previously published in Main and Al-Kindy (2002). Here a discrete version is derived to explain differences in calculating entropy by using linear and logarithmic increments. This was done by Prof. Ian Main. We propose that this theoretical framework may be used as a tool for assessing the proximity to criticality of a system with gamma type statistics. I also use the theoretical results to produce entropy-energy phase-diagrams for earthquake seismicity in the three criticality regimes for different power-law exponents. Some of the results of this chapter are also published in Al-Kindy and Main (2003).

3.2 The *gamma* distribution (GD)

> *'Only the gamma distribution satisfies both conditions: simplicity and satisfactory approximation of available [earthquake] data'* - Kagan (1993).

3.2.1 Overview

We have seen in section 2.6 that power-laws show correlation spanning all length scales as demonstrated by equation 2.20 and the Gutenberg-Richter (GR) law. Although this infinity can be demonstrated for geometrical objects on paper or those generated numerically on a computer screen, Earth is not infinite in size. This spatial limit at least for higher magnitudes can be accounted for by the use of a modified gamma function (section 3.2.4) that is in the form

of a power-law with an exponential tail that rolls off at larger scales (equation 3.1).

$$p(E) \sim E^{-(B+1)} e^{-E/\theta} \tag{3.1}$$

Here, $p(E)$ is the probability density of a state with energy E, B is the power-law scaling exponent and θ is a temperature term.

The difference between a pure power-law (effectively the Gutenberg-Richter law) and a gamma distribution (GD) as usually observed from earthquake data is demonstrated in figure 3.1.

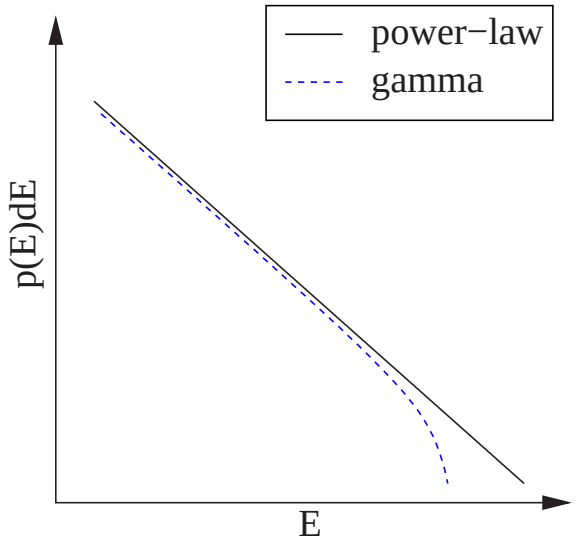

Figure 3.1: Plot of frequency-energy distribution from equation 3.1 for a pure power-law with $\theta = \infty$ (solid line) and for a gamma distribution with $\theta > 0$ (dashed line) which shows a roll-off at larger scales.

The y-axis in figure 3.1 denotes the incremental probability[1] $p_i = p(E)\delta E$ of an event of a particular size. Often this is also given as the numbers or frequencies of events. Sometimes probability is integrated and given as the cumulative number of events (e.g. Burroughs and Tebbens, 2002). However, taking the cumulative (which is used to 'smooth' the data) can often introduce or indeed obscure factors such as breaks in scaling or noise (Main, 2000). For this reason I will show incremental frequencies in the rest of this thesis unless explicitly stated

[1]The probability $p(E)dE$ is usually calculated by counting the number of events in a particular size range $E \pm \frac{\delta E}{2}$ and dividing by the total number of events.

otherwise. Two main features normally observed in data are shown in figure 3.1. Firstly, the cut-off size of the largest event will be smaller for the gamma distribution than for an equivalent pure-power-law[2]. Secondly, at the larger scales, the likelihood of having an event of a given size will be smaller for the gamma distribution than for a pure power-law distribution. Note that the observations in figure 3.1 are for the critical and sub-critical regimes which are usually observed from real data. A third case called 'super-critical', which is sometimes suggested from historic and palaeoseismic data, is discussed in section 3.3.3.

The GD has been used to describe various natural systems. For example, in the percolation model described in section 2.6.3, the cluster size-frequency distribution will follow a GD bellow the critical point to account for the largest cluster not being effectively infinite (Stauffer and Aharony, 1994). GDs are also represented in the band limiting effect of dissipation in cellular automata models of seismicity (Olami et al, 1992) and system finite size effects in other earthquake models (Jánosi and Kertész, 1993; Christensen and Olami, 1993). The GD has also been observed in magnetic domain patterns to account for the size limiting effect of magnetic damping at larger length scales (Bak and Flyvbjerg, 1992). These various accounts of the GD verify its applicability to both geometric (e.g. cluster size) and dynamic (e.g. earthquake energy release) type systems.

3.2.2 Seismicity: gamma and other distributions

The gamma distribution as applied to earthquake seismicity has its roots in statistical physics and information theory (see section 3.2.4) and can be thought of as an 'energy' distribution as in equation 2.1 (section 2.2) but with a geometric power-law degeneracy. It has been extensively used as a fit to earthquake seismicity data for both real (Main and Burton, 1989; Wu, 2000; Kagan, 1993; 1997; 1999; 2002) and model (synthetic) earthquake catalogues (Main et al. 2000; Vere-Jones et al., 2001). A gamma distribution fitted to three real earthquake cumulative-frequency data ensembles from The Harvard Centroid Moment Tensor catalogue (described in chapter 5) is shown in figure 3.2 (from Kagan, 1999). The fits shown are for three different earthquake source depth ranges.

[2] Although this is what is mostly observed, the opposite is true for the super-critical regime (section 3.3.3).

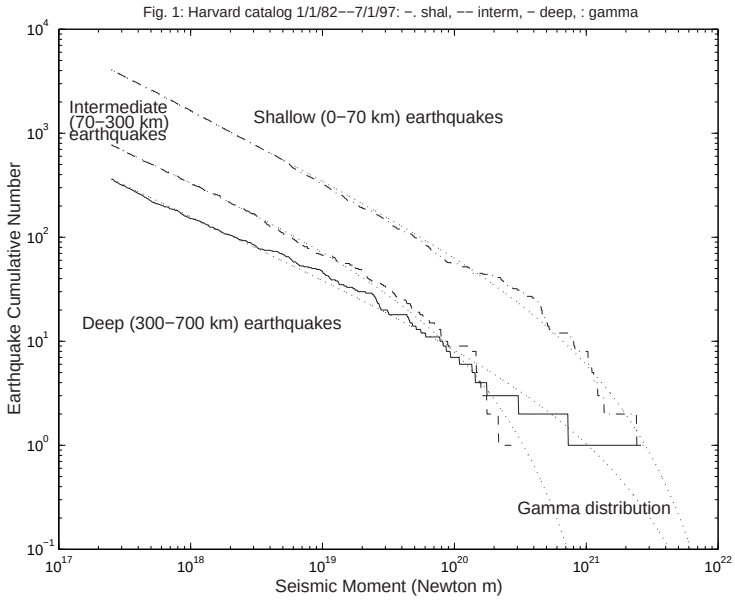

Figure 3.2: Cumulative frequency seismic moment distributions for earthquake data for three different depth ranges with fitted gamma distributions (from Kagan, 1999).

Although the gamma distribution (and variations thereof) currently seems to be the simplest and most consistent with available earthquake data (see Leonard et al., 2001), there are alternatives in the literature mentioned here for completeness. For example, it has been suggested that there may be two scaling regimes within an earthquake population with larger and smaller earthquakes obeying different scaling laws (Pacheco et al., 1992; Scholz, 1997) which in effect means fitting two GR laws with different b values to a data population. The premise of a break in slope of the GR law has been criticised on both statistical grounds as such a fit requires more parameters to be defined (Main et al., 1999) and/or on the grounds of being artefacts of noise or due to the use of cumulative statistics (e.g. Main, 2000). Sometimes related to the gamma distribution is the *characteristic earthquake model* which is discussed in section 3.4. In summary, it can be said that for a given energy range $E_{max} - E_{min}$, the gamma distribution is the simplest distribution in terms of the number of free parameters after the pure GR law that can fit most observed earthquake populations as well as having a statistical physics basis as derived from information theory (see section 3.2.4 below).

3.2.3 The 'temperature' term θ and the scaling exponent B

The two main components of equation 3.1 are as follows:

θ: This is referred to as the *temperature* term because it dimensionally replaces the temperature terms kT in Boltzmann's distribution (equation 2.1 in section 2.2) and must not be thought of as an actual temperature in the thermodynamic sense; it merely determines the magnitude of fluctuations in the system. The θ value is often used to estimate or predict the size of the largest *probable* event in seismic hazard studies (Main and Burton, 1989; Kagan, 1999). In other words, θ is related to a correlation length. One important aspect of the θ term is that it is analogous to the probability p in the percolation model (section 2.6.3) in the sense that it determines whether a system is in the 'sub-critical' ($\theta > 0$, 'critical' ($\theta^{-1} = 0$) or 'super-critical' ($\theta < 0$) regime, depending on its value. These three criticality regimes are discussed in section 3.3.

B: The scaling exponent B for earthquake seismicity is reported as being a universal constant (referred to as *universality* in this thesis) with $B \sim 0.60 - 0.65$ (Kagan, 2002) although studies have shown that B can vary in space (Ogata et al., 1991) and/or time (Smith, 1991; Wyss and Wiemer, 2000). For example, it is apparent from figure 3.2 that the deep earthquakes have a lower slope (B value) than the shallower ones. Temporal variations of B have been studied as possible precursors to large events in seismicity of earthquakes (Smith, 1981) as well is rock fracture experiments (Sammonds et al., 1992). Physically B can be indicative of the level of spatial clustering of faults (Öncel et al., 2001) or earthquake epicentres in space (Henderson, 1992) since, at least mathematically, it is related to the fractal dimension D (section 2.8.3). Variations in B in space or time might also be symptomatic of changes in the local physical dynamics of a system (e.g. Main, 1987, Olami et al., 1992). However, variations in B should be treated with some caution because measured values may be influenced by the assumptions or methods used in obtaining them (Bender, 1983).

3.2.4 Derivation of the gamma distribution

This derivation is given here in accordance with Shen and Mansinha (1983) and Main and Burton (1984) and then generalised to include the constraints using the theory summarised by Jaynes (1957). The derivation of Shannon or statistical entropy is given in Appendix A of this thesis and defined for an energy probability distribution $p_i = p(E)dE$ with incremental microstates E_i as:

$$S = -\sum_{E_{min}}^{E_{max}} p_i \ln p_i \tag{3.2}$$

where E_{min} and E_{max} are the minimum and maximum possible energy states observed in the system. To ensure unit probability for all states we set

$$\sum_{E_{min}}^{E_{max}} p_i = 1 \qquad i = 1, ..., N. \tag{3.3}$$

The expectation or mean of $f(E_i)$ for N constraints is

$$< f(E) >= \sum_{E_{min}}^{E_{max}} p_i f(E_i) \qquad i = 1, ..., N \tag{3.4}$$

where $f(E_i)$ are independent functions of the energy. In accordance with Jaynes (1957), the maximum entropy distribution is the most likely subject to the information available. We therefore look for $\delta S = 0$, using the method of Lagrangian undetermined multipliers, subject to (3.3) and (3.4) then

$$p_i = e^{-\lambda_0 - \lambda_1 f(E_1) - \lambda_2 f(E_2) - ... - \lambda_N f(E_N)}. \tag{3.5}$$

The constants λ_i are Lagrangian undetermined multipliers, to be determined by substituting (3.5) into (3.3) and (3.4). Given the constrains of (3.3) we can define

$$\lambda_0 = \ln Z \tag{3.6}$$

where Z is the partition function defined as

$$Z = \sum_{E_{min}}^{E_{max}} e^{-\lambda_0 - \lambda_1 f(E_1) - \lambda_2 f(E_2) - ... - \lambda_N f(E_N)} \tag{3.7}$$

and following from this, it can be shown that (generalised from Main and Burton, 1984)

$$< f(E) >= -\partial \ln Z / \partial \lambda_i. \tag{3.8}$$

We can see that once Z is known, all the other macroscopic variables f_i can be calculated from its partial derivative using (3.8). One example is the mean energy. One can now put the energy constraint $f_1 = E$, and finite natural log energy $f_2 = \ln(a_2 E)$ to obtain

$$p_i = \frac{e^{-\lambda_1 E - \lambda_2 \ln a_2 E}}{Z}. \tag{3.9}$$

Substituting $\lambda_1^{-1} = \theta$, $\lambda_2 = B + 1$ and $a_2 = E_0^{-B}$ for dimensional consistency, where E_0 is is a reference energy state, we then have

$$p_i = \frac{E_0^B E^{-B-1} e^{-E/\theta}}{Z} \tag{3.10}$$

and

$$Z = \sum_{E_{min}}^{E_{max}} \frac{E^{-B-1}}{E_0^{-B}} e^{-E/\theta}. \tag{3.11}$$

Equation 3.10 has the form of the gamma distribution (equation 3.1) but here, the partition function Z ensures that (3.10) has unit total probability. The occurrence of the degeneracy 'power-law' term in earthquakes can be thought of in geometrical terms since the energy release is related to the fault rupture area A where $E \sim A^{3/2}$ (section 2.8.3) and there are fewer ways of fitting a large fault to a given area and vice versa for small faults (Kanamori and Anderson, 1975). This geometric constraint is addressed by Main and Burton (1984) in their derivation of the power-law GD. The approach of maximising entropy subject to information available has also been used by Nagahama (1992) to derive a formula to calculate shear strain with distance from a naturally occurring shear zone. More recently, a similar approach has been applied to derive statistical physical models for strain in fibre bundle models (Pride and Toussaint, 2002; Toussaint and Pride, 2002a; 2002b) using the principles of maximum entropy. I now re-examine the characteristics of the GD formally in relation to criticality.

3.3 The three criticality regimes

Equation 3.10 it is composed of a power-law (degeneracy) term with slope B and a Boltzmann exponential 'tail' at a characteristic energy θ. For statistical systems such as the percolation and Ising models discussed in section 2.6.3, the system will behave differently below and above

the critical point (where the system is a pure power-law). The three criticality regimes are dependent on θ in their definition as follows:

3.3.1 The sub-critical regime ($\theta > 0$)

If the θ term is positive, there will be a roll-off at the higher energies with larger energies less probable than a pure power-law (figure 3.3). This is what is observed for the majority of earthquakes populations (e.g. figure 3.2 after Kagan, 1999; Leonard et al., 2001).

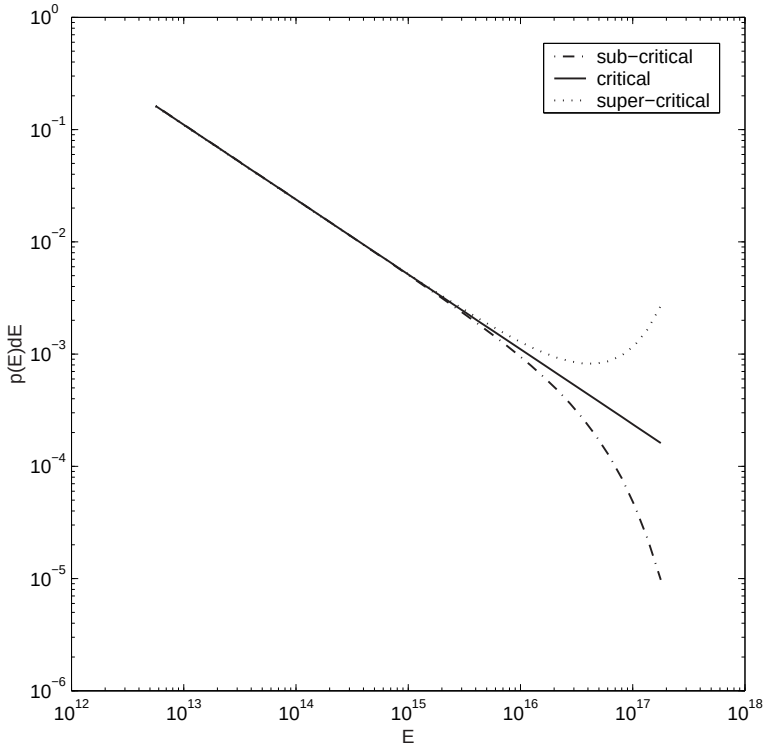

Figure 3.3: Theoretical probability distribution for the three criticality regimes with $\theta > 0$ (sub-critical), $\theta^{-1} = 0$ (critical) and $\theta < 0$ (super-critical).

The observation of a sub-critical regime is also predicted from various analytical solutions of SOC models. For example, in mean-field approximations of the SOC model, sub-criticality is predicted when finite dissipation is introduced in to the system (Lauritsen et al., 1996). The dissipation can have the same effect as the system size on limiting the extent or magnitude of the maximum event size. Again, these observations are more akin to real systems which are

usually both limited in size and dissipative.

3.3.2 The critical regime ($\theta^{-1} = \theta_c^{-1} = 0$)

When the temperature term θ is effectively infinite, we achieve a pure power-law (figure 3.3) since for $\theta \rightarrow \infty$, the exponential term in equation 3.10 disappears and the Gutenberg-Richter law is retrieved. The critical regime is what was found in the original BTW model (Bak et al., 1987) where there is no internal dissipation in the system and is analytically predicted for a one-dimensional sand pile model (Helander et al., 1999).

An important point regarding the literature on the Earth as a 'critical system' must be clarified here. The power-law observed in the original BTW model was referred to as '*1/f*-noise' since the relation between the duration of the avalanches and their size was found to be a power-law[3]. However, some of the literature addressing Earth's criticality in association with *1/f*-noise refers to a power-law observed in the Fourier analysis frequency-power distribution of say borehole wire-log data (e.g. Leary, 1991; Bean, 1996; Leary and Al-Kindy, 2002), or in the Fourier analysis of Earth surface landscape altitude data (Turcotte, 1997). The observed power-laws in these examples are true *1/f*-noise since they examine the power-frequency content of a time series. These should neither be confused with the dynamic power-laws observed in the probability distribution of radiated seismic energy nor with the critical point observations associated with accelerated seismicity discussed in section 2.8.4. The term 'critical' is too often used in the earth science literature to mean 'power-law' regardless of what parameters the observed power-laws are associated with. Just as with the critical point (CP) concept, *1/f*-noise in the crust, despite being self-organised, is a static observation ingrained in the crust in the form of deformation and fracture asperities, whereas SOC is a dynamic and evolving process. These are two different faces of criticality that must be better differentiated in the literature.

[3]This power-law had a different slope to that found for the avalanche frequency-size distribution. It was later decided that the term '*1/f* noise' in the BTW publication was not appropriate (Jensen, 1998).

3.3.3 The super-critical regime ($\theta < 0$)

If θ is negative, the system is said to be super-critical (figure 3.3). Vere-Jones (1976) states that 'no system is likely to survive in a supercritical state'. I highlighted the difference between equilibrium thermodynamic systems and SOC systems at the critical point in section 2.7.2. I now highlight how they are phenomenologically different in the super-critical regime.

1. Let us take an extreme case in the percolation model of $p \rightarrow 0.99$, one would effectively get a spike located close to the size of the largest cluster or indeed, the system size (figure 3.4). There is, however, no equivalent statement of $p \rightarrow 0.99$ for θ in Earth seismicity; θ can take any value ($-\infty < \theta < \infty$) rather than the bounded $0 < p < 1$ for the percolation model. Note also that unlike θ, p can only have positive values.

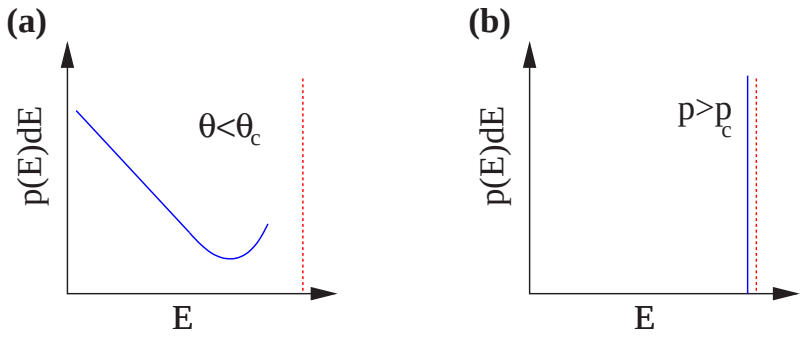

Figure 3.4: Probability distributions for a) gamma distribution with $\theta < \theta_c$ and b) the percolation model with $p > p_c$. The dashed line indicates the system size.

2. Also, the super-critical state in the dynamic sense refers to there being an above average number of largest possible events; this is possible in a dynamic driven system which is constantly updating itself (e.g. sand entering and leaving a sand pile). However, we cannot, say in the percolation model, have a super-critical distribution of clusters in the same way since this would require simultaneously fitting more than one 'infinite' cluster into the system which is impossible.

3. Earthquakes in practice tend not to span the size of the system i.e., there are no faults whose lengths are the circumference of Earth. So, although the correlation length is denoted as 'infinite' for the percolation model above p_c, it is not in practice for Earth

above θ_c. A correlation length can perhaps only be regarded as 'infinite' if it exceeds the length scale of an observed sub-region of the system as a whole. Here 'sub-region' can either refer to a geographic location such as Cyprus for example and/or an area defined by a physical restriction such as seismogenic depth or a plate boundary geometry.

3.4 'Characteristic' earthquakes

Characteristic earthquakes are earthquakes of a particular size or magnitude that occur more often (a higher recurrence rate) than would be statistically predicted by the standard GR law (e.g. Schwartz and Coppersmith, 1984). Following from the definition of super-criticality above (section 3.3.3), the largest events in the super-critical distribution can be regarded as 'characteristic' since there are more of them than expected, but the opposite is not true i.e. 'characteristic' does not necessarily mean 'super-critical'. I demonstrate this in figure 3.5. It

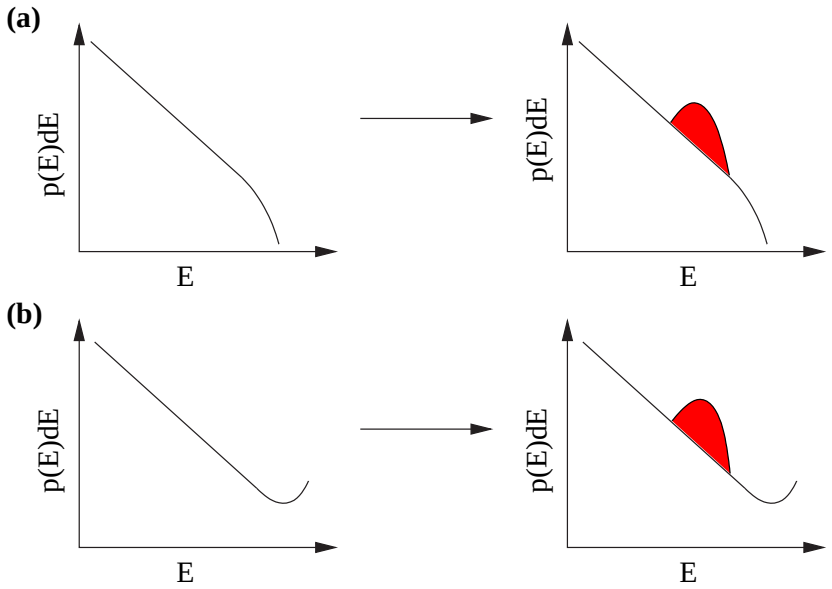

Figure 3.5: Log-log plots of a) sub-critical and b) super-critical energy probability distributions both showing 'characteristic' earthquakes (shaded area).

can be seen in figure 3.5 that the deviant, more frequent earthquakes do not necessarily occur at an energy that corresponds to θ, otherwise this would simply be a 'critical' case. Also, the characteristic earthquakes can overprint both a sub-critical and super-critical distribution

making the resulting distribution difficult to define. Figure 3.6 shows an example of real 'characteristic' earthquakes for magnitudes $4.5 < M < 5$ in the seismicity of Mount St. Helens (after Main, 1987). Characteristic earthquakes tend to be observed in isolated cases and are often criticised as being a by-product of statistical bias or as artefacts of data analysis or quality (Kagan, 1993). However, characteristic earthquakes have also been observed under certain conditions in numerical models of seismicity (e.g. Ben-Zion et al., 1999). It is ambiguous to me as to which of the three criticality regimes characteristic earthquakes should belong to, if any. Indeed, the characteristic earthquake hypothesis is *'yet to be proven'* (Kagan, 1993).

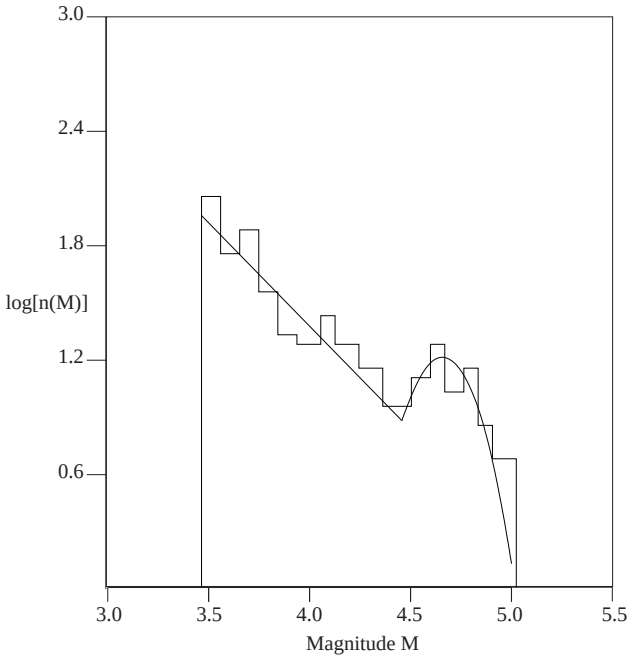

Figure 3.6: Incremental frequency-magnitude plot for the Mount St. Helen's volcano (re-drawn from Main, 1987). The straight portion of the line represents a power-law at low magnitudes, and the Gaussian peak at larger magnitudes. The elevated probability away from the power-law trend implies the distribution is 'characteristic'.

3.5 Apparent super-criticality

I have mentioned that a super-critical regime is one where there is a greater number of large events than would be expected than a linear extrapolation. I demonstrate a hypothetical scenario

where this is observed despite not being inherent or intrinsic to the system's dynamics. Because of the infrequency of large events (recurrence rates in the order of tens to hundreds of years), these are usually documented historically. However, let us take a hypothetical case that follows a Gutenberg-Richter law (Figure 3.7) where the largest events are historical ones estimated from documented human accounts of damage etc. It can be seen in figure 3.7 that if say two or three events have been underestimated, or indeed smaller events overestimated, these will shift the distribution from a linear GR trend to a characteristic, or more likely, super-critical trend. I call this *apparent super-criticality* since it is a statistical or sampling artefact. In addition to historically based magnitude estimates, another cause of under or over estimation of event size can also be due to instrumental saturation in wave energy measurements (Rieter, 1990). A recent example of many super-critical distributions observed for data populations from the period 550 BC-2000 AD in the Aegean area is given by Koravos et al. (2003). It was unclear in the Koravos et al. study if the super-criticality observed was real or a by-product of uncertainties in the historical earthquake magnitude estimates. In this thesis, the earthquake data analysed (chapter 5) will be from the CMT catalogue that only spans the last 30 years and measures the moment magnitude; it is therefore free from any historical or instrumental impediments.

3.6 Gamma entropy

In chapter 2, we saw how entropy plays an important role in the portrayal of the level of organisation in a system and its proximity to criticality. Here, an analytical solution is derived for the entropy of the modified gamma distribution[4] $d \ln E$. Equation $A6$ in Main and Al-Kindy (2002) should therefore read $S = \ln Z - B \ln E_O + (B+1)\langle \ln E \rangle + \langle E \rangle / \theta$. This error was resolved by a submission of a corrigendum to the Journal *Geophysical Research Letters* in which the derivation was first published (Main and Al-Kindy, 2004). The discrete derivation by Ian Main given here is more appropriate since the data analysed in chapters 4 and 5 are

[4] After the publication of Main and Al-Kindy (2002) -see appendix- and the submission of this thesis, it was noted that there was an error in this derivation (Chen and Chang, 2004). The incorrect derivation was then subsequently removed from this thesis. This error is in equation $A5$ of Main and Al-Kindy (2002) which should read $S = Z^{-1} \int_{E_{min}}^{E_{max}} (\frac{E^{-B}}{E_O}) e^{-E/\theta} \ln \left[\frac{1}{Z} \frac{E^{-B-1}}{E_O} e^{-E/\theta} \right.$

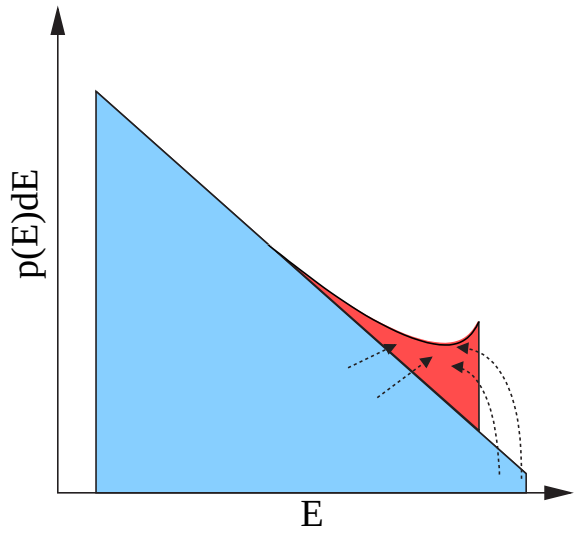

Figure 3.7: Apparent super-criticality where erroneous estimation of larger (or smaller) events can lead to an increase in the frequency of events of a particular size (energy). The arrows point towards the underestimated or overestimated earthquake energy probabilities.

treated discretely. Fortunately due to the nature of the error, non of the results or conclusions of this thesis were in any way affected.. The rationale for this derivation is to predict from a theoretical point of view how S will be influenced by the energy E, the temperature term θ and the scaling exponent B below, at and above the critical point. The mathematical derivation presented in this section was done by Prof. Ian Main. Because the radiated seismic energy is over several orders of magnitude, it is often binned using logarithmic bin widths ($d \ln E$) rather than linear bins (dE) in constructing the frequency-energy plots (chapter 5). Here a discrete solution is given of the entropy for a gamma distribution as apposed to a continuous one as in Main and Al-Kindy (2002).

The incremental probability p_i with energy level E_i and linear bin width dE is expressed generally by

$$p_i = p(E)dE \tag{3.12}$$

where for the limit $dE \to 0$, the probability density is defined as

$$p(E) = dp_i/dE. \tag{3.13}$$

The modified gamma distribution (as in equation 3.10) for a discrete function can therefore be expressed as

$$p(E) = \alpha E_i^{-B-1} e^{-E_i/\theta} \tag{3.14}$$

where α is a constant that insures the summation of all probabilities equals unity. Because the data is analysed using logarithmic bins, we use the substitution

$$d\ln E = dE/E \tag{3.15}$$

Combining 3.13, 3.14 and 3.15, we now have

$$p_i = \alpha E_i^{-B} e^{-E_i/\theta} d\ln E. \tag{3.16}$$

Comparing this with equation 3.10 we get

$$p_i = \frac{E^{-B} e^{-E_i/\theta}}{Z} \tag{3.17}$$

where Z is the partition function and the constant $\alpha = d\ln E/Z$. Because

$$\sum_{i=1}^{n} p_i = 1, \tag{3.18}$$

the partition function for n increments will be

$$Z = \sum_{i=1}^{n} E_i^{-B} e^{-E_i/\theta}. \tag{3.19}$$

Now, for a Discrete function $f(E)$, we can define a mean or expectation value as

$$\langle f(E) \rangle = \sum_{i=1}^{n} p_i f(E_i) \tag{3.20}$$

and the 'Shannon' entropy for a discrete function as

$$S = -K \sum_{i=1}^{n} p_i \ln p_i. \tag{3.21}$$

Putting the constant $K = 1$, and substitution 3.17 into 3.21, we find

$$S = -\sum_{i=1}^{n} \frac{E^{-B}e^{-E_i/\theta}}{Z} \ln\left[\frac{E^{-B}e^{-E_i/\theta}}{Z}\right] \tag{3.22}$$

which can be expanded as

$$S = -\sum_{i=1}^{n} \frac{E^{-B}e^{-E_i/\theta}}{Z}[\ln(E_i^{-B}) + \ln(e^{-E_i/\theta}) - \ln Z] \tag{3.23}$$

which gives

$$S = -\sum_{i=1}^{n} \frac{[\ln(E_i^{-B})]E_i^{-B}e^{-E_i/\theta}}{Z} + \sum_{i=1}^{n} \frac{[E_i/\theta]E_i^{-B}e^{-E_i/\theta}}{Z} + \sum_{i=1}^{n} \frac{[\ln Z]E_i^{-B}e^{-E_i/\theta}}{Z} \tag{3.24}$$

From 3.19, 3.20, 3.24 reduces to

$$\boxed{S = \ln Z + B_S\langle \ln E\rangle + \tfrac{\langle E\rangle}{\theta}} \tag{3.25}$$

I call this *gamma entropy* (or S_γ for short) since it is derived assuming a gamma distribution. To avoid confusion, B is replaced with B_S since it is an inferred scaling exponent and is not calculated directly by measuring the slope of the linear part of the energy-frequency distribution (B). For the critical regime $\theta \to \infty$, the last term in 3.25 vanishes. So for a **critical regime**, equation 3.25 can be expressed as

$$\boxed{S = S_O + B_S\langle \ln E\rangle} \tag{3.26}$$

where S_O is a constant equal to $\ln Z$. Now we calculate the entropy for linear increments dE. We use 3.14 to get

$$p_i = \frac{E_i^{-B-1}e^{-E_i/\theta}}{Z}. \tag{3.27}$$

Solving as we did to derive equation 3.25 we find for linear bins that when $\theta \to \infty$ we have

$$\boxed{S = S_O + (B_S + 1)\langle \ln E\rangle} \tag{3.28}$$

Note that the case for the logarithmic bins (equation 3.25) is exactly the same as the case for linear bins (equation 3.28) except that respectively, B_S is replaced with $B_S + 1$. In summary, as $\theta \to \infty$, we have for logarithmic increments

$$\partial S/\partial\langle \ln E\rangle = B_S \tag{3.29}$$

and for linear increments

$$\partial S/\partial\langle \ln E\rangle = B_S + 1 \tag{3.30}$$

On a plot of S vs. $\langle \ln E\rangle$, we can therefore predict a straight line with slope $\sim B$ and intercept S_O for data analysed using logarithmic bins. Conversely, because equation 3.26 is true for the critical or very near critical regime ($\theta \rightarrow \infty$), any deviation from it is indicative of a sub-critical or super-critical regime.

3.6.1 Characteristics and factors

- **Information content**: Let us now consider equation 3.26 more closely. Equation 3.26 is a linear equation close to the critical regime that depends on the expectation of the logarithm of the energy $\langle \ln E\rangle$. B_S on the other hand is a constant that will be proportional to the mean B value of a given data population. This suggests that the entropy measured (which is a single number) will contain information on the level of organisation in a system as a function of the average B, θ and $\langle \ln E\rangle$ with the advantage of only having to essentially measure p_i. This 'boiling down' of variables to the probability distribution of energetic microstates, as well as being standard practice in Boltzmann's thermodynamics (chapter 2), is a useful tool with which to compare the level of self-organisation between different seismic regions (as will be done in chapter 5).

- **Energy expectations**: There will be at best a weak correlation between $\langle E\rangle$ and $\langle \ln E\rangle$ in equation 3.25. This may seem to be counter intuitive but can be qualitatively explained thus: $\langle E\rangle$ will vary over several orders of magnitude due to its power-law nature. This also means that $\langle E\rangle$ will be strongly and almost solely influenced by the size of the largest energy fluctuations and accordingly θ. However, $\langle \ln E\rangle$ to a certain extent diminishes the effect of the largest events by taking their logarithms so $\langle \ln E\rangle$ will be predominantly affected by the smaller (more numerous) energies in a population. So, unless there is a correlation between the large and small fluctuations, the assumption that $\langle E\rangle$ and $\langle \ln E\rangle$ are not correlated remains true. Mathematically $\partial\langle \ln E\rangle/\partial\langle E\rangle \sim 0$. The prior assumption of a lack of correlation has been verified *a posteriori* for real earthquake data in Chapter 5 of this thesis and by Main and Al-Kindy (2002).

- ***Spread* and *Shape***: Entropy in general will depend on two factors for a given population's probability distribution: these are *shape* and *spread*. The effects of these two factors are depicted in figure 3.8. For the first factor, '*shape*', the entropy calculated will depend on how peaked the probability distribution is for a given energy range. A very peaked distribution means that we are more certain of the outcome of a particular energy level (lower entropy) whereas a flat distribution will mean more uncertainty (higher entropy). As can be seen from figures 3.8 a and b, for a gamma distribution, S will be related to θ (figure 3.8a) and B (figure 3.8b). θ will influence both the spread and the shape of a gamma distribution; in figure 3.8a, the peakness was increased by having a negative θ and hence a lower entropy relative to the distribution with a positive θ.

  A higher B value in effect will also increase the peakness of a distribution (figure 3.8b). This is in slight contrast to the entropy of an equilibrium system such as say a gas which is always a Boltzmann distribution whose 'peakness' is dependent on the number of gas molecules within the system (Mandl, 1988). The second factor is the band-width of the data or the *spread* which in the case of earthquakes is effectively $E_{max} - E_{min}$ (figure 3.8c). This makes sense since the broader the energy distribution, the more energy levels there are to choose from and hence there is a larger degree of freedom (entropy) in the system. A more quantitative approach to the way S is influenced by B, θ etc. is given in section 3.7.

3.7 Analytical predictions

3.7.1 Entropy phase-diagrams and the three regimes

In order to illustrate predictions of the analytical theory outlined above, I create synthetic phase-space plots to show the change of entropy with $\langle E \rangle$, $\langle \ln E \rangle$ and B in the sub-critical ($\theta > 0$), critical ($\theta \to \infty$), and super-critical ($\theta < 0$) regimes. The plots are constructed as follows:

The energies are created using standard energy-magnitude relations (Kanamori and Anderson,

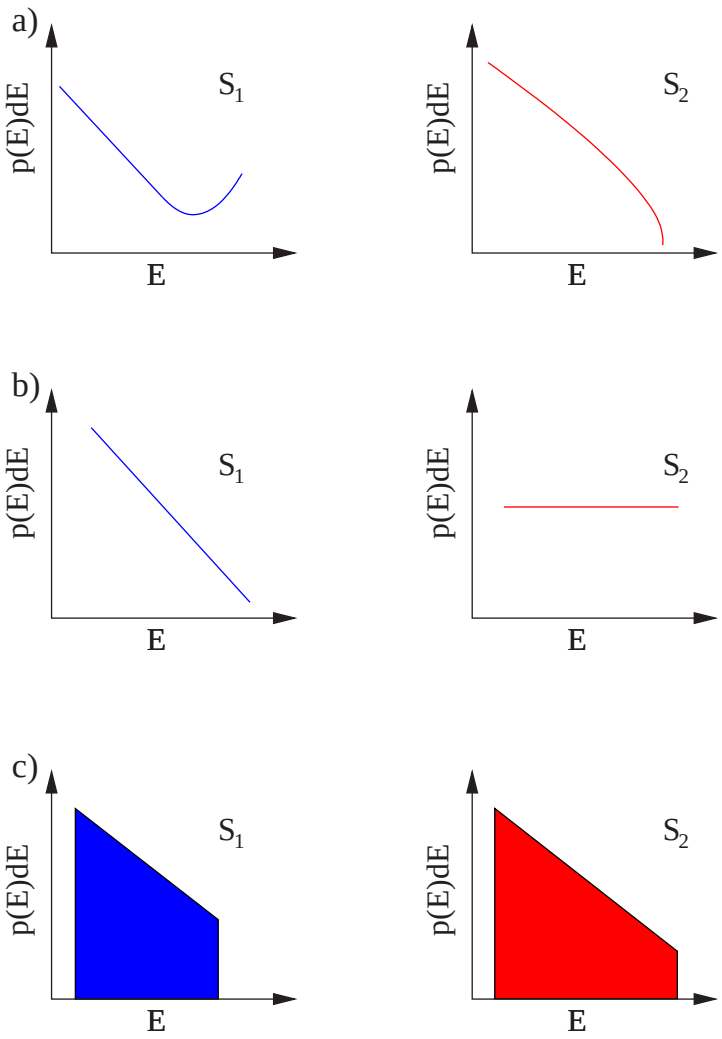

Figure 3.8: Effect of *spread* and *shape* on entropy S: a) Lower θ increases 'peakness', b) higher B increases 'peakness' and c) higher E_{max} increased spread. For all cases, $S_1 < S_2$.

1975) for energies in Joules

$$E = 10^{1.5m+4.8} \tag{3.31}$$

$$\theta = 10^{1.5m_\theta+4.8} \tag{3.32}$$

by varying the values of the magnitude m corresponding to the range $5.8 < m < 8.5$ for a given bin width δm. These values of m are chosen because they correspond to the values of m for real data that will be analysed in chapter 5. It is only within this range that the Harvard Centroid Moment Tensor (CMT) catalogue is considered to be complete over its history (Kagan, 1997). I then calculate values of θ for values of $7 < m < \infty$ both in the positive (sub-critical) and negative (super-critical) sense which will include the critical regime for both when θ is large. The range $7 < m < \infty$ is chosen to constitute to what tend to be the *largest* events. The values obtained from 3.31 and 3.32 are substituted into 3.17 to calculate $p(E)$ for different values of B (from -1 to 1) and θ. From the different values of $p(E)$, the corresponding values of $\langle E \rangle$ and $\langle \ln E \rangle$ can be calculated directly using

$$\langle E \rangle = \sum_{E_{min}}^{E_{max}} p_i E_i \tag{3.33}$$

$$\langle \ln E \rangle = \sum_{E_{min}}^{E_{max}} p_i \ln E_i \tag{3.34}$$

The corresponding values of S are calculated using

$$S = -\sum_{E_{min}}^{E_{max}} p_i \ln p_i \tag{3.35}$$

The phase diagrams for the variation of S as a function of B and $\langle E \rangle$ and $\langle \ln E \rangle$ for the three criticality regimes can be seen in figures 3.9 and 3.10 respectively. The solid line corresponds to $\theta \to \infty$. B for real earthquake seismicity can be observed in the range $0.5 < B < 1$ (e.g. Ogata et al., 1991; Kagan, 1997) so the negative values calculated here are unrealistic but are included to give an overall view.

Both phase diagrams show that the global maximum possible entropy occurs at the regions close to $B \sim 0$ which is to be expected since that is where the probability distributions are

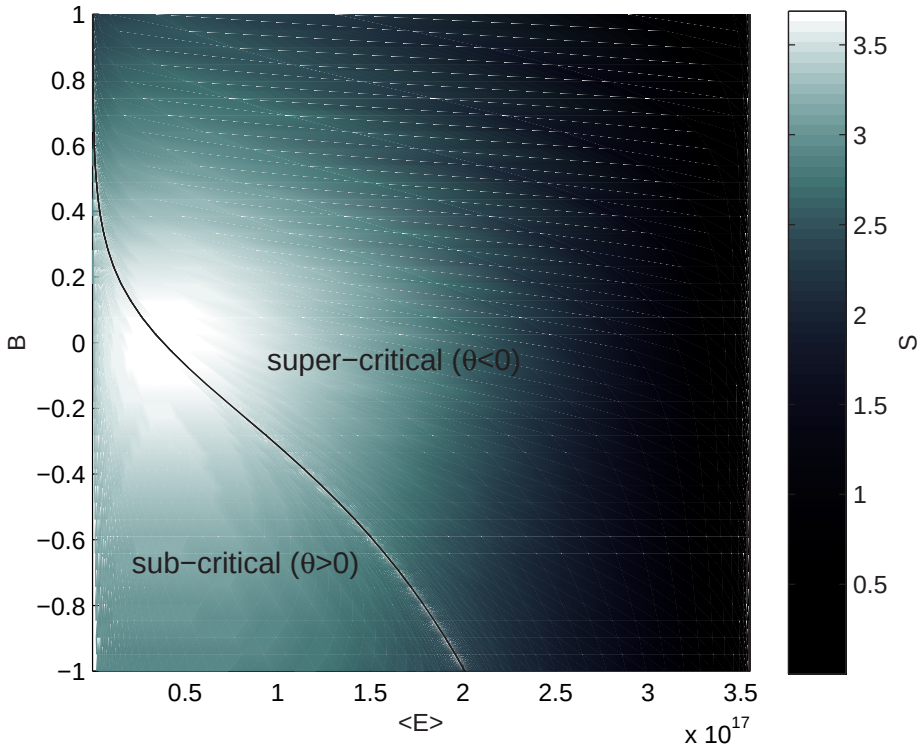

Figure 3.9: B - $\langle E \rangle$ phase diagram for the three criticality regimes. The solid curve corresponds to the critical regime ($\theta \to \infty$) and the brightness is proportional to the entropy S.

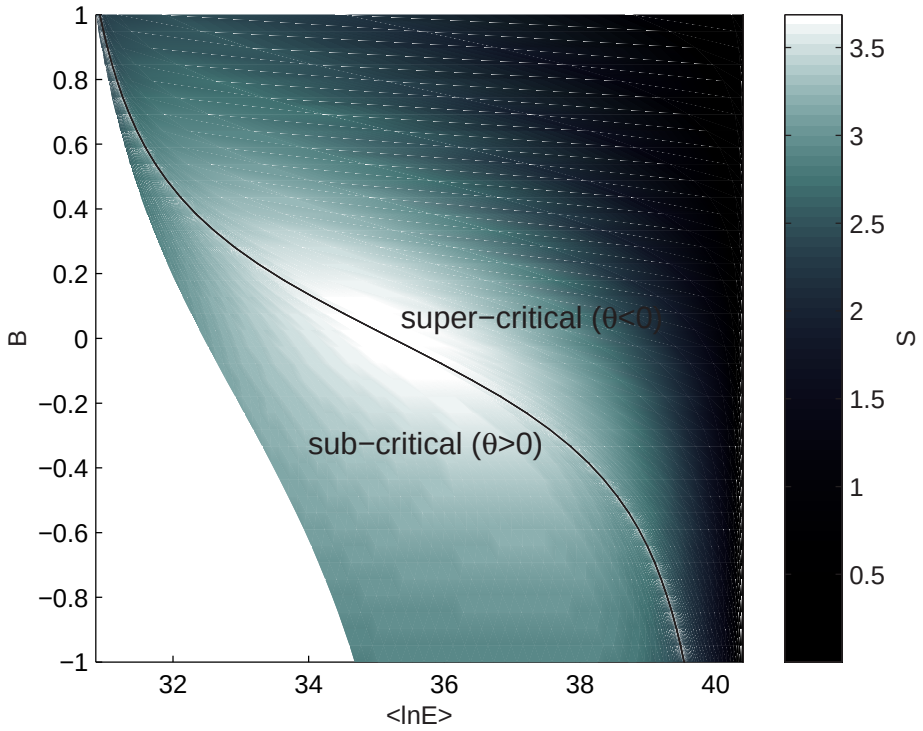

Figure 3.10: B and $\langle \ln E \rangle$ phase diagram for the three criticality regimes. The solid curve corresponds to the critical regime ($\theta \to \infty$) and the brightness is proportional to the entropy S.

flattest (least certainty). This is highlighted in figure 3.11 where searching the phase space for the maximum entropy for a given B value occurs at $B = 0$ for both $\theta > 0$ and $\theta < 0$. The figure also confirms the effect of B on the level of organisation in a system; the higher the B value (negative or positive), the greater the level of organisation.

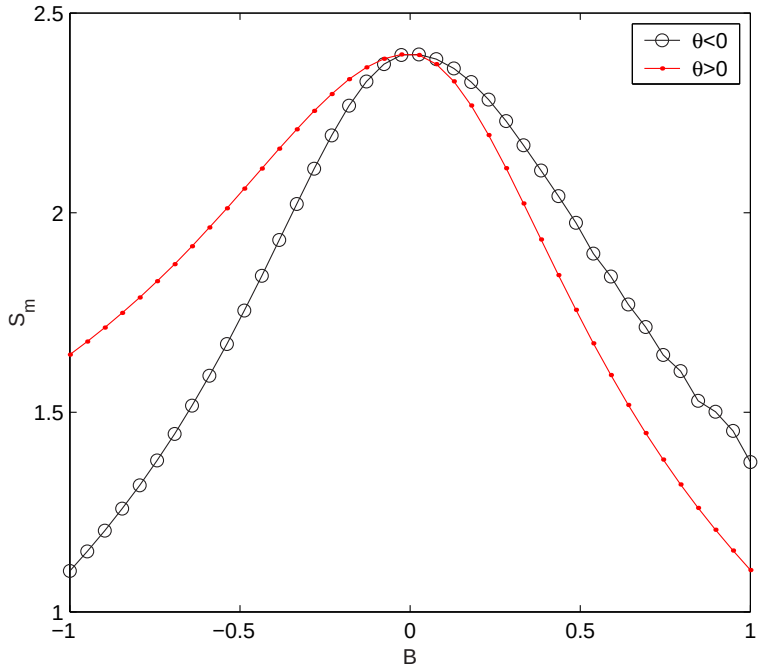

Figure 3.11: Maximum entropy S_m for a given value of B for both sub-critical ($\theta > 0$) and super-critical ($\theta < 0$) regimes. Note that in both cases, the maximum entropy occurs at $B = 0$.

3.7.2 Criticality and phase transitions

It is common to refer to where the transition between a sub-critical and super-critical regime as the critical *point*. However, it can be seen from figures 3.9 and 3.10 that the critical point is in fact a critical *line* that is a function of B *and* θ in a two-dimensional phase space. One can therefore conclude from the phase-space plots that for a given gamma type population, any momentary change in B must be accompanied by a change in $\langle \ln E \rangle$ for the system to remain critical. A change in one and not the other will be indicative of a departure from the criticality, similar to a phase transition. This is analogous to a fluid pressure-temperature diagram ($P-T$) (figure 3.12) or a pressure-volume (P-V) phase diagram where a phase transition can occur at

a given temperature and pressure (or volume) along a defined curve (Mandl, 1988; Kondepudi and Prigogine, 1998).

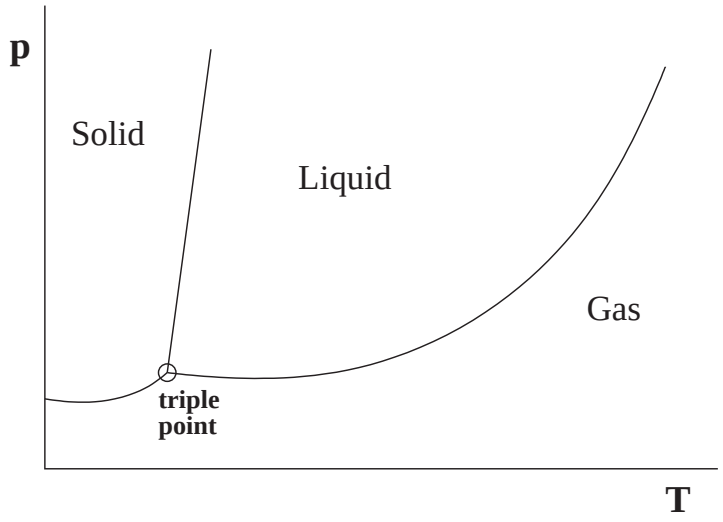

Figure 3.12: Pressure-temperature (P-T) phase-diagram for a fluid with a 'critical' line between the different phases. Redrawn from *Kondepudi and Prigogine* (1998), pg. 176.

It must be emphasised that the changes in B and $\langle \ln E \rangle$ mentioned here must be in the short term or must refer to two separate non interacting systems. Any long-term trends would suggest that the system is not in a stationary steady-state and would therefore be difficult to define.

To further compare the phase-space of a gamma system with that of an equilibrium system, I construct horizontal cross-sections of figure 3.9 and 3.10 for $B = -2/3$, $B = 0$ (non-degenerate system) and $B = 2/3$ (earthquakes) in figure 3.13.

We have seen in section 2.5.2 in chapter 2 that for a non-degenerate equilibrium system, the critical point occurs where the entropy is a maximum. This is borne out by figure 3.13b. However, It can be seen from figure 3.13 that the critical points for $B = 2/3$ ($B = -2/3$) occur below (above) the maxima as indicated by the arrow for both $\langle E \rangle$ and $\langle \ln E \rangle$. Therefore, for power-law systems that are observed in nature ($B > 0$), the equivalent of a phase transition between a sub-critical and a super-critical regime will occur for lower values of mean energy as highlighted by figure 3.13.

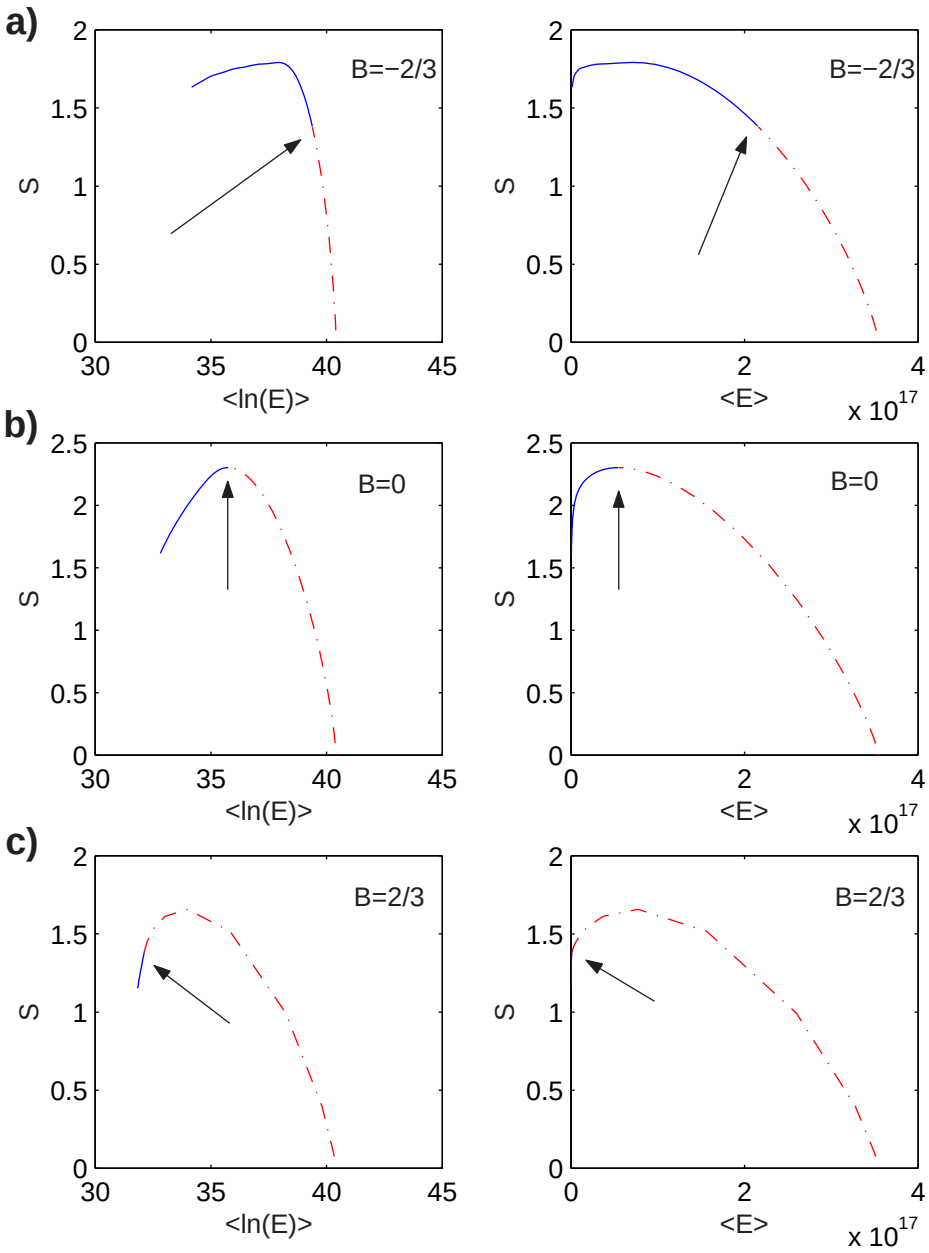

Figure 3.13: Cross-sections of S vs $\langle E \rangle$ and $\langle \ln E \rangle$ phase spaces for (a)$B = -2/3$ (b)$B = 0$ and (c)$B = 2/3$. The solid line indicates the sub-critical regime and the dotted line indicates the super-critical regime with the arrows indicating the critical regime.

3.7.3 Effect of bin width

The nature of equation 3.35 is that the absolute entropy will depend on the bin width of our discrete elements when calculating $p(E_i)$ for each energy level. This is because for a given range of energies, the more discretised our sample, the more the apparent degrees of freedom. I show this effect for synthetic data in figure 3.14 by calculating S for different values of bin width δm for $B = 2/3$ and $B = 0$. I assume $\theta \to \infty$ to restrict our focus on the effect of δm. It can be seen from this figure that the narrower the bin width, the higher the entropy (uncertainty) as one would expect for a larger number of energy elements. Goltz and Böse (2002) acknowledge this problem by normalising the spatial entropy for different grid sizes (essentially different bin widths) for a population of earthquake data. This was useful for comparing the spatial entropy of the data at different resolutions. I follow a similar procedure and normalise the data by dividing the entropies at different bin widths by the maximum entropy for the same bin width (S_m) as shown in figure 3.14. It can be seen in figure 3.14 that although the effect of bin width is reduced, it is not eliminated for the $B = 2/3$ case. The effect is as expected, eliminated for the $B = 0$ case since the maximum possible entropy for a power-law distribution (for a given energy range) is for the flat case ($B = 0$).

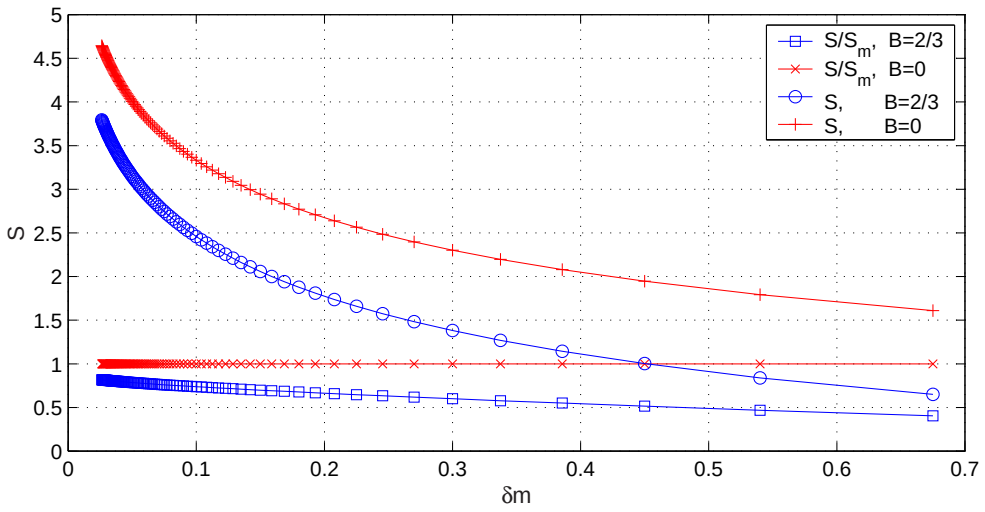

Figure 3.14: Plot of calculated S as a function of bin width δm for $B = 2/3$ and $B = 0$. The upper two curves correspond to non-normalised synthetic data and the lower two curves to data normalised by dividing the maximum entropy for a given bin width S_m.

To solve this problem, I will fix the bin width to a chosen value throughout my analysis of

earthquake data in chapter 5 ($\delta m = 0.25$). By fixing the value of the bin width, any differences or changes in entropy calculated will only be influenced by the overall origination of an earthquake population (spread and shape) making comparison of data ensembles quantitative. From a pragmatic point of view, the bin width of $\delta m = 0.25$ is chosen similar to the uncertainties in the magnitude determination for earthquake data available. There would not be enough data points in each bin if the bins were too narrow. Larger bins on the other hand would constitute too few values of $p(E_i)$ which would destabilise the calculation of S. The effect of bin width will also be discussed in chapter 5.

3.8 Thermodynamics?

I have mentioned in section 2.5.1 that the free energy of a system F is a measure of how much energy the system has available to do work (equation 2.8). Free energy can therefore be an important factor when examining the Earth's crust since logically, the more free energy there is, the more energy available to 'do work' in the form of earthquakes. However, can we derive an analytical expression for the free seismic energy stored in the crust? This is a difficult question to answer for the following reasons:

- It is physically impossible to measure all the energy stored and transported in the crust be it in the form of strain, heat etc. Therefore, we can only assume some arbitrary values based on what we observe at the surface.
- Not all the energy released by the Earth's crust is seismic since some will be aseismic in the form of heat, deformation, radioactive decay and so on.
- Although we know that the energy released by earthquakes is in the form of a modified gamma distribution, we do not know independently the form of the distribution of the stored free energy.

Fortunately we can make some reasonable assumptions based on what we do know. Firstly, it has been shown for cellular automata models of seismicity that on average, the radiated seismic energy will be proportional to the internal energy of the system (e.g. Main et al., 2000). This

is also true in general for open driven SOC systems (Dewar, 2003). Although the concept that 'the more energy coming out of a system, the more energy there is in the system' may seem counter intuitive, this is the norm for driven threshold systems provided they remain driven. An analogy is that of a house heating radiator system. While the radiator is switched on, it will acquire a temperature that will eventually warm the room and the room-radiator system as a whole will reach a steady state. The more heat being emitted from the radiator, the higher the temperature of the room. Note how this is different from the ice in a glass example (chapter 1) where the water decreases in temperature and the ice increases in temperature until the entire system reaches an equilibrium state. Dewar (2003) also derives a mean-field expression for a SOC sand pile model with the assumption that the average amount of sand entering a pile must equal the amount of sand leaving it in the form of avalanches. Therefore, we could perhaps say that in the crust, areas of higher seismicity (bigger events) will have greater free energy F *on average* and accordingly greater potential for further large events. This is a different way of looking at the idea that what has happened in the past (events) in more likely to recur in the future.

3.9 Remarks and conclusions

- In this chapter, I examine the modified gamma distribution in the three criticality regimes. I show how the three regimes differ from critical regimes of equilibrium systems and those of time-series analysis. Although the gamma distribution is currently the most reliable in explaining a variety of systems, it does not in its simple form fit the characteristic earthquake hypothesis although the hypothesis is yet to be verified. I also show how super-criticality can be an artefact of historic data rather than some inherent physical process.

- Following from this, the derivation of the discrete version of entropy for a modified gamma distribution close to and at the critical regime is given. I call this *gamma entropy* or S_γ. The theoretical result shows that the level of organisation for a gamma type system is related to the expectation of the logarithm of the energy $\langle \ln E \rangle$ and the scaling exponent B. Any deviation from this equation is indicative of a sub-critical or super-

critical regime.

- I then construct a series of phase diagrams as a function of B and $\langle \ln E \rangle$ (θ) and show that the criticality can be maintained provided that both B and $\langle \ln E \rangle$ are changing. A deviation from this is also indicative of a departure from the critical regime. This result predicts that if the crust were close to criticality -at least on a regional level-, we would observe a higher B value in areas of a lower mean seismicity relative to areas of higher seismic activity.

- In addition, the phase diagrams show that the global maximum entropy occurs for a flat distribution ($B = 0$). Also, for power-law systems the critical point occurs below (above) the expected critical point for $B > 0$ ($B < 0$). This predicts that criticality can be reached at the expense of less mean energy for power-law systems with $B > 0$ which is always the case for earthquakes and most natural systems.

Chapter 4

Self-organisation in numerical models of seismicity

4.1 Introduction

In the previous chapter, it has been shown analytically how the entropy and hence degree of self-organisation in a system will be related to the scaling exponent B and the mean energy of the system. Phase diagrams were also used to demonstrate the relations between the various thermodynamic variables and the scaling exponent B around criticality. In this chapter I examine self-organisation and its relation with dissipation using numerical, or more specifically, cellular automata models of seismicity. The investigations and results of this chapter are divided in to two parts.

- **Part I**: Here I treat a cellular automaton model of seismicity as a self-organising dissipative structure. I measure internal and external thermodynamic variables such as energy and entropy and investigate their dependence on dissipation. This is in the hope of extrapolating the results to a real system such as the Earth's crust.
- **Part II**: I then probe SOC; given that *'the lack of a general understanding [of SOC] prevents the construction of a unifying framework'* (Sornette, 2000, p.g. 323), I examine some aspects of the original Bak, Tang and Wiesenfeld (Bak et al., 1987) model of SOC to pin down some of its characteristics in relation to our assessment

of earthquakes as an SOC system. In particular, I look at spatial and some temporal characteristics of the original BTW model.

Some of the main results presented in this chapter have been written as a paper to be submitted.

4.2 Cellular automata (CA)

Cellular Automata are numerical (computer) models commonly used to simulate physical systems. The models usually consist of an array composed of a large number simple microscopic 'elements', 'sites' or 'cells' that interact in accordance with a pre-specified set of rules or algorithms. Despite the very basic rules that govern the way in which the individual cells interact, CA models are capable of producing complex patterns and dynamics similar to physical, biological and turbulent systems found in nature. Examples of such systems include geomagnetic activity (Chapman and Watkins, 2001) and earthquakes (e.g. Anglo-Brown and Munõz-Diosdado, 1999; Kumagai et al., 1999) . These models give impetus for conjecturing simple explanations to very complex phenomena observed, natural or otherwise. Cellular automata models are also extensively used in engineering problems. For example, figure 4.1 shows an example of the fluid flow over a cylinder (from Wolfram, 1986). The exact solution of simultaneous flow equations for such a system would be computationally prohibitive but can be simply calculated on a cell-to-cell basis using a CA model.

4.3 Why use models of seismicity?

There are many reasons to use numerical models of seismicity and are summarised as follows:

– Simple cellular automata models of seismicity can reproduce the power-law statistics observed in real earthquake populations such as the Gutenberg-Richter relation (e.g. Kumagai et al., 1999) and foreshock and aftershock activity (Jaumé et al., 2000).

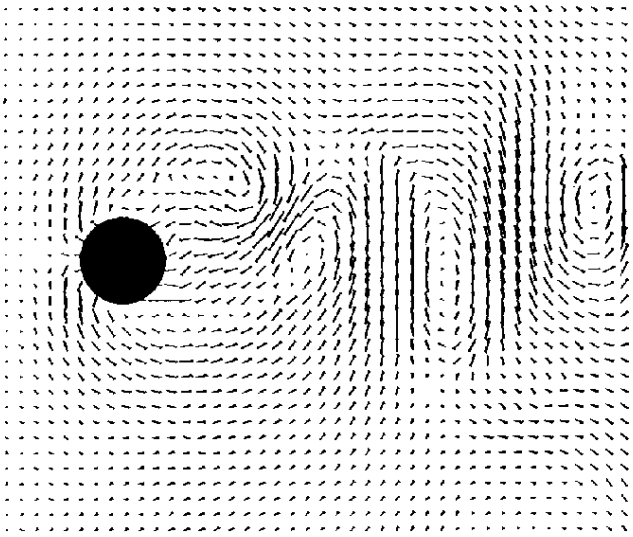

Figure 4.1: Fluid flow and resulting vortex around a cylinder in cellular-automata model (from Wolfram, 1986).

– In the crust, we can only measure the radiated seismic energy and its corresponding probability density distribution. Any knowledge of the internal strain energy (or indeed any other internal parameters) are difficult to measure and can only be inferred or guessed through the use of models (Main et al., 2000; Viti et al., 2001). However, in numerical models, we can measure both the internal and external properties of the system (e.g. Lu et al., 1998) and test the hypothesis that they are related.

– Complete and reliable earthquake data catalogues only span tens of years or so. For example, the Harvard Centroid Moment Tensor (CMT) catalogue -which is the most reliable- only spans the last 30 years. However, with numerical models of seismicity, the length of the catalogue simply depends on the length of the model run. We can therefore produce data that would require hundreds to thousands of years to accumulate naturally. Statistically, we will have data that is both stable and reliable when compared to natural data.

– Unlike real data, the synthetically-produced data will be free of any noise, or bias in instrumental saturation or data selection. The synthetic data will therefore be complete over all ‘magnitudes’ in comparison to earthquake data that is usually only recorded for events bigger than a particular size. Usually this is above magnitudes 4.5 or as high as 5.5 depending on the catalogue. Many catalogues can also satu-

rate for very large earthquake magnitudes (Kanamori and Anderson, 1975; Reiter, 1991).

However, there are some drawbacks in the use of cellular automata models of seismicity. For example, CA models are 'coarse grained' as they are composed of discrete elements or cells whereas most natural systems such as the crust are best described as continuous (non-discretised). Also, CA models are predominantly two-dimensional whereas fault interactions in the crust at the very least occur in three dimensions. The models also oversimplify or exclude known laws of elastodynamics that govern fault interaction in the crust (e.g. Rice, 1993). Nonetheless, CA models remain a useful and powerful primary tool in reproducing and investigating earthquakes statistics and have been used in assessing their hazard (e.g. Malamud and Turcotte, 1999). The philosophy is therefore to make the simplest model possible that can explain or predict general observations.

4.4 Aspects of seismicity models

4.4.1 Driving conditions

Specifically for models of seismicity, there appear to be two main modes of 'driving' CA models (analogous to tectonic loading in the Earth). Driving here refers to the addition of energy or 'strain' or a force to the model. This driving force can be global or local.

Global: A global or 'homogenous' or 'uniform' driving force as the name may suggest is when all elements or cells within the model are updated simultaneously. In the case of earthquakes models, this is when *'the stress at all points on the fault increases by the same amount'* (Lomnitz-Adler, 1993). Examples include the Olami Feder and Christensen (OFC) model described below (Olami et al., 1992), and those of Jánosi and Kertész (1993) and Main et. al (2000). Although a global driving force is often used in the literature, it can introduce problems. For example, it was found that for a low conservation parameter, a global driving force can introduce 'phase locking' between neighbouring elements in a system with open boundary conditions (defined below) (Jánosi and Kertész, 1993; Middelton and Tang, 1995). This is because we are in effect introducing a spatial correlation to the system causing it

to produce a periodic or sinusoidal signature in its energy fluctuations that would not occur under local driving (defined below) conditions (e.g. Bak and Tang, 1989). A global driving force can also cause more than one site to be activated simultaneously (the formation of more than one cluster at a time). This can add considerably to computation times in the model. This problem has been solved by using a very slow driving force and the addition of noise (e.g. Mousseau, 1996). This however required the addition of another parameter and could be considered to be a form of tuning of the model.

Local: A local or 'random' driving force is when only a single cell is randomly selected and updated at every time step (Lomnitz-Adler, 1993). This insures that we do not trigger more than one 'earthquake' at a time and is what is used in the original BTW model (Bak et al. 1987) described below. Because sites are selected at random in space, the driving can be considered on average to be 'global' in the long run. The modelling in this chapter will only use a local 'random' driving.

Note that I specifically use the terms 'local' and 'global' driving to mean 'random' and 'uniform' not in accordance to what is commonly used in the literature. This is because one could, in theory, have a uniform driving force that is random (simultaneously updating all cells with a random value) as well as have a local driving force that is uniform (updating the same single cell over and over again). However, I do not consider these possibilities here.

4.4.2 Boundary conditions

The boundary conditions for CA models are the rules that govern what happens at the edges of our model array or grid. They are also believed to play a critical role in the observation of critical behaviour of some models (Lise and Paczuski, 2001). For the purpose of this thesis, they can be divided into two types: Open[1] and periodic. Figure 4.2 shows the difference between the two. For open boundary conditions, any activated

[1]The terms 'closed', 'free' and 'fixed' boundary conditions are also used in the literature. These usually refer to specific 'spring-block' models where there are special rules that govern how the edge springs interact with the 'outside' (see article by Lise and Stella, 1998). Here I only give generalised definitions that are sufficient for the models to be used in this thesis.

cell at the edge or 'halo' will lose energy out of the system (figure 4.2a). The edges can be thought of as infinitely absorbent to energy. However, with periodic boundary conditions, any energy lost at the edge will be immediately reintroduced from the other side so energy is conserved. Periodic boundary conditions are used to reduce the edge effects within a finite size system (e.g. Grassberger, 1994). The boundary conditions will therefore play a role in the way a system dissipates energy. Periodic boundary conditions can also be responsible for a system reaching a periodic state 'with only earthquakes of one size' occurring for smaller conservation (Lise and Paczuski, 2001). Open boundary

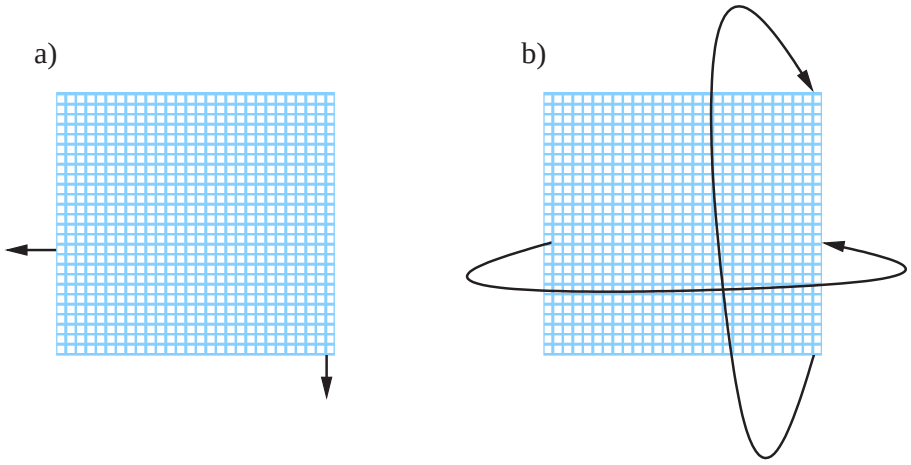

Figure 4.2: Models with a) open boundary conditions and b) periodic boundary conditions. Energy is dissipated at the edges under open boundary conditions whereby it is conserved by being reintroduced into the system with periodic boundary conditions.

conditions are commonly used in the literature and are *'more relevant for real earthquakes than simulations with periodic boundary conditions'* (Grassberger, 1994). I shall therefore only use models with open boundary conditions in this thesis.

4.4.3 Energy conservation

There are two ways in which models of seismicity can lose energy. First is at the boundaries as mentioned above and secondly through internal interactions. If a site or cell breaks in a model and passes all its energy to its neighbouring sites, it is said to be *conservative*. Alternatively, if only a fraction of the energy is passed on, the system is said

to be *dissipative*. The most common dissipative model of seismicity is that of Olami et al. (1992) described below (section 4.5.3). The amount of energy lost per break is usually controlled by the *conservation* (or *dissipation*) factor commonly denoted by α in the literature (e.g. Olami et al., 1992; Ceva, 1995; de Carvalho and Prado, 2000).

4.5 Models of seismicity

There are numerous models of seismicity to be found in the literature. For example, Lomnitz-Adler (1993) creates 40 CA models of seismicity using different combinations of conservation, driving force, boundary conditions etc. to examine under what conditions the Gutenberg-Richter law is reproduced. Here I summarise what I feel are the three fundamental models from which most other models in the literature are derived. They are in chronological order the Burridge and Knopoff model (Burridge and Knopoff, 1967), The Bak, Tang and Wiesenfeld SOC model (Bak et al., 1987), and the Olami Christensen and Feder non-conservative model (Olami et al., 1992; Christensen and Olami, 1992). The three models are summarised as follows using the original publication notation[2] where appropriate:

4.5.1 The Burridge and Knopoff (BK) model

The Burridge and Knopoff (1967) model (BK) is not a CA model and is mentioned here for its historical role in numerical seismicity. Burridge and Knopoff (1967) conducted both laboratory and numerical spring block model experiments to reproduce some of the statistics observed for earthquakes such as aftershocks and the Gutenberg-Richter law. Their model is somewhat more complicated than a simple CA model whereby they use exact dynamic equations of motion and friction for a one-dimensional driven chain of blocks connected by springs. An IBM computer was used to solve non-linear differential equations governing ten connected driven blocks. The computations included measuring the internal energy between connecting springs and radiated energy due to blocks slipping. Details of the model are beyond the scope of this chapter and are only

[2]The notations quoted in these examples should be considered independent from ‘standard’ notation used throughout this thesis since they are given in this section ‘as is’ from the original publications.

partially reproduced for the CA version of the model mentioned below (the OFC model). Nonetheless, the BK model is seen as a starting point for the use of numerical models of seismicity and was the inspiration behind models that followed. To my best of knowledge, it was the first model of any type to demonstrate the origin of the Gutenberg-Richter law and aftershocks in terms of the non-linear dynamics of a many-body complex system.

4.5.2 The Bak, Tang and Wiesenfeld (BTW) model

The term 'Self-Organized Criticality' was first coined by Bak et al (1987). In their seminal paper, they demonstrated through the use of a 'sand pile' numerical model (the BTW model here on) how a system with 'extended degrees of spatial freedom' can naturally evolve to a critical state with power-law statistics. This model was then proposed as 'a general mechanism leading to the power law distribution of earthquakes' (Bak and Tang, 1989). The BTW model was considered by Bak and Tang (1989) to have the essence of the Burridge and Knopoff 'spring block' model (Burridge and Knopoff, 1967) but greatly simplified in its dynamics. Their model is described as follows in accordance with Bak et al.(1987) and Bak and Tang (1989):

– The model consists of two-dimensional array of $i \times j$ particles or cells on a square grid. The starting conditions are such that the force at each cell in the grid is $Z_{i,j} = 0$. Then for every time step t, a cell is selected at random and a driving force is applied to it according to the rule:

$$Z(i,j) \rightarrow Z(i,j) + 1 \tag{4.1}$$

– Step 4.1 is repeated until the force on a cell at position (i,j) reaches a breaking point Z_C where in their model $Z_C = 4$. For $Z(i,j) > Z_C$, the cell releases its 'strain' to its 4 closest neighbours according to the rule:

$$Z(i,j) \rightarrow Z(i,j) - 4$$

$$Z(i \pm 1, j \pm 1) \rightarrow Z(i \pm 1, j \pm 1) + 1 \tag{4.2}$$

If by a domino type effect the neighbouring cells acquire a force $Z(i,j) > Z_C$ due to the redistribution of strain, the process is repeated until all cells have strain $Z \leq Z_C$ and we return to process 4.1. Note that for the BTW model, Z is always an integer.

– The total number of cells broken for every cycle of process 4.1 defines a cluster size or total energy released during an earthquake[3](Bak and Tang, 1989). Any cells at the boundary that break will lose their energy out of the system (open boundary conditions). This form of dissipation at the edges is essential since because the BTW model is internally conservative (no energy is lost from a broken cell except to its neighbouring cells), having periodic boundary conditions would results in an infinite cluster or 'avalanche' (repetition of rule 4.2 indefinitely). A steady state is eventually reached and there is a balance between the system input and output.

– Note that there are therefore two times in the system. The 'external' time between events and the 'internal' relaxation time within a given event -i.e., the duration of an avalanche. The system after some transient time is found to reach a steady state and the energy released follows a power-law where

$$p(E) \approx E^{-\tau} \tag{4.3}$$

where $p(E)$ is the probability of having a cluster of energy E and τ is a scaling exponent with $\tau \approx 1$ for a two-dimensional model similar to what is seen for real earthquakes (section 2.8.3). The model as well as showing a power-law for the size distribution of the clusters, also shows a power-law in the internal time for the durations of the individual events following

$$p(t) \approx t^{-a} \tag{4.4}$$

where $p(t)$ is the probability of having an event of duration t and $a \approx 0.42$ for a two-dimensional model.

Despite its simplicity, the BTW model was and is seen as poignant in the 'self-organization' literature. However, it was by no means revolutionary. Wolfram (1983) had pioneered

[3]For real earthquakes, the moment energy release E is found to be related to the fault rupture area A whereby $E \sim A^{3/2}$ (Kanamori and Anderson, 1975). Also see chapter 2, sections 2.8.1 and 2.8.3

the use of cellular automata models and had produced simple algorithms that show both 'self-organization' and power-law statistics. Kantz (1986) also produced a simple model of 'propagating brittle failure in heterogeneous media' that showed power-law statistics from very basic rules. The infamy and success of the BTW CA model may be attributed to its simplicity both in form and reproducibility. Also, the authors put efforts in proposing SOC as a simple solution to a variety of complex problems including earthquakes to a wide scientific community. In addition, they to a degree highlight SOC's association with the bigger field of 'critical point' systems (section 2.7.2). But perhaps more importantly, Bak et al. (1987) gave their observation a catchy and apt name, 'Self-Organized Criticality'.

4.5.3 The Olami, Feder and Christensen (OFC) model

The BTW model is strictly internally conservative since energy is only lost at the boundaries. An investigation into whether criticality can still be achieved if internal dissipation is introduced was carried out by Olami et al (1992). The model, referred to here as the OFC model, also has its roots in the Burridge and Knopoff (BK) model (Leung et al., 1997; Jensen, 1998) and is described as follows:

Just as with the BTW model, the OFC model is defined by a square $L \times L$ array with i and j the integer coordinates of elements within the array where i and j take values between 1 and L. In accordance with the BK model, the OFC model as shown in figure 4.3 can be thought of as blocks interconnected by springs to their four nearest neighbours. The individual blocks are also connected via springs to a driving plate above them and frictionally to a fixed plate below them. As one plate moves relative to each other, the blocks will experience a force. For a block at position (i, j) that experiences a displacement $dx_{i,j}$, the force $F_{i,j}$ will be:

$$\begin{aligned} F_{i,j} &= K_1[2dx_{i,j} - dx_{i-1,j} - dx_{i+1,j}] \\ +K_2[2dx_{i,j} - dx_{i,j-1} - dx_{i,j+1}] &+ K_L dx_{i,j} \end{aligned} \tag{4.5}$$

where K_1,K_2 and K_L are elastic constants (figure 4.3). As the plates slide with relative velocity V, the force will increase uniformly in the array by an amount $K_L V$ until a site

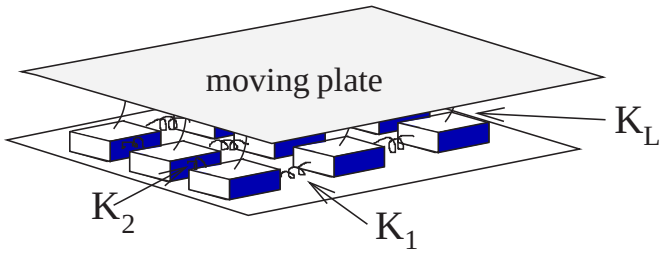

Figure 4.3: The physical representation of the OFC model with elastic constants K_1, K_2 and K_L (redrawn from Olami et al., 1992).

reaches a threshed value. This will trigger an earthquake and the strain will relax to it four nearest neighbours in a fashion similar to the BTW model as follows:

$$\begin{aligned} F_{i\pm1,j} &\rightarrow F_{i\pm1,j} + \delta F_{i\pm1,j}, \\ F_{i,j\pm1} &\rightarrow F_{i,j\pm1} + \delta F_{i,j\pm1}, \\ F_{i,j} &\rightarrow 0 \end{aligned} \tag{4.6}$$

where the increase in force of the nearest neighbours is

$$\begin{aligned} \delta F_{i\pm1,j} &= \frac{K_1}{2K_1 + 2K_2 + K_L} F_{i,j} = \alpha_1 F_{i,j}, \\ \delta F_{i,j\pm1} &= \frac{K_2}{2K_1 + 2K_2 + K_L} F_{i,j} = \alpha_2 F_{i,j}, \end{aligned} \tag{4.7}$$

Where α is the 'elastic' or conservation (dissipation) parameter. In the case of the OFC model, it is assumed that the system is isotropic so $\alpha_1 = \alpha_2 = \alpha$, and the boundaries are open or 'fixed' with $F = 0$ at the edges. The model is now reduced to only a few parameters and is run using the following algorithm:

- All sites are assigned a value between 0 and a threshold value F_{th}.
- For any site with $F_{i,j} \geq F_{th}$, the force is redistributed following the rule:

$$\begin{aligned} F_{i\pm1,j\pm1} &\rightarrow F_{i\pm1,j\pm1} + \alpha F_{i,j}, \\ F_{i,j} &\rightarrow 0 \end{aligned} \tag{4.8}$$

– Process 4.8 is repeated until all $F_{i,j} < F_{th}$. note that for a model with four neighbours, α can have values $0 \leq \alpha \leq 0.25$.

– The block with the largest force F_{max} is located and then all sites are given a force $F_{th} - F_{max}$ which will cause another 'earthquake' and process 4.8 is repeated and so on.

The most important results from the model are that (1) criticality (a power-law) is maintained despite the introduction of dissipation and (2) the slope of the linear part of the power-law distribution is dependant of the conservation parameter α. This is shown in figure 4.4 (after Olami et al., 1992). The results questioned the 'universality' idea that the scaling exponents should be independent of microscopic details of a system (Lise and Paczuski, 2001). This is more in tune with natural systems that are predominantly dissipative and may show different scaling exponents (Bak, 1997). Also, their findings suggest that internal conservation of energy is not a requirement for criticality. However, there is some debate concerning whether 'criticality' can exist in the non-conservative OFC model (e.g. Manna et al., 1999; de Carvalho and Prado, 2000; Christensen et al., 2001) and regarding the mechanisms responsible for the criticality observed. This issue is an 'unsettled question' (Sornette, 2000) yet to be categorically resolved (Jensen, 1998).

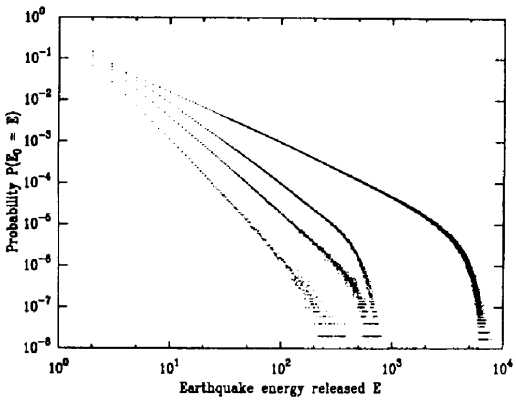

Figure 4.4: Incremental energy probability distributions for (top to bottom) $\alpha = 0.25, 0.20, 0.15$ and 0.10. From Olami et al. (1992).

4.6 A generalized BTW model

In order to investigate thermodynamic aspects of SOC in relation to earthquakes, I use a generalized model that is a cross between the BTW model and the OFC model. This model is chosen because it is very close to the original SOC model of Bak et al. (1987) with the addition of dissipation. A similar model is used to investigate criticality for non-conservative sand pile models by Ghaffari et al (1997). Here the model is defined as follows:

- As with the BTW and OFC models, the generalized model is composed of an $N \times N$ square array.
- The model is initialised with the 'stress' σ in each cell between some random value $0 < \sigma < 4$.
- For every time step t, A random number generator is used to select a point on the array (x, y) to which a stress of 1 is added thus

$$\sigma_{x,y} = \sigma(x, y) + 1 \tag{4.9}$$

- Any site with $\sigma_{x,y} \geq \sigma_C$ fails or 'breaks' and redistributed its stress to its 4 nearest neighbours (figure 4.5) following

$$\begin{aligned} \sigma_{x\pm1,y\pm1} &\rightarrow \sigma_{x\pm1,y\pm1} + \alpha\sigma_C/4 \\ \sigma_{x,y} &\rightarrow \sigma_{x,y} - \alpha\sigma_C \end{aligned} \tag{4.10}$$

  where α is the conservation factor with $0 \leq \alpha \leq 1$. For $\alpha < 1$, σ can take non-integer values.
- process 4.10 is repeated until all sites have $\sigma < \sigma_C$. The total area A effected by rule 4.10 defines the cluster or event size[4].

The model is run with open boundary conditions. Note that we retrieve the BTW model when $\alpha = 1$ so I shall refer to the model as the non-conservative BTW model or NBTW

[4] I have found that the total number of elements that break for a given perturbation (4.9) does not always equal the cluster size since sites within a cluster can break more than once within a single event (see figure 4.20). This is especially true for the case $\alpha = 1$. I nonetheless for comparison, stick with the BTW definition and equate the cluster size to the total area affected by an avalanche process.

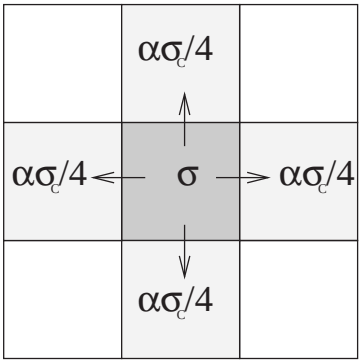

Figure 4.5: A site (centre) with stress σ failing and redistributing its stress to its four nearest neighbours.

Property	**BTW**	**OFC**	**NBTW**
Driving	local	global	local
Boundaries	open	open	open
Dissipation	no	yes	yes
σ values	integers	continuous	continuous
Failed site	$\sigma \rightarrow \sigma - \sigma_C$	$\sigma \rightarrow 0$	$\sigma \rightarrow \sigma - \sigma_C$

Table 4.1: Table of differences between the BTW, OFC and NBTW models of seismicity.

here on. The main differences between BTW, OFC and NBTW models are summarized in table 4.1. This completes the definition of the NBTW model which is used in this chapter. Now I shall use the model to address the issues outlined in the introduction of this chapter.

4.7 Part I: Self-organisation and dissipation

I now use the NBTW model to investigate some of the thermodynamic characteristics of a self-organising dissipative structure and their dependence on the level of dissipation. For the NBTW model outlined I measure the following internal and external parameters as follows:

4.7.1 Energy

For a $N \times N$ lattice, the externally radiated and internal 'strain' energies E_e and E_i at a time t and conservation parameter α are defined respectively as:

$$E_e(t, \alpha) = a_1 A \tag{4.11}$$

where A is the cluster area[5] i.e. the number of connected cells effected by an avalanche process and

$$E_i(t, \alpha) = a_2 \sum_{n=1}^{N^2} \sigma_n^2 \tag{4.12}$$

over all cells in the array. The mean internal energy at a given time increment t is then

$$\overline{E_i}(t, \alpha) = \frac{a_2}{N^2} \sum_{n=1}^{N^2} \sigma_n^2 \tag{4.13}$$

where a_1 and a_2 are arbitrary constants that will depend on the system. For simplicity, I put $a_1 = a_2 = 1$. Note that at any time t, $\overline{E_e} = E_e$ since only one cluster is allowed to occur at every time increment. Here we can also define the energy dissipated irreversibly through the factor α. Every cell that fails will dissipate an amount $(1 - \alpha)\sigma_C$ in the process of redistributing its energy to its neighbours. Since the number of cells that fail for a given event is proportional to E_e, we can broadly define the dissipated energy E_{dis} as

$$E_{dis} \sim (1 - \alpha)\sigma_C E_e \tag{4.14}$$

Note that E_{dis} here is only an approximate value since it excludes energy lost at the boundaries and doesn't take into account the arbitrary constants a_1 and a_2 in 4.11 and 4.12 respectively. E_{dis} can be seen as analogous to energy lost irreversibly in the crust as heat or plastic deformation and so on.

For a model run of length t_n where t_n in the steady state[6], I define the mean external and internal energies for a given α to be

$$\langle E_e(\alpha) \rangle = \frac{1}{t_n} \sum_{t=1}^{t_n} E_e(t, \alpha) \tag{4.15}$$

[5]The relationship found between fault rupture area and radiated seismic energy for real earthquakes is $E_e \sim A^{3/2}$ (Kanamori and Anderson (1975). However, I take $E_e \sim A$ in accordance with Bak et al. (1987) so results presented in this thesis may be easily compared to those of the original publication.

[6]The system is first allowed to run for a period to stabilise and reach a steady-state. All data during this stabilisation period is not included in t_n.

and

$$\langle E_i(\alpha)\rangle = \frac{1}{t_n}\sum_{t=1}^{t_n} E_i(t,\alpha). \tag{4.16}$$

The expectation of the logarithm of external and internal energies are respectively

$$\langle \ln E_e(\alpha)\rangle = \frac{1}{t_n}\sum_{t=1}^{t_n} \ln[E_e(t,\alpha)] \tag{4.17}$$

and

$$\langle \ln E_i(\alpha)\rangle = \frac{1}{t_n}\sum_{t=1}^{t_n} \ln[E_i(t,\alpha)]. \tag{4.18}$$

From the energies calculated using 4.11 and4.12, we can also construct histograms that will give us energy probability distributions $p(E_e)$ and $p(E_i)$. I do this by binning the energy data with increments of $\delta E = 1$. The data are then normalized such that for both p we have

$$\sum p = 1 \tag{4.19}$$

4.7.2 Entropy

From $p(E_e)$ and $p(E_i)$ we can, after a transient time t_n, calculate the external and internal entropies of our system for a given α as follows:

$$S_e(\alpha) = -\sum_{E_e min}^{E_e max} p(E_e)\ln p(E_e) \tag{4.20}$$

and

$$S_i(\alpha) = -\sum_{E_i min}^{E_i max} p(E_i)\ln p(E_i). \tag{4.21}$$

By measuring both the internal and external entropies, we can test Prigogine's conjecture that organisation within a system is at the expense of increasing the entropy globally (Kondepudi and Prigogine, 1998). Although it is generally assumed that the internal (strain) and radiated energies for the crust are correlated (e.g. Rundle et al., 1993; Dahmen et al., 1998; Main and Al-Kindy, 2002), the correlation between internal and external entropies (or indeed entropy productions) are unknown. Measuring these at least for a model could shed some light on self-organisation in the crust. As far as I am aware, the results in this chapter are the first to test this hypothesis formally for a randomly driven model.

4.7.3 'Temperature'

In section 2.5.1 (chapter 2) a definition of temperature was given from a thermodynamic point of view. For the discretised model presented here, a 'statistical' definition is more appropriate. In accordance with Mandl (1988), a temperature can be seen as a measure of how large the fluctuations in a system's energy are. It can also be *'a parameter that quantifies the degree of stochasticity of the system'* (Sornette, 2000). The magnitude of these fluctuations is a function of the standard deviation of the energy ΔE defined by (Mandl, 1988):

$$(\Delta E)^2 = \overline{(E - \overline{E})^2} = \overline{E^2} - \overline{E}^2 \tag{4.22}$$

With reference to equation 2.3 and differentiating $\ln Z$ twice we have

$$(\Delta E)^2 = \frac{\partial^2 \ln Z}{\partial \beta^2} = -\frac{\partial \overline{E}}{\partial \beta} = -\frac{dT}{d\beta}\frac{\partial \overline{E}}{\partial T} = kT^2 C \tag{4.23}$$

Where C is the heat capacity and k is Boltzmann's constant. So we can say that for a given system:

$$\Delta E \sim T_T \tag{4.24}$$

I put the statistical temperature $T = T_T$ here to distinguish it from thermodynamic temperature. Therefore, by measuring the standard deviations of E_e and E_i we can also calculate a form of external and internal 'temperature' for our system T_e and T_i. This chapter, to my best of knowledge, is the first time these temperatures are measured from the external *and* internal energy fluctuations for a numerical seismicity model. Statistical temperature used in the literature is sometimes referred to as 'effective temperature' (D'Anna et al., 2003) or 'tectonic temperature' (Main et al., 2000) which are both a measure of the fluctuation amplitudes and therefore predictability of the system rather than a traditional 'heat' temperature.

4.8 Model runs and results

I run the NBTW model for $t = 5 \times 10^5$, $\sigma_C = 4$ (as in the original BTW model), and varying the conservation factor α from 0.05 to 1.0 at increments of 0.05 giving a

total of 20 runs and 10^7 events[7]. In order to ensure the runs have reached a stationary 'steady state', the first 10^5 events are discarded. This cut off value is chosen based on observation of $E_i(t, \alpha)$ (see below). The results of the runs are as follows:

4.8.1 External energy E_e

The radiated energies are calculated from the cluster sizes of each event using 4.11. Figure 4.6 shows $E_e(t, \alpha)$ for $\alpha = 0.1$, 0.5 and 1.0. Note that for all three cases, the data are punctuated with no apparent signs of any transient trends such as periodic behaviour even with high dissipation ($\alpha = 0.1$). There is also a very notable contrast between the size of the largest and smallest events for the conservative case ($\alpha = 1$) when compared to the non-conservative runs ($\alpha < 1$). Then, from E_e I produce probability distribution plots. Figure 4.7 shows the probability distributions for $\alpha = 0.1$ to 1 on a log-log plot. A line (dashed) is drawn with a slope equal to unity for reference. The power-law type distribution can be clearly seen for the case $\alpha = 1$ with scaling exponent ~ 1. This result as expected, is identical to that of Bak et al. (1987). Note that if I were to put $E_e \sim A^{3/2}$ in relation 4.11 above in accordance with Kanamori and Anderson (1975), the slope of the exponent for $\alpha = 1$ in figure 4.7 would be $2/3$ (section 2.8.3) as found for earthquake moment data (e.g. Kagan, 1997) rather than 1 as found here for the BTW model.

However, looking at the cases for $\alpha < 1$ in figure 4.7, we can see that the distributions roll off from a power-law very quickly (low θ, see chapter 3). The maximum event sizes are much smaller than the system size (sub-critical) and are systematically related to α. The gamma distribution gives a very good fit to the data as I demonstrate for two cases $\alpha = 0.95$ and 0.55 in figure 4.8. Figure 4.8 shows a sub-critical distribution for the two chosen values of α and the equations for the corresponding fits. The same can be said for all $0 < \alpha < 1$. This is in agreement with mean field predictions that *'criticality in the sand pile model is lost when dissipation is present'* (Lauritsen et al., 1996) as well as other similar numerical models (e.g. Ghaffari et al., 1997). The results also show that the gamma distribution discussed in chapter 3 is best suited to describe such scaling be it in models or real earthquake data since it can cater for power-law ($\theta \to \infty$) and exponential

[7]Note that the entire length of the Harvard CMT catalogue for real earthquake data for which it is complete consists of < 10000 points.

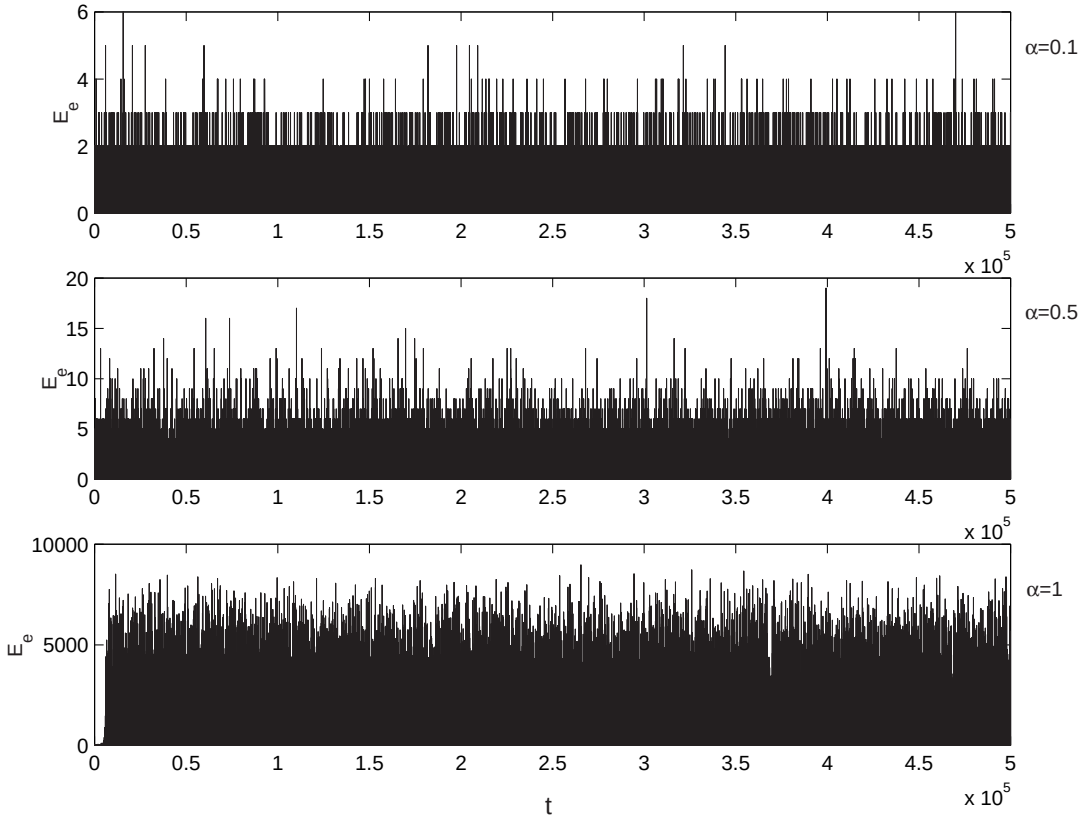

Figure 4.6: Radiated energy $E_e(t, \alpha)$ for $\alpha = 0.1, 0.5$, and 1. Note the large differences in scale in the y-axis for the three plots.

($B = 0$) distributions or a combinations of both.

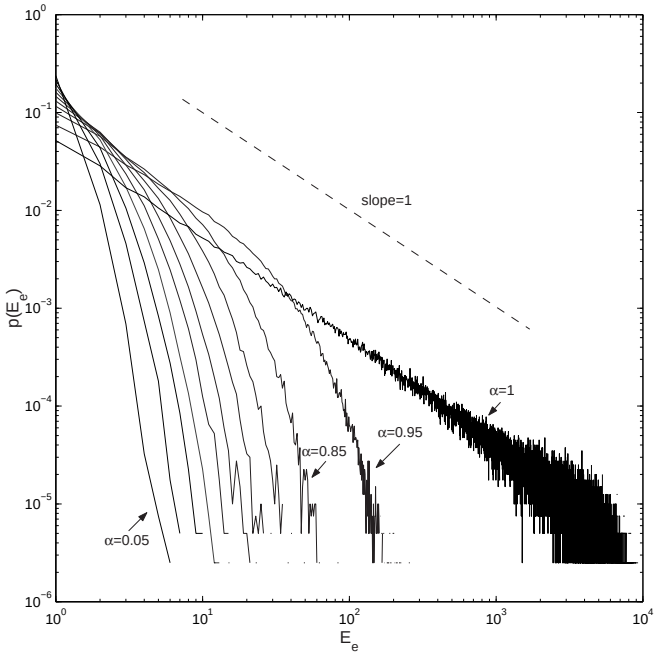

Figure 4.7: Incremental probability distribution for the radiated energy E_e from $\alpha = 0.1$ to $\alpha = 1$. The dashed line is drawn with slope$= 1$ for reference.

To ensure that the distribution of $P(E_e)$ in figure 4.7 does not depend on the grid size, I calculate $P(E_e)$ for another two runs, with grid size 5×50 and 200×200. These results are shown in figure 4.9. It can be seen that the results for the case $\alpha < 1$ are indistinguishable. For the case $\alpha = 1$, the slopes of the distribition are the same however the cut-off as the higher energies are restricted by the system size. This is highlighted in the figure with the arrows that mark system size for the three distributions.

4.8.2 Internal energy E_i

The internal energy for different runs is measured using 4.12 for different values of α. The results for $E_i(t, \alpha)$ are shown in figure 4.10. We can see from figure 4.10 that the system reaches a stationary steady state at $t > 100000$ showing Boltzmann type fluctuations similar to an equilibrium system despite it being far-from-equilibrium. The results reported here for internal energy are very different to those reported for globally 'uniformly' driven systems in that they lack any periodic behaviour such as found by Jánosi

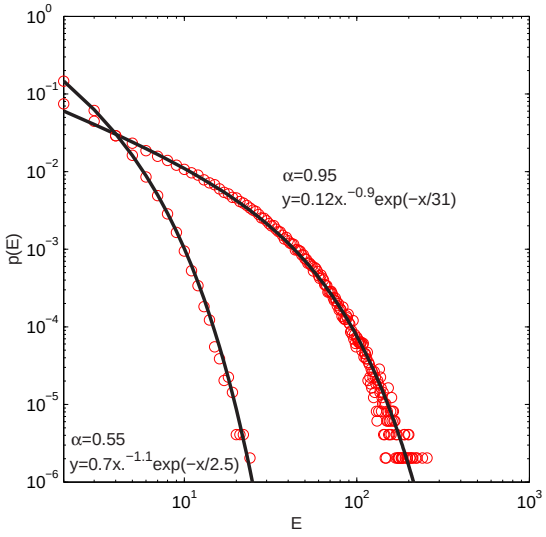

Figure 4.8: Gamma fit on energy probability distributions for runs with $\alpha = 0.55$ and $\alpha = 0.95$ showing a sub-critical distribution.

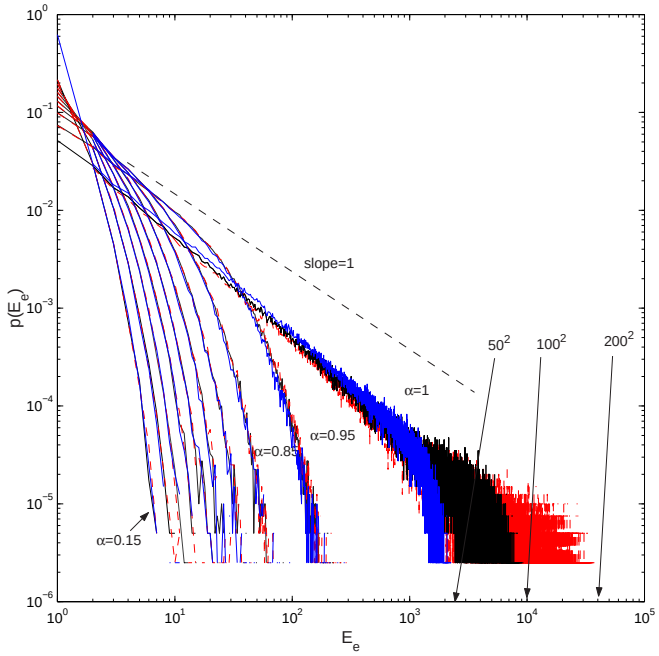

Figure 4.9: Incremental probability distribution for the radiated energy E_e from $\alpha = 0.1$ to $\alpha = 1$ for grid size 50×50, 100×100 and 200×200. The dashed line is drawn with slope$= 1$ for reference.

and Kertész (1993) and Main et. al. (2000). It is noted however that the fluctuations become less erratic (lower frequency content) as α is decreased. To further investigate the

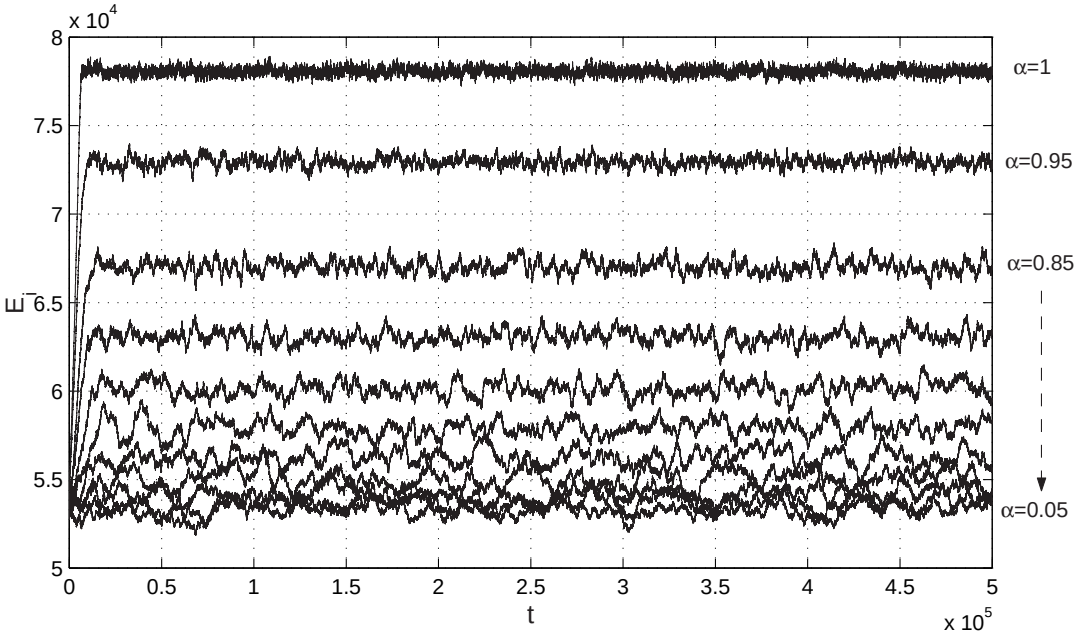

Figure 4.10: plot of internal energy $E_i(t, \alpha)$.

frequency content of E_i for different α, I construct time-series Fourier power-frequency plots for the steady-state regions for different runs as shown in figure 4.11 The power-frequency plots do not show any peaks that would be indicative of any form of periodic behaviour i.e. the dominance of a particular frequency. It is also interesting to note from the power-spectra that they all follow a power-law distribution with a slope ~ 2. A slope of 2 in power-spectra is what is usually obtained from the frequency analysis of Brownian noise in gasses or 'random walk' simulations (Feder, 1988; Turcotte, 1997). It is unclear to me at this time why the slopes of the power-spectra appear to be independent of α. In summary, the internal energy fluctuations reported here for a steady-state far-from-equilibrium system appear to be similar to those of equilibrium systems.

Now I examine the density distribution of the internal energy in the steady-state for different values of α. My results are shown in figure 4.12. The figure shows three interesting characteristics. Firstly, although the radiated energies follow a gamma distribution, the internal energy is closer to a peaked Gaussian or 'normal' distribution which is similar

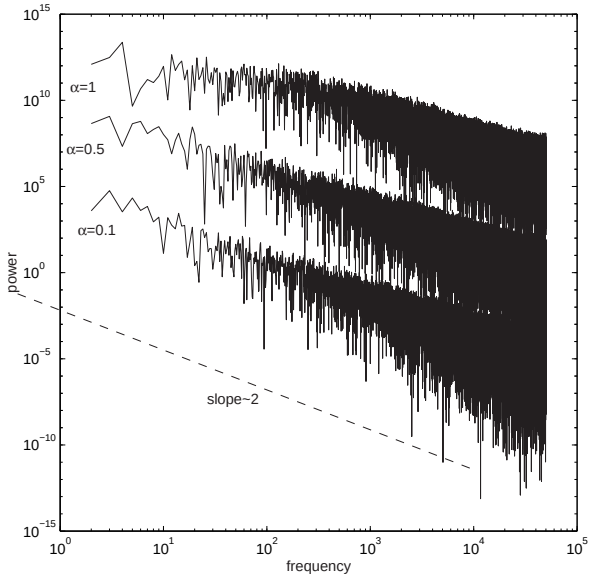

Figure 4.11: Fourier power-frequency plots for E_i with$\alpha = 1, 0.5$ and 0.1. The dotted line is drawn with slope ~ 2 for reference. The plots have been shifted vertically for clarity.

to what is found for an equilibrium system such as a gas (e.g. Mandl, 1988). This is also true for $\alpha = 1$. Secondly, it can be seen that as dissipation increases, the average internal energy decreases; the mean energy of the system is therefore a function of the level of energy dissipation. Finally, the distributions are more peaked for higher conservation and broaden as dissipation is increased. Note that this final point is contrary to what we observe for the radiated energy E_e (figure 4.7) where the distributions broaden as α increases.

Finally, I test the assumption that radiated energy (that can be measured for the crust) and internal energies (that cannot) are correlated by plotting $\langle E_i(\alpha)\rangle$ against $\langle E_i(\alpha)\rangle$ for all runs. It can be seen in figure 4.13 that there is a positive correlation between the two. This is in agreement with the results of the globally driven model of Main et al. (2000) but shown here to be also true for a locally random driven system. Although the positive correlation between internal and radiated energy cannot be conclusively shown for the crust, the NBTW model does not suggest the contrary.

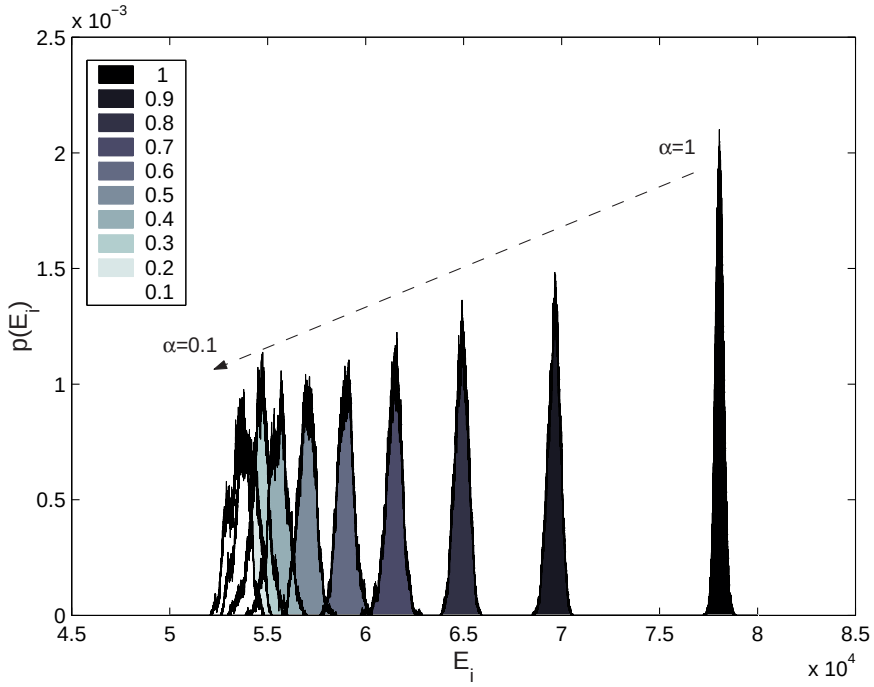

Figure 4.12: Incremental probability distribution for the internal energy E_i from $\alpha = 0.1$ to $\alpha = 1$. The dashed arrow indicates the direction of increasing dissipation.

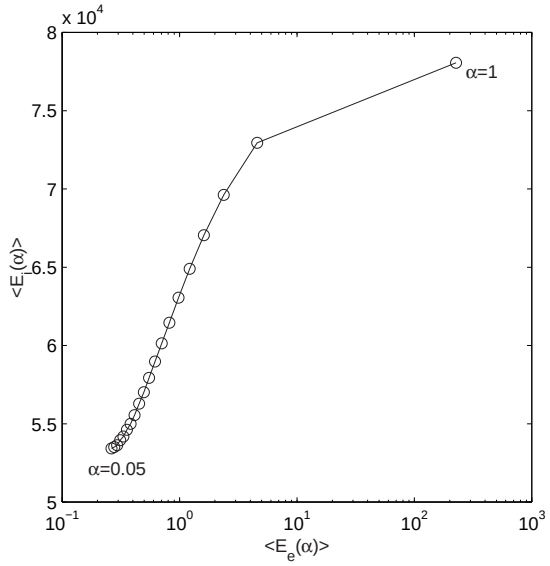

Figure 4.13: Plot of internal energy $\langle E_i(\alpha) \rangle$ against radiated energy $\langle E_i(\alpha) \rangle$ showing a positive correlation between the two. The plot is done using a log-linear scale for clarity.

4.8.3 Entropy and effective 'temperature'

I now measure the external and internal entropies and corresponding temperatures for the NBTW model and their dependence on dissipation. It must be noted here that the entropy production of a system approaches zero as the entropy approaches a maximum to achieve equilibrium (Kondepudi and Prigogine, 1998). However, here we are dealing with a far-from-equilibrium system. I therefore focus my interest in the change in external and internal entropy as a function of dissipation (decreasing α). The aim is to test the notion that driven dissipative systems self-organisation (lower their entropy internally) is at the expense of increasing entropy globally. I first examine the effect of dissipation on the internal and external entropies which are measured on the steady-state part of the runs using 4.20 and 4.21. Figures 4.14a and b shows how S_e and S_i depend on α. We can see that whereby an increase in dissipation (decreasing α) increased S_i, it decreases S_e. This is a significant result demonstrating how internal and external entropies are negatively related for a dissipative driven system and how the two vary with the level of dissipation. This results is further illustrated by plotting S_e against S_i in figure 4.15 confirming the negative correlation.

I now examine the predictions of equation 3.26 (chapter 3) on the correlation between the external and internal expectation of logarithm of energies and their corresponding entropies shown in figure 4.16a and b. We can see from figure 4.16a that there is a positive correlation between the expectation of the logarithm of the radiated energy $\langle \ln Ee \rangle$ and the entropy S_e confirming the prediction of equation 3.26. However, this positive correlation is curved which, based on the 'thermodynamic' criteria outlined in section 3.6 (chapter 3), further suggests that the BTW model in the non conservative regime (NBTW) is not critical. Conversely, we can see a negative correlation between the expectation of the internal energy $\langle \ln E_i \rangle$ and the entropy S_i. This is interesting since as with $p(E_i)$, it is more in accordance with what one would expect for an equilibrium system whereby the system's increase in entropy is accompanied by a lowering of its internal energy, like a collapsing house say that will become more disorganised (higher S) and will lose energy (lower E_i) to its surroundings (higher E_e). This is 'anti' self-organisation.

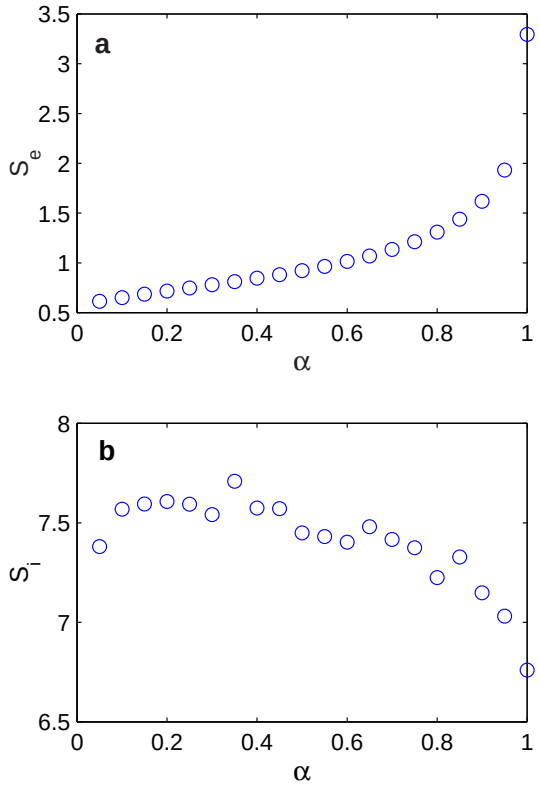

Figure 4.14: Plot of external and internal entropies S_e and S_i as a function of α.

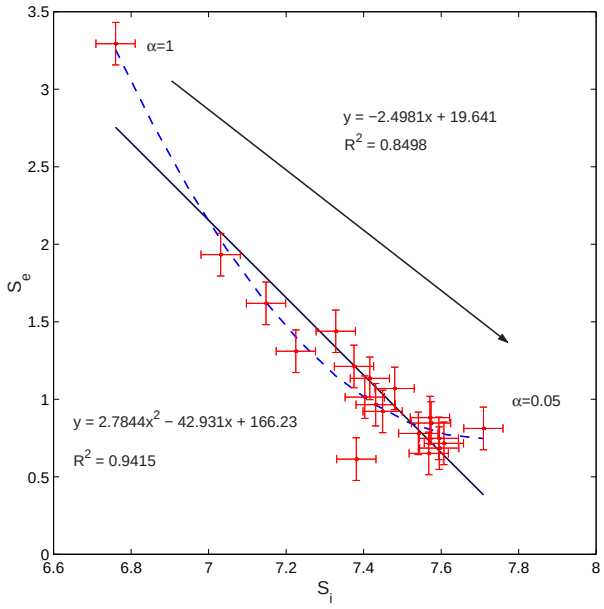

Figure 4.15: Plot of the external entropy S_e against internal entropy S_i. The two entropies show a negative correlation fitted here with linear (solid line) and polynomial (dashed line) least-squares fit. The arrow points towards the direction of increasing dissipation.

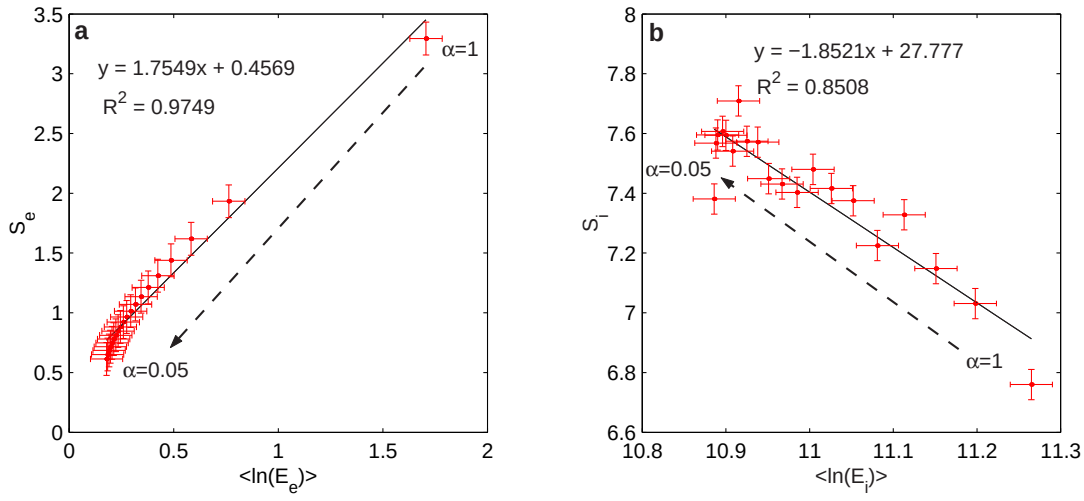

Figure 4.16: Plot of a) S_e against $\langle \ln E_e \rangle$ showing a positive correlation and b) S_i against $\langle \ln E_i \rangle$ showing a negative correlation. The dashed arrow points towards the direction of increasing dissipation.

Moving on to temperature, I follow the definition 4.24 and measure the standard deviations of E_e and E_i and to see how external and internal temperatures are related to entropy, energy and α. I show my results in figure 4.17. I find that there is a positive correlation between the entropies of the system and their corresponding temperatures (figure 4.17a). Lower temperatures are usually seen to be a property of 'ordered' systems (lower entropy) such as say a quartz crystal as apposed to a hot 'disordered' gas. Temperature is an important property of self-organising systems because the 'hotter' a system, the larger the energy phase-space it can explore to find a lowest energy state (Sornette, 2000). Looking at the relation between energy and temperature, we can see in figures 4.17c and 4.17d that T_i of the system is highest for the lowest energy state E_i. Finally, looking at the relation between the temperatures and the dissipation, I find as expected that the correlation between the two for the internal and external temperatures are different. This is shown in figures 4.17e and f. An increase in dissipation therefore increases the internal temperature of a system whilst decreasing the temperature of the energy or 'matter' radiating from it.

4.8.4 Effect of conservation α on radiated energy $\langle E_e \rangle$

We have seen in figure 4.7 that the maximum radiated energy E_e will decrease with decreasing α. This result is also seen for other globally driven models (e.g. Olami et al, 1992, Main et al., 2000). Lise and Jensen (1996) find that for a random neighbour version of the OFC model (one where the energy is redistributed to 4 randomly chosen cells rather than the 4 immediate neighbours) that

$$\xi \sim (\alpha_C - \alpha)^{-1.5} \tag{4.25}$$

where ξ is the cut-off in avalanche size (the maximum possible cluster size for a given α). A similar power-law result was found by Christensen and Olami (1993) through a mean filed approximation although they used a conservative model with α being a measure of the number of neighbours to which energy is redistributed. Here I numerically test if the results also hold for the NBTW model. Plotting $\langle E_i \rangle$ against α in figure 4.18a, we see that there is a positive correlation with an exponential increase in $\langle E_e \rangle$ as $\alpha \rightarrow 1$. Note the similarities with figure 2.13 (chapter 2). Following the results of equation 4.25, I set

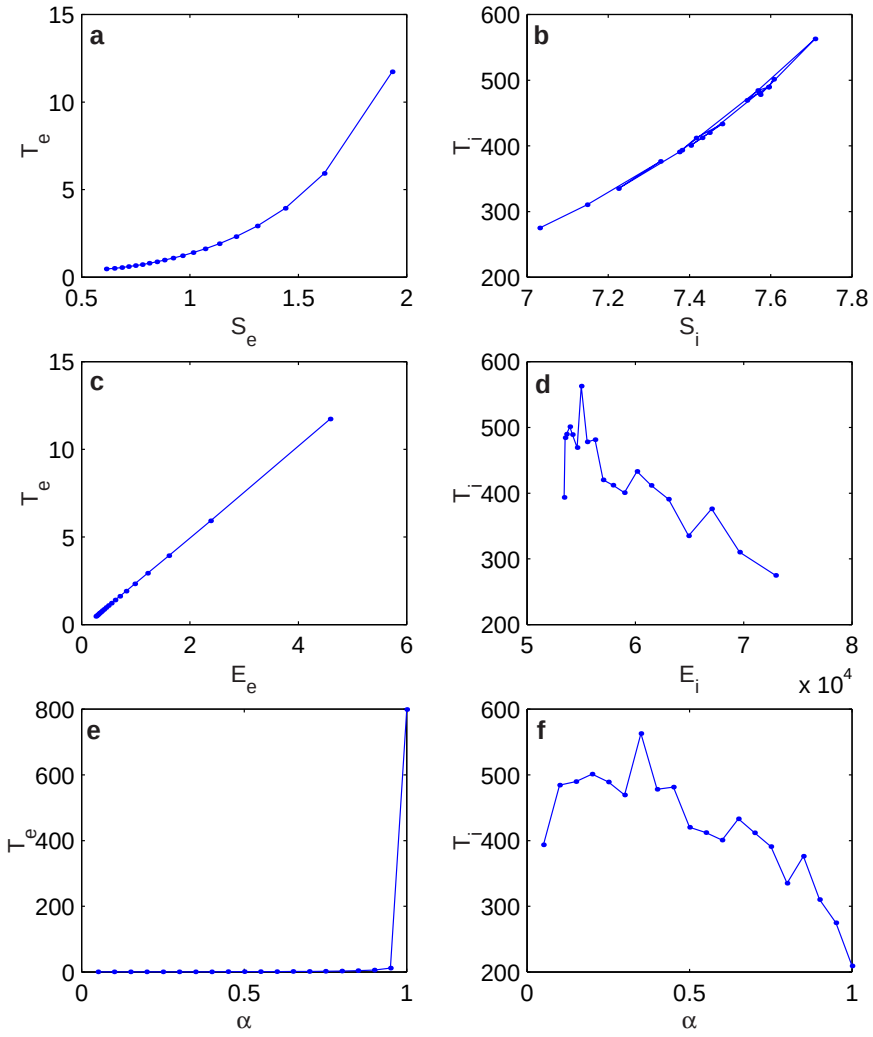

Figure 4.17: Plot of $a)S_e$ against T_e, $b)S_i$ against T_i, $c)\langle E_e \rangle$ against T_e, $d)\langle E_i \rangle$ against T_i, $e)T_e$ against α, $f)T_i$ against T_α.

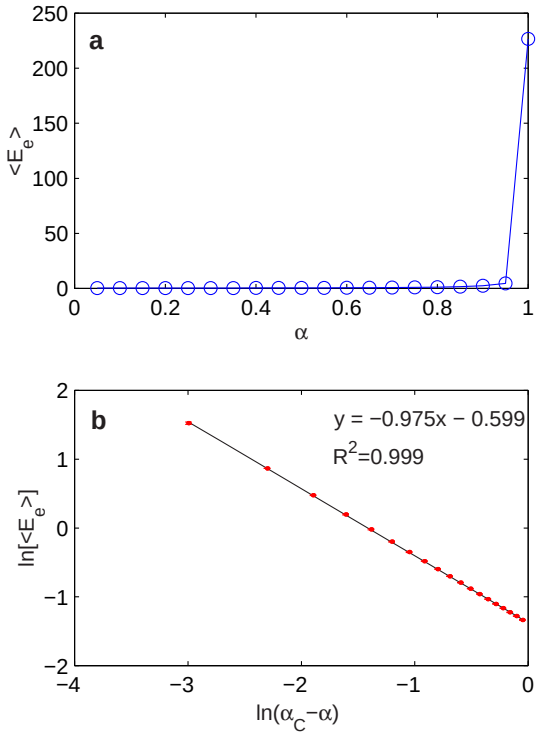

Figure 4.18: Plot of a) $\langle E_e \rangle$ againts α and b) $\ln\langle E_e \rangle$ against $\ln(\alpha_C - \alpha)$ where $\alpha_C = 1$.

α	$\langle E_e \rangle$	$E_e max$	$\langle \ln E_e \rangle$	$\langle E_i \rangle \times 10^4$	$\langle \overline{E_i} \rangle \times 10^4$	$\langle \ln E_i \rangle$	S_e	S_i	T_e	T_i
0.05	0.263	6	0.179	5.342	5.134	10.886	0.614	7.381	0.471	393.421
0.10	0.278	6	0.184	5.351	5.144	10.888	0.651	7.568	0.51	484.238
0.15	0.294	7	0.191	5.363	5.154	10.89	0.685	7.595	0.555	489.627
0.20	0.312	8	0.197	5.395	5.186	10.896	0.716	7.607	0.604	501.219
0.25	0.332	12	0.205	5.419	5.209	10.9	0.748	7.594	0.662	489.265
0.30	0.356	11	0.213	5.461	5.249	10.908	0.78	7.541	0.722	469.363
0.35	0.383	15	0.223	5.5	5.286	10.915	0.812	7.709	0.794	562.919
0.40	0.414	18	0.234	5.555	5.339	10.925	0.847	7.574	0.874	478.06
0.45	0.452	15	0.245	5.628	5.409	10.938	0.882	7.571	0.976	481.324
0.50	0.496	22	0.259	5.701	5.48	10.951	0.922	7.449	1.089	420.232
0.55	0.55	23	0.275	5.793	5.569	10.967	0.965	7.431	1.227	412.261
0.60	0.618	29	0.294	5.898	5.669	10.985	1.014	7.403	1.4	400.714
0.65	0.705	29	0.317	6.014	5.78	11.004	1.07	7.48	1.62	433.138
0.70	0.82	38	0.344	6.145	5.906	11.026	1.135	7.416	1.914	411.857
0.75	0.98	49	0.378	6.305	6.06	11.052	1.212	7.375	2.321	390.817
0.80	1.218	56	0.424	6.49	6.238	11.081	1.31	7.225	2.927	335.043
0.85	1.611	83	0.487	6.704	6.444	11.113	1.439	7.328	3.932	376.163
0.90	2.38	120	0.583	6.962	6.669	11.151	1.619	7.148	5.924	310.393
0.95	4.587	254	0.763	7.295	7.011	11.198	1.933	7.031	11.731	274.998
1.00	226.6	9122	1.706	7.806	7.503	11.265	3.294	6.76	798.81	209.274

Table 4.2: Summary of results of model runs for $\alpha = 0.05$ to $\alpha = 1$.

$\alpha_C = 1$ since its is at $\alpha = 1$ that we get the largest mean energy. Plotting $\langle E_e \rangle$ against $1 - \alpha$ in figure 4.18b, I find that

$$\langle E_e(\alpha) \rangle \sim (1 - \alpha)^{-0.975} \tag{4.26}$$

The results of Christensen and Olami (1993) and Lise and Jensen (1996) are therefore quantitatively confirmed here for a locally driven NBTW model. It is interesting to note from equations 4.25 and 4.26 that α has a similar effect on cluster size as temperature and percolation probability do on non-driven systems as given by equation 2.22 in section 2.6.3 (chapter 2). The results of this section are summarised in table 4.2

4.9 Part II: Investigating SOC in the BTW model

I have outlined that the definition of SOC remains somewhat vague. This is a problem when trying to assess whether the Earth's crust is a SOC system or not. Therefore, I now

examine the BTW model in some detail in relation to earthquakes. I will also extend this investigation to the NBTW model ($\alpha < 1$). The three main questions I attempt to address are

1. Is spatial heterogeneity present in the BTW model of SOC? This question is important because spatial heterogeneity is observed in the statistics of earthquake populations (e.g. Ogata et al., 1991; Öncel et al., 2001). If heterogeneity is found in the BTW model, then the assumption that SOC systems are unpredictable in space need not be made as part of its definition. Extrapolating from this, the notion that the Earth's crust is at the point of global failure *everywhere* (e.g. Grasso and Sornette, 1998; Zöller et al., 2001) also need not be made.

2. Is universality a requirement of SOC? Although universality in a dissipative model such as the OFC model is a subject of debate (section 4.5.3) because of the non-uniqueness of the scaling exponent, it is not the case for the BTW model of SOC which has a fixed scaling exponent for the energy release. However, if spatial heterogeneity is found in the BTW model, how will this generally affect the power-law statistics observed on a subsection of the model?

3. Although the BTW model is inherently unpredictable in time (Bak et al., 1987), there have been observations of time dependant processes in real earthquake data such as accelerated seismicity before a large event (section 2.8.4 in chapter 2). Here I ask the question that assuming such an observation happened by complete coincidence, would it still be compatible with the statistics of the BTW model? In other words, does the BTW model have the statistical raw material to show accelerated seismicity before a large event?

By covering these questions, the main aspects of the BTW model and therefore SOC would have been investigated; space and time.

4.9.1 Spatial variations

I now investigate spatial heterogeneity in the original BTW model by putting $\alpha = 1$ in the NBTW model. My primary interest is on the recurrence rate of event occurrence in

space. In order to do this, I define a second $x \times y$ square lattice $C_{x,y}$. This is my 'counter' lattice. For every cell $\sigma_{x,y}$ that fails due to process 4.10 we have:

$$C_{x,y} = C_{x,y} + 1 \tag{4.27}$$

Note that an event can involve the several failed cells that form a cluster for a given time step t. Therefore,

$$\sum C > t \tag{4.28}$$

where $t \in [1, t_n]$. Again, I run the model for a 100×100 lattice for a total of 500000 time steps. Finally, I calculate the probability $p_{x,y}$ of a site breaking in a given position (x, y) for each site in the lattice:

$$p_{x,y} = \frac{C_{x,y}}{\sum C} \tag{4.29}$$

The results are shown in figure 4.19. It can be clearly seen from figure 4.19 that the probability of a cell breaking increases as we get away from the boundaries; **spatial heterogeneity exists in the BTW model**. This is perhaps somewhat expected because the edge cells interact with three neighbours[8] whereby all other cells interact with four

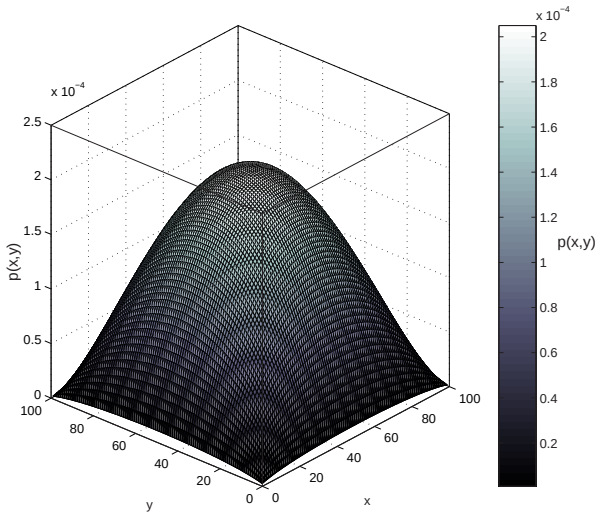

Figure 4.19: Probability $p_{x,y}$ of a site breaking in space for a two-dimensional BTW model.

and are therefore on average more likely to receive energy and break. Let us consider this

[8]Except for the cells at the corners of the array which only have two neighbours.

schematically in figure 4.20. Figure 4.20 is a simplified one dimensional BTW model that starts off close to breaking point ($\sigma_C = 2$). A cell in the centre is given an 'energy' increment (figure 4.20a). The cell breaks and redistributes its energy to it two neighbours and so on until the avalanche ends (figure 4.20f).

There are two things we can gather from this example. Firstly we see how from the counter at the bottom of the schematic that the cells away from the edges break more frequently. Secondly, for this conservative case, the total number of cells broken (9) exceeds the size of the resulting cluster (5). Although this is an simple example, it does conceptually explain the result shown in figure 4.19.

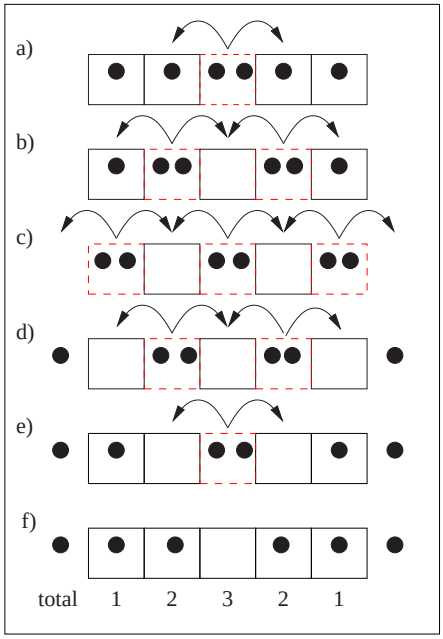

Figure 4.20: One dimensional BTW model showing the effect of open boundaries on causing sites to topple more frequently away from the edges. The dashed squares indicate breaking sites. The number of broken sites (9) exceeds the resulting cluster size (5).

One could now also ask if the magnitude of a triggered event depends on its initiation position (x, y)? I investigate this by constructing a second counter similar to C which I call $C2$. For a an event for energy E_E triggered due to an update at position (x,y):

$$C2_{x,y} = C2_{x,y} + E_e \tag{4.30}$$

so in theory, if larger events are initiated in the centre away from the edges, $C2_{x,y}$ should

be systematically bigger towards the centre. The results of this are shown in figure 4.21 We can see from figure 4.21 that there doesn't appear to be any spatial dependence of

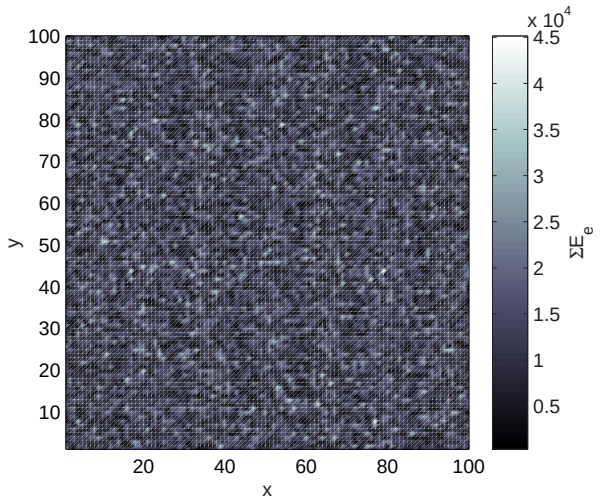

Figure 4.21: Two dimensional counter showing no dependence of the size of the triggered events on their point of initiation.

event size on the position of initiation. Larger events are just as likely to be triggered at the edges as in the centre of the array.

Now I ask the question, is this as suggested by figure 4.20 an artefact of the conservative case? To answer this, I carry out a similar 'counter' analysis for $\alpha < 1$. I show the results of this analysis in figure 4.22 for $\alpha = 0.1$ to $\alpha = 1$. We see in figure 4.22 that the spatial signature observed for $\alpha = 1$ disappears when dissipation is present contrary to what is observed in globally driven dissipative models (e.g. Middleton and Tang, 1995). The effect of the probability of site failure in the x direction ($y = 50$) for $\alpha = 0.1$ to $\alpha = 1$ is shown as a composite plot in figure (4.23).

To ensure that the distinct spatial variation for the case $\alpha = 1$ is not due to the system size, I calculate it for a further two runs with for grid sizes 50×50 and 200×200. This is shown in figure 4.24. It can be concluded that this spatial variation is intrinsic to the system at 1 and not due to system finite size effects. Overall, the results suggest that unless very close the boundary, a dissipative BTW model will not show any spatial heterogeneity in contrast to the conservative case ($\alpha = 1$). Nonetheless, spatial heterogeneity in general appears not to contradict SOC.

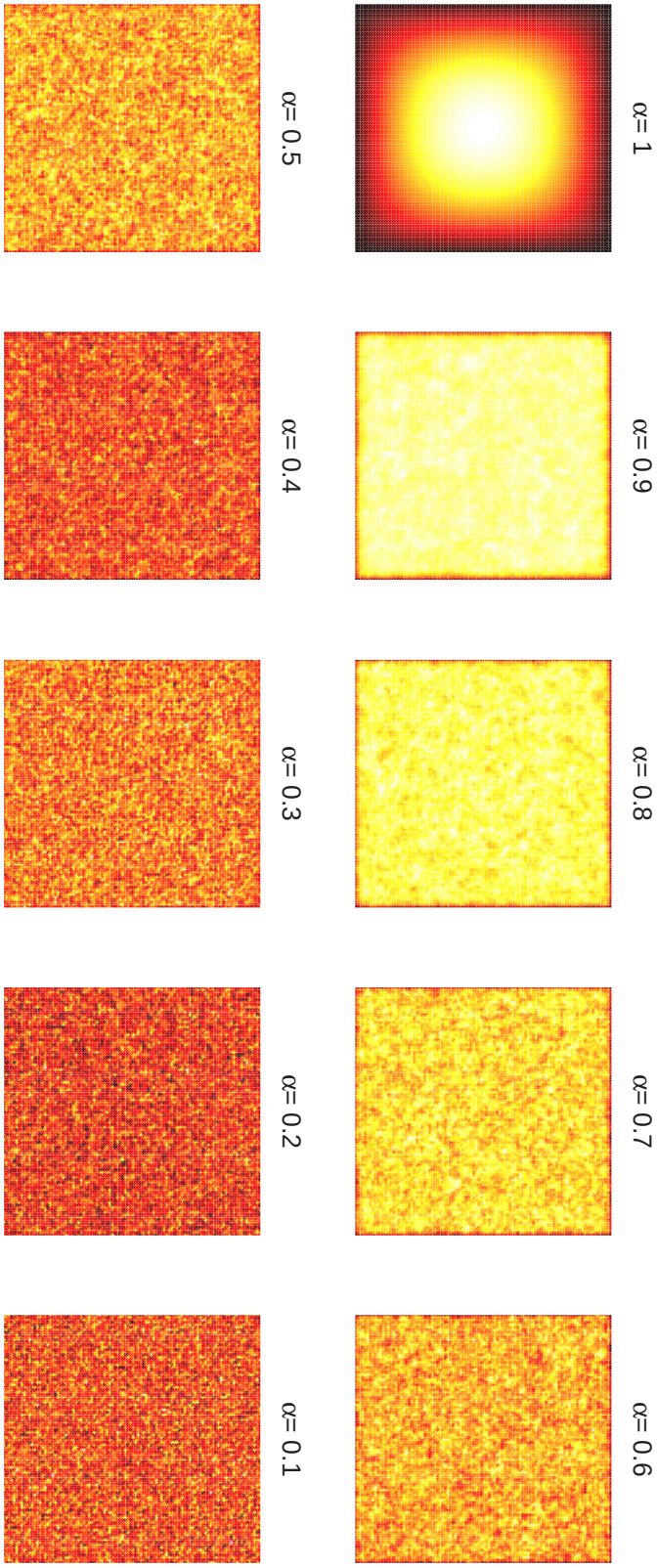

Figure 4.22: Plot of variation of probability $p(i,j)$ of sites breaking in space for 100×100 grid from $\alpha = 0.1$ to $\alpha = 1$. The brightness is proportional to $p(i,j)$

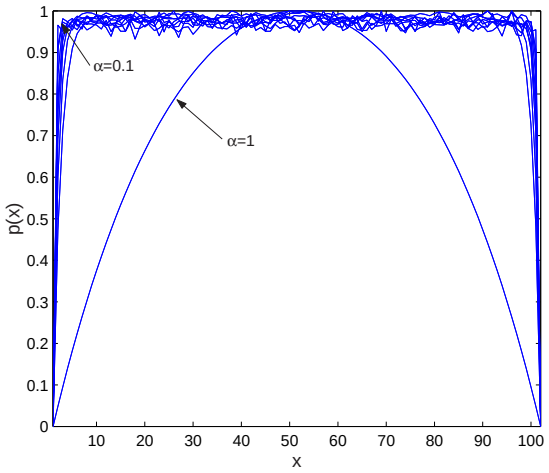

Figure 4.23: Probability $p(x)$ of a site breaking at position x for conservation factor $\alpha = 0.1$ to $\alpha = 1$. There is clear spatial heterogeneity for $\alpha = 1$ which is absent for $\alpha < 1$.

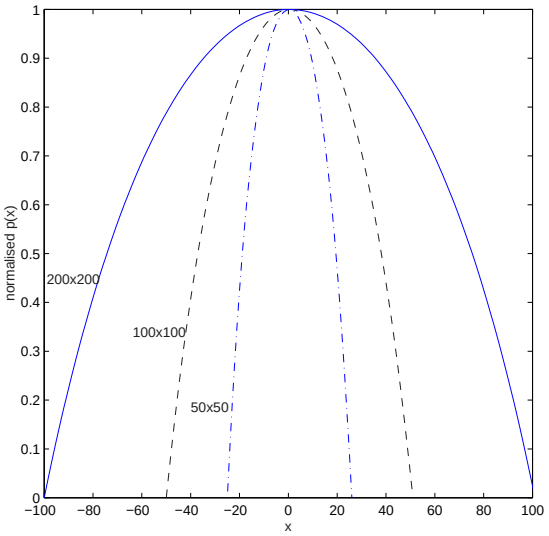

Figure 4.24: Probability $p(x)$ of a site breaking at position x for conservation factor $\alpha = 1$ for grid size 50×50, 100×100 and 200×200. There is clear spatial heterogeneity for $\alpha = 1$ despite the variation in system size (shifted x values and normalised y values are plotted for comparison).

4.9.2 Testing universality in scaling

I have established that there is a spatial bias in the BTW model. I now investigate whether this spatial heterogeneity has any effect on the universality within sub regions of the system. That is, if we are to subdivide the BWT model spatially, will the sub-regions have the same statistical characteristics as each other depicted by a constant scaling exponent B. To do this, I run a BTW model which is sub-divided into two equal areas $A1$ and $A2$ as can be seen in figure 4.25. The regions are chosen in this way because firstly there will be more events in $A1$ than $A2$ (with reference to figure 4.19). Secondly, $A1$ will not be affected by the size limiting effect of the edges whereby $A2$ will. We would therefore expect a bigger maximum event size for $A1$. The model is run as with previous runs

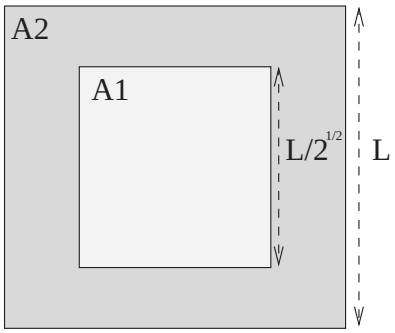

Figure 4.25: BTW model of area A divided into to sub-regions with areas $A1$ and $A2$ where $A1 = A2$ and $A1 + A2 = A = L^2$.

with $t = 500000$. The cluster sizes formed within $A1$ and $A2$ are measured separately for every time step t. From this, I calculate two energy-probability distributions denoted $p(E_{A1})$ and $p(E_{A2})$. These are shown in figure 4.26. Although the two distributions as expected have different maximum event sizes, they both show an identical scaling exponent $B \sim 1$ although the distribution for $A2$ is more gamma than power-law due to the edge effect of the boundaries. This suggests that for the original BTW model, spatial heterogeneity caused by boundary effects should not influence the universality of the system (the value of B) although it can influence the shape of our gamma distribution. **In summary, it appears that systems that show a gamma distribution do not contradict SOC. However, systems that show a regional variation in the scaling exponent**

B will be in contradiction to what has been found for the original BTW model of SOC.

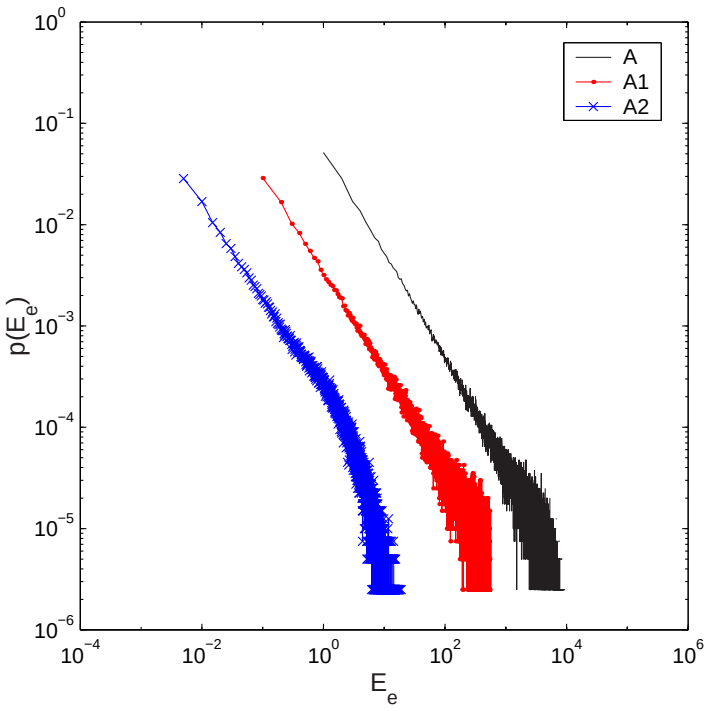

Figure 4.26: Energy probability distributions for region A and sub-regions $A1$ and $A2$ as illustrated in figure 4.25. The $A1$ and $A2$ distributions are shifted to the left along the x-axis for clarity.

4.9.3 Accelerated seismicity and α

The final aspect of the SOC that I test on the BTW model is that of accelerated seismicity. That is, a time dependant acceleration in the radiated energy preceding a large event in the form (Zöller and Hainzl, 2001)

$$\sum \sqrt{E_t} = A - B(t_C - t)^m \tag{4.31}$$

with A, B and m positive constants and t_C is the time of *failure*. Although the issue of precursors occurring before large events for earthquake populations have been reported (e.g. Bowman et al., 1998), these remain controversial and are usually only detected retrospectively after an event has occured (Geller, 1997; Mulargia, 2001). Such precursory phenomena are not observed in the BTW model although there are models that

mimic accelerated seismicity (e.g. Jaumé et al., 2000). The question I ask here however is: although accelerated seismicity is not observed in the BTW model of SOC, would accelerated seismicity contradict it in any way? In other words, can we have an accelerating energy release within a population of events and still have a power-law or gamma energy-density distribution for the data overall?

To answer this, I take $E_e(t, \alpha)$ for all runs and simply re-shuffle it in order of ascending energy. In other words, I am forcing an accelerated seismicity for a population of gamma type data to see if it will follow a power-law increase similar to the reverse Omori law (equation 2.38, chapter 2). It must be noted that the energy probability distributions for data are independent of their transient properties because we are binning in energy rather than time. There is therefore no reason to assume that all systems with power-law statistics are unpredictable in time. Figures 4.27a and b show the unordered and ordered data from $\alpha = 0.1$ to 0.9 (I exclude the case for $\alpha = 1$ from the plots because even though it shows the same results, it out-scales the remainder of the data and obscures them due to its much larger energies). It can be seen from figure 4.27a that the data

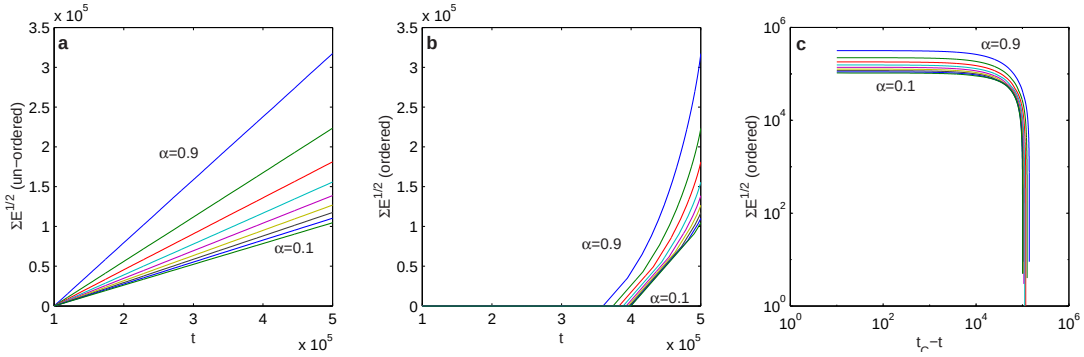

Figure 4.27: $\sqrt{E_e}$ against (a) t (unordered) and (b) ordered, (c) against $(t_C - t)$ on a log-log plot .

un-ordered closely resemble what is usually found in CA models of seismicity (e.g. Angulo-Brown and Muñoz-Diosdado, 1999). Ordering the data (figure 4.27b) shows an exponential type time increase in seismicity as we approach the largest event which becomes more linear as α decreases. To test equation 4.31 on the data, I plot $\sum \sqrt{E}$ against $(t_C - t)$ on a log-log plot (figure 4.27c. It can be seen that the results in figure 4.27c do not follow the predictions of equation 4.31 for this model. This results suggest

that accelerated seismicity is not compatible with SOC at least in a statistical sense.

4.10 An alternative to SOC?

I have shown that although SOC can accommodate for both power law and gamma statistics in the energy release, it cannot accommodate for varying scaling exponents. I therefore propose an alternative; *self-organised sub-criticality* (SOSC). This is simply in accordance with characteristics of the NBTW model rather than the BTW model. SOSC is simply a more 'relaxed' version of SOC that can include internal dissipation, as most natural systems will have, as well as variations in the scaling exponents and correlation length. This is a looser form of SOC that does not rule out any of its characteristics.

4.11 Chapter summary

In this chapter I examined two things: 1. the thermodynamic aspects of self-organisation in a generalized version of the BTW model of SOC. 2. Spatial and temporal characteristics of SOC. The main conclusions are as follows:

- For the Generalized BTW model (NBTW), I find that when dissipation is present ($\alpha < 1$), criticality is lost in the system and the radiated seismic energy is best described by a sub-critical gamma distribution rather than a pure power-law.
- Unlike the external energy properties (E_i and $P(E_i)$), the internal energy fluctuations at steady-state resemble those of equilibrium systems in two ways. Firstly, they show a Gaussian distribution in their fluctuations and secondly, a Brownian noise signature, as shown from the time series analysis. These two observations are similar to what is seen in say gasses at equilibrium (D'Anna et al., 2003). This is an important result that suggests that our perception of the criticality of a driven system may be observer dependant. That is, if the observer is *inside* or *outside* the system.
- The external and internal entropies are negatively correlated. This is consistent with the idea that systems self-organise to increase entropy globally (e.g. Bridgman, 1950).

- The external and internal energies of the locally driven system shown here are found to be positively correlated. This is what is also found for globally driven CA models (e.g. Main et al., 2000).
- The relation between S_e and $\langle \ln E_e \rangle$ was found to follow a curve rather than a straight line (see section 3.6, chapter 3). This is further evidence that we are dealing with a sub-critical system when dissipation is present. Conversely, we get a negative correlation between S_i and $\langle \ln E_i \rangle$
- For both internal and external cases, the temperatures T_T was found to correlate well with their relative entropies. This is in agreement with the notion that statistically 'hot' systems are less predictable (Rinaldo et al., 1996; Sornette, 2000).
- The prediction that the mean radiated energy and conservation parameter α are related by a power-law was confirmed for the NBTW model where $\langle E_e \rangle \sim (\alpha_C - \alpha)^{-0.975}$ (note $\alpha_C = 1$).

Moving on to SOC, there are several important results found here that question our current understanding of SOC and how it should be applied:

- Spatial heterogeneity exists in the BTW model of SOC. This is in the form of more cells breaking away from the edges. This observation disappears when dissipation is present (but so does criticality!). This is due to cells being more likely to break away from the edges since they have more neighbours to interact with and therefore statistically more likely to receive energy and fail.
- Despite the spatial bias observed, the size of events do not appear to be related to their position of initiation. This can explain why we still get a power-law despite the spatial bias (point above).
- Analysing the BTW model on a regional level, it was found that the energy probability distributions for the sub-regions follow a power-law in the centre and a gamma 'sub-critical' distribution at the edges. Despite this, the distributions still show the same slope ($B \sim 1$). This confirms that for a model of SOC, universality is conserved.
- From a temporal point of view, the NBTW model was found to be statistically in disagreement with what is claimed of accelerated seismicity preceding large events.

– I propose a more lenient version of SOC which I refer to as self-organised sub-criticality (SOSC). This is simply in accordance with the NBTW model and can accommodate gamma distributions, internal dissipation and variations in scaling exponents and correlation lengths; more in tune with natural systems.

4.12 Afterthoughts

Looking at the model from a thermodynamic prospective, what predictions can we make about the Earth's lithosphere? We have seen that the internal and external energy here are correlated reassuring us that for a driven system, the free energy is proportional to the amount of energy being released. This may appear counter intuitive when compared to equilibrium systems. We have also seen the dominating effect of even a small amount dissipation on the system energy and spatial heterogeneity. Dissipation may therefore strongly influence the amount of energy stored in the crust; the higher the dissipation the lower the free energy and the higher the energy dissipated irreversibly (such as through heat). Dissipation also influences the shape of the probability density distribution (and therefore the entropy) from a power-law to a gamma with increasing energy loss. One could suggest from this that for seismically active areas, if dissipation is high, the earthquakes will follow a gamma distribution with a low θ (and perhaps higher B?) and there will be more heat loss. This will also be represented in dissipative areas having a lower S_e.

On the other hand, spatial variations in B values would violate what is observed from the regional study of the BTW model even if we are to relax the definition of SOC to include gamma type statistics. Ironically, spatial variations in the amount of seismicity are found not to contradict SOC, this reassures the notion that SOC systems need not be on the point of global failure everywhere (e.g. Sornette, 2000). The relevance of these predictions will be investigated on real earthquake populations in the following chapter.

Chapter 5

Testing criticality in global earthquake populations

So far, we have seen the statistical and thermodynamic aspects of self-organisation and dissipation analytically and through the use of a numerical model. It has been shown through the gamma entropy equation, relating the mean expectation of the logarithm of energy $\langle \ln E \rangle$ and the entropy S, how one may assess the 'criticality' of a gamma type system. The analytical predictions were then tested on a generalised numerical model of seismicity in the previous chapter. Self-organised criticality (SOC) in the Bak et al. (1987) numerical model (BTW) was also examined in some depth to pinpoint characteristics of SOC.

In this chapter I test some of the predictions and conclusions of the last three chapters on *real* global earthquake data. I do this to attempt to answer some remaining questions regarding criticality in the crust. I must at the expense of repetition emphasise that when I use the term 'critical', I do not exclusively mean SOC. With 'critical' I refer thermodynamically to the criterion outlined in chapter 3. That is, a linear relationship between the entropy S and its corresponding energy $\langle \ln E \rangle$ ($\theta \rightarrow \infty$). Conversely, with 'SOC', I refer to the phenomenological characteristics I demonstrated from the original BTW model of SOC in chapter 4. Keeping this distinction between the two in mind, I accordingly attempt to answer the following questions, as in the last chapter, in two parts. The first part looks at thermodynamic aspects and investigates the following points:

1. Is the analytical prediction relating entropy and energy applicable to real earthquake data? Also, given the thermodynamic criteria encapsulated by the gamma entropy equation in chapter 3, is the Earth's crust in a critical state? I assess criticality from a thermodynamic perspective by testing the expression for gamma entropy derived in chapter 3 ($S \sim B\langle \ln E \rangle$) on real earthquake populations.
2. If the crust is critical, does criticality hold temporally *and* spatially? It is important to address these two separately since any temporal variations, for example, may be smoothed out by grouping the data spatially and vice-versa. In this chapter, I test the gamma entropy equation on earthquake populations that are grouped first temporally and then spatially.

The second part looks at self-organised criticality in relation to earthquakes and addresses the following issues:

1. Looking at the criteria deduced from the study of the BTW model in chapter 4, is the crust strictly SOC? I have shown for the BTW model of SOC that the B exponent does not change regionally and universality is maintained (section 4.9.2). Can the same be said about the crust?
2. Does SOC best describe the crust or are there other hypotheses that are more consistent with the data?

Some of the main results of this chapter are published in Main and Al-Kindy (2002) and Al-Kindy and Main (2003) (see appendix).

5.1 'Critical'?

To reiterate some of the points made in chapters 2 and 3, is the crust 'critical'? This appears to depend on what an author means by 'critical'. There are many studies assessing 'criticality' (or 'self-organised criticality') in the crust on real data populations, many of which use 'critical' to mean different things. Unfortunately, these are often conducted using confused or even erroneous assumptions. I highlighted in chapter 2 (section 2.7.2) how a driven 'critical' system is different from the classical equilibrium thermodynamic definition of a critical point (CP) system. However, Zöller and Hainzl

(2001), for example, use a spatial correlation length that grows in a power-law fashion with time preceding a large earthquake as an indicator to the crust being a critical point (CP) phenomena. Similar approaches are given by Shaw et al. (1992), Bowman et al. (1998), Robinson (2001) and Zöller et al. (2001). However, a growing correlation length preceding large events is not a property of an open driven or SOC system (Jensen, 1998; Sornette, 2000). I confirmed this statistically for a numerical model of SOC in section 4.9.3. The growing correlation length approach should only be applied to an equilibrium system such as the Ising or percolation model that has a specific critical point rather than the attractor critical state associated with SOC. Therefore, for a driven system, a systematically growing correlation length prior to a large event should not be a requisite for a system to be in a state of SOC.

Another approach used in earthquake 'prediction' is that of *fracture criticality* where variations in time delays associated with shear wave splitting are reported to occur before large earthquakes (Crampin, 1994; Crampin et al., 1999). The term 'criticality' here is used to describe the sensitivity of the rock to breaking (analogous to the percolating model close to the percolation threshold (section 2.6.3). This is more in tune with equilibrium systems close to the critical point rather than driven dissipative systems. Similarly, Grasso and Sornette (1998) examine criticality in triggered earthquakes but correctly define 'criticality' in terms of 'large susceptibility' and its association with SOC. It is this 'loose' use of the word 'critical' that leads me to emphasise what is meant by it here and to avoid any confusion. Here I use a thermodynamic approach derived in chapter 3 in assessing the criticality from the seismic energy release from the crust. In summary, for logarithmic bins -as used throughout this chapter-:

$$S = B\langle \ln E \rangle \quad \rightarrow \quad critical \tag{5.1}$$

$$S \neq B\langle \ln E \rangle \quad \rightarrow \quad non - critical \tag{5.2}$$

5.2 The Harvard Centroid Moment Tensor (CMT) Catalogue

I mentioned in chapter 2 that earthquakes usually occur when strain energy stored in the Earth's lithosphere is suddenly released; a frictional resistance along a fault plane is overcome and relative motion or 'slip' occurs (figure 5.1). The analysis of this motion can be used to give information on the size and orientation of the fault plane. This analysis is called a *focal mechanism solution* (Kearey and Vine, 1996). The arrivals of the seismic waves from the fault are measured by a series of global multi-component seismographs that measure the amplitude of the arriving seismic waves in three dimensions. The radiated amplitudes of seismic waves along three axis can be reduced to what is

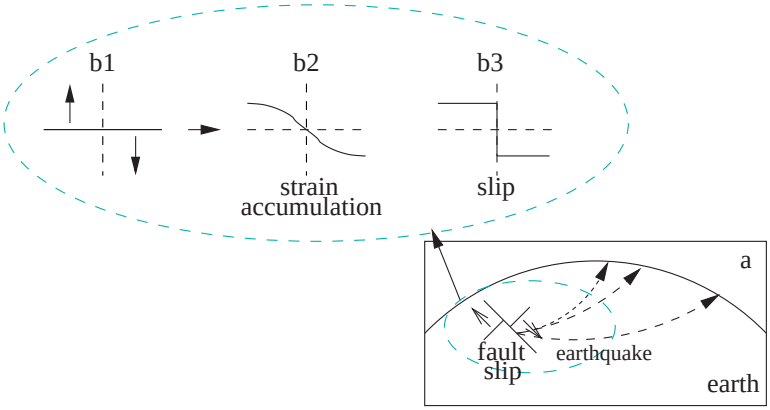

Figure 5.1: Earthquake process in the crust: a) Earth cross-section showing activated fault with radiated seismic waves (dashed arrows) and b) Seismic process: b1. fault after rupture, b2. accumulation of strain and b3. a slip along a fault.

known as the *scalar seismic moment* or M_O which is measured in Nm. The details of how this is calculated are not relevant here. What is important is that *'the best measure of earthquake size and energy release is the static (or scalar) seismic moment* (Stein and Wysession, 2003). This is why I shall primarily use the scalar moment as a measure of earthquake size in this study.

The primary source of moment data internationally is the Harvard Centroid Moment Tensor catalogue, usually referred to as the CMT catalogue. From the moment data

solutions, we can calculate a corresponding *moment magnitude*[1] m using (e.g. Kagan, 2002)

$$m = \frac{2}{3}\log_{10} M - 6.0 \tag{5.3}$$

and the corresponding seismically radiated energy E can be calculated approximately using (Kanamori and Anderson, 1975; Scholz, 2002)

$$\log_{10} E = 1.5m + 4.8 \tag{5.4}$$

where E is in Joules. The CMT catalogue's record begins in 1977 and at the time of writing this thesis is published at http://www.seismology.harvard.edu/.

5.3 Analysis

In this chapter, the thermodynamic parameters of the data are measured in a similar way to the methods used in chapter 4. Because of the nature of the crust, internal properties (those with subscript i in the results section of chapter 4) such as strain cannot be measured so only external properties derived from the radiated energy are calculated. However, in the previous chapter, I was dealing with a large synthetic data set with no notable measuring errors. Here, with real data, more caution is required.

5.3.1 Data and magnitude range

Smaller earthquakes are not recorded in global data sets. To estimate the cut-off magnitude, the incremental probability-magnitude distribution is plotted in figure 5.2. This shows that the deviation from the Gutenberg-Richter law occurs at $m \sim 5.5$. Data for the values $m \geq 5.5$ are therefore considered to be complete for the purposes of this study. Kagan (1997; 2002) reports that the CMT catalogue is complete only for magnitudes $m \geq 5.4$ for the period 1987 onwards and $m \geq 5.6$ from 1982 onwards. Figure 5.3 shows the number of earthquakes recorded per year n for $m \geq 5.5$ 1977-2000. It can be seen that there is a sudden increase in the numbers after 1982. However, I have found that this does not significantly influence the results calculated here (see figure 5.15 which has data for period 1977-2000).

[1] The moment magnitude is denoted M_W in the literature but for simplicity denoted m here.

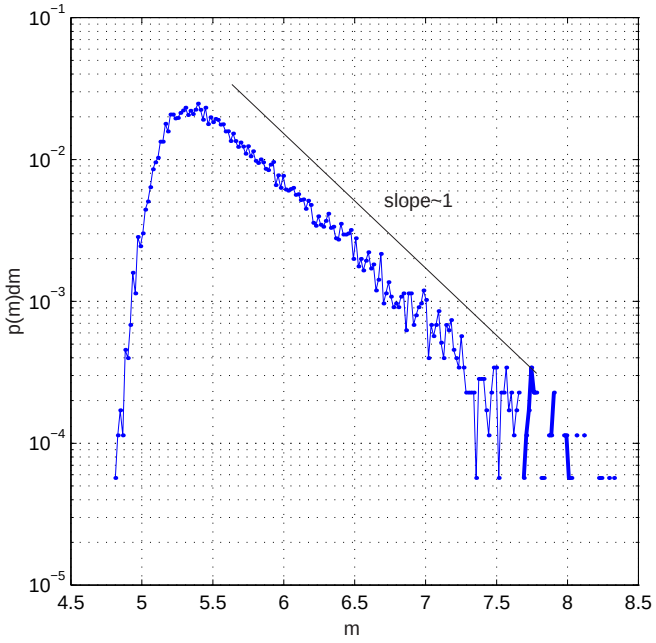

Figure 5.2: Incremental magnitude probability distribution for all CMT data 1977-2000 showing data completeness for $m \geq 5.5$. The solid line is of slope -1 for reference.

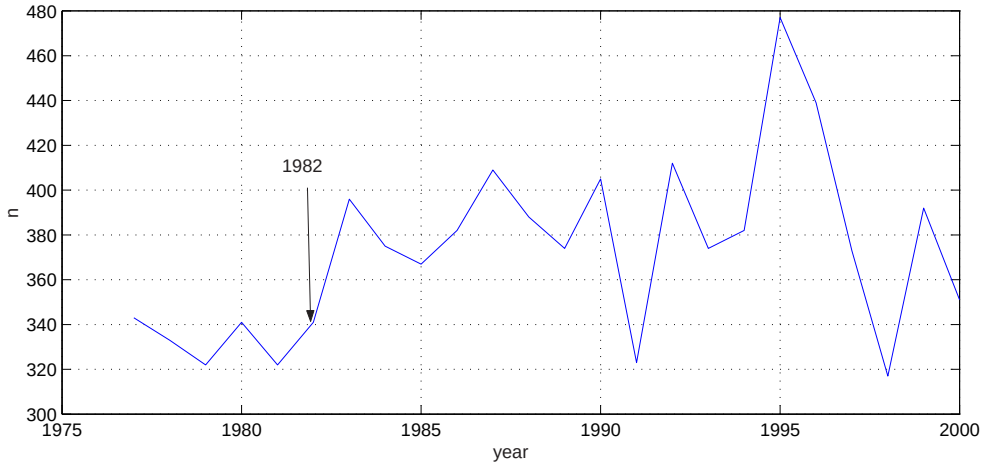

Figure 5.3: Number of recorded events per year n for period 1977-2000 inclusive for moment magnitudes $m \geq 5.5$.

In summary, I use the CMT data for $M \geq 5.5$ for the period 1977-2000 for all depth ranges giving a total of 9042 events. All data are shown in figure 5.4.

5.3.2 Bin widths

The data are binned in the magnitude domain δm (equivalent to logarithmic bin widths $\delta \ln E$). Because the data are limited in numbers, the bin width used to produce the energy incremental probability distribution must be chosen with caution. If it is too narrow (more bins) there will be more empty bins that will destabilise the calculations of S, B, etc. This is shown in figure 5.5a. Conversely, if the bin widths are too wide, we may be filtering out characteristics of the probability distributions. This is depicted in figure 5.5b. By trial and error, I determine that the ideal bin-width for this study is $\delta m = 0.25$. From the binned energy data (equation 5.4), I follow the same procedure in chapter 4 (section 4.7) to calculate $p(E)$, S and so on.

5.3.3 Scaling exponents

In addition to the parameters already outlined, I also investigate universality to see if the earthquake energy probability distributions give a constant scaling exponent B consistent with requirements of SOC, or if they vary in contradiction to it. Although there are numerous studies on the variation of scaling exponents with space and time (e.g. Ogata et al., 1991; Öncel et al. 2001; Cao and Gao, 2003), there are also studies that suggest it is constant (e.g. Frohlich and Davis, 1993; Kagan, 1999; Godano and Pingue, 2000). It is difficult to quantitatively compare the results of these studies in terms of scaling exponents for the following reasons:

1. The studies use different techniques to calculate the scaling exponents that may cause variations in the results. These include Aki's maximum likelihood method (Aki, 1965), rank ordering statistics (Sornette et al., 1996), linear least squares fits (Scholz, 1997; Godano and Pingue, 2000; Al-Kindy and Main, 2003; Amitrano, 2003) and fitting the gamma distribution and variations thereof (Main and Burton, 1986; Kagan, 1997; Koravos et al., 2003).

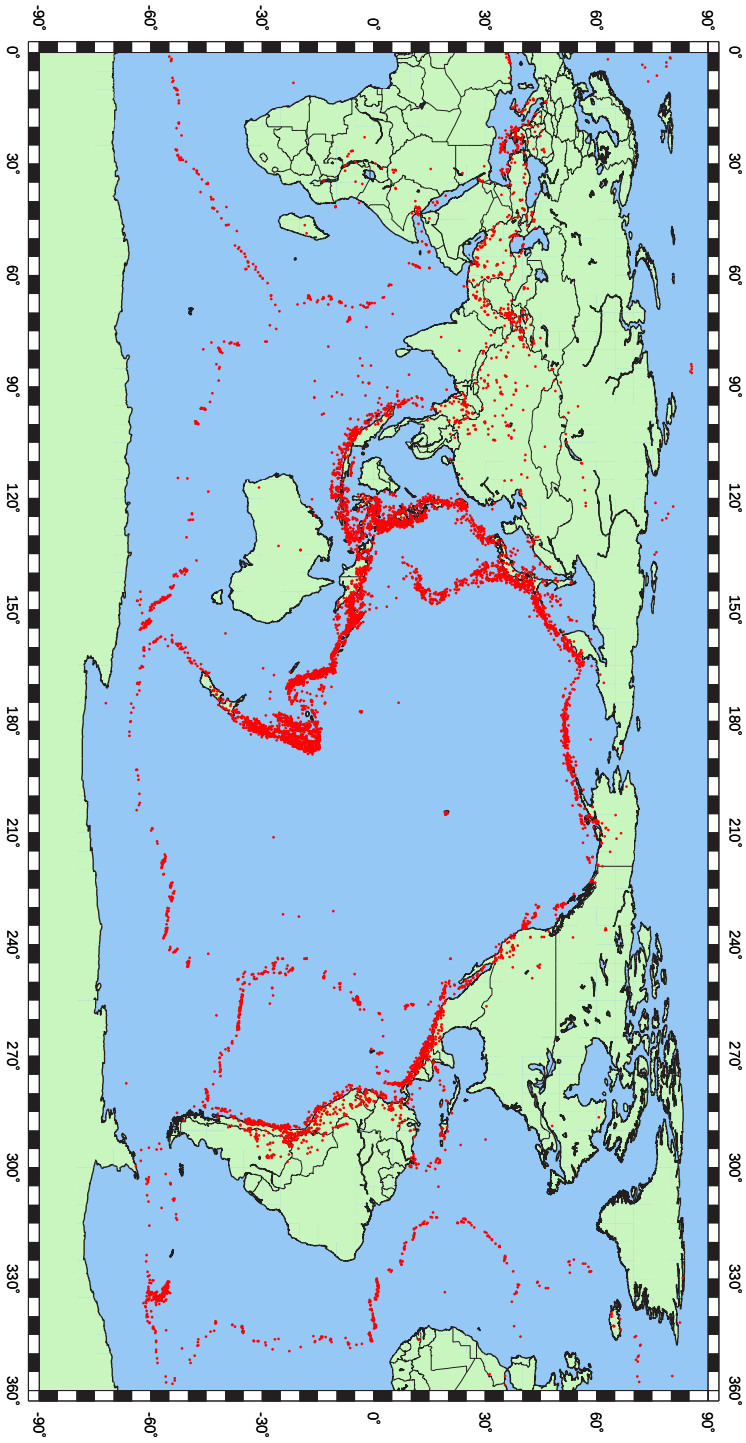

Figure 5.4: World map showing all CMT earthquake data locations for $M \geq 5.5$, 1977-2000.

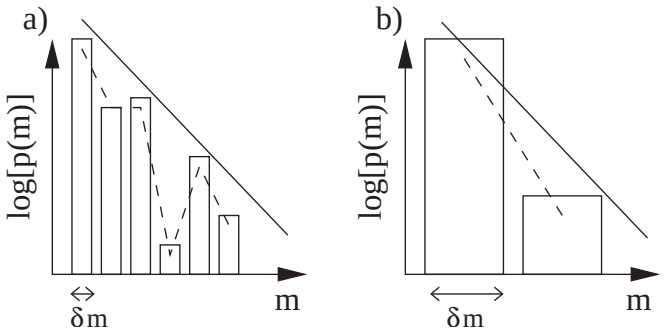

Figure 5.5: The effect of bin width δm being a) too narrow, b) too wide.

2. The majority of these studies mentioned calculate the scaling exponent on the cumulative frequency distribution. This smoothes the data and may introduce bias in the results (Main, 2000). I therefore, as in chapter 4, only use incremental distributions.

3. Regional studies on the scaling exponents tend to cover a specific area chosen for a particular study. In this study, I will follow the method of Kagan (1997) regionalising the data using the standard Flinn-Engdahl classification (Flinn and Engdahl, 1974) described below.

For these reasons, I use three methods to calculate the scaling exponents in this study. The results can then be compared with other studies and with one another:

1. I calculate B using a **Least Squares Fit** (LSF) through the linear (power-law) part of the energy probability distributions. I refrain from fitting a gamma fit since my primary interest here is in the slope of the distribution. Therefore, there is no need to introduce the extra parameter θ. B as mentioned in chapter 2 usually takes an average value of $\sim \frac{2}{3}$ worldwide (e.g. Frohlich and Davis, 1993)

2. The b (called b_1 hereon) value using **Aki's maximum likelihood method** (1965) is calculated by measuring the mean magnitude:

$$b_1 = \frac{\log_{10} e}{\langle m \rangle - m_C} \tag{5.5}$$

Here $\langle m \rangle$ is the mean magnitude, m_C is the minimum cut-off magnitude (5.5 in this case) and $b_1 \sim 1$ globally on average. This method is extensively used in

the literature and interestingly shares some similarities with the gamma entropy equation. Note that b_1 depends mainly on the mean of the magnitude, similar to S_γ, which depends on $\langle \ln E \rangle$ and $m \sim \ln E$ (chapter 2). Although we calculate a scaling exponent, it is not certain from the obtained value that the distribution of m is necessarily a power-law. m indeed might follow any distribution. I therefore use this calculation in conjunction with B which confirms whether the distribution of m or E is a power-law. Using this somewhat 'popular' method makes comparison of my results with other published results feasible.

3. I finally calculate a scaling exponent b_2 using rank order statistics (ROS). This statistical method has been used in various disciplines including linguistics and DNA analysis (Mantegna et al., 1995) and has also been applied to earthquake populations (Sornette et al., 1996; Sornette, 2000). The method simply involves putting events in order of their size with the largest event being rank 1 and the second largest rank 2 and so on. The event sizes are then plotted against their rank. In accordance with Sornette et al. (1996), if the slope of a power-law scaling exponent is μ, then the slope of the size vs. rank plot will be $\frac{1}{\mu}$. For the case of magnitude data, the slope of the magnitude vs. rank plot will be $\frac{1}{b_2}$.

5.4 The temporal study

I now examine the CMT data in time. I bin the data in yearly intervals and calculate the external thermodynamic variables I examined in chapter 4.

5.4.1 Testing criticality

The magnitudes and energies are calculated from the moment data using equations 5.3 and 5.4 respectively. The magnitude and energy release data are shown in figure 5.6. Note the similarities between figure 5.6 and the numerical results of figure 4.6. The mean energies released per year are calculated by taking the annual averages of all values of $\ln E$ and E to give $\langle \ln E \rangle$ and $\langle E \rangle$ respectively. I then bin the yearly data to produce discretized probability distributions calculating $p(E)$ from which I also calculate the

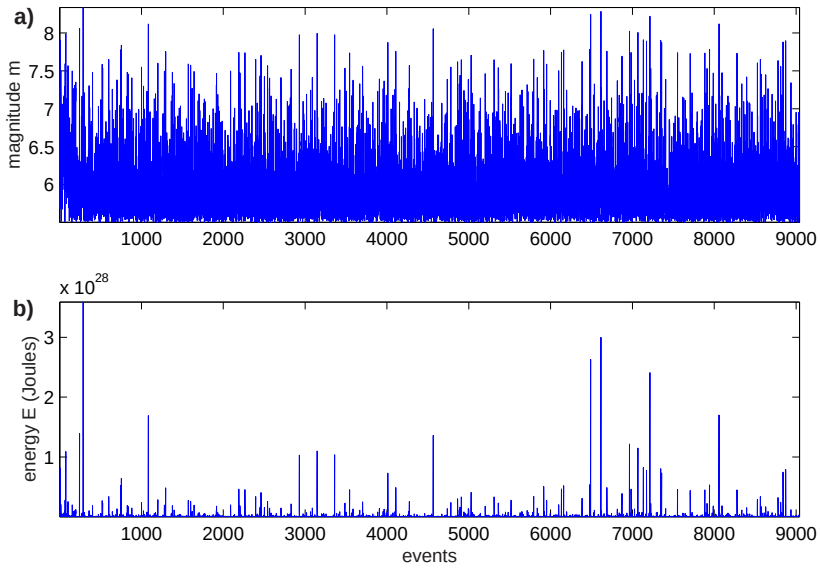

Figure 5.6: Plot of a) moment magnitude release and b) energy release for all data $m \geq 5.5$.

entropy (equation 3.21). I also measure the maximum energy released in a year E_{max}. The results of this analysis are shown in figure 5.7. Note from figure 5.7 that there is a good correlation between S and $\langle \ln E \rangle$ as predicted by equation 3.26 (chapter 3). I then check to see if the temporal data are critical by plotting S against $\langle \ln E \rangle$ in figure 5.8. Figure 5.8 firstly confirms that **the prediction of the gamma entropy equation is applicable to a real earthquake population**. Because of the linear nature of the fit, the results also suggest that earthquake seismicity *temporally* is 'critical' or at least very nearly critical following the criteria outlined in chapter 3. It should also be noted here that the slope of the linear line ($y = 0.6275x - 18.73$) gives a slope of $B_S \sim \frac{2}{3}$ which is in agreement with global estimates (e.g. Kagan, 2002). It must be said that although the inferred slope is a *pleasing* result, it is somewhat coincidental. As I demonstrated in chapter 3 (section 3.7.3), the calculated value of S will depend on the number of bins used. Keeping everything constant, If I were to increase or decrease δm here, this would alter the calculated value of B_S. It was another assumption associated with the derivation of the gamma entropy equation that $\langle E \rangle$ and $\langle \ln E \rangle$ are not correlated. I tested this in figure 5.9. We can see from figure 5.9 that there is a negligible correlation between the two with $R^2 = 0.09$.

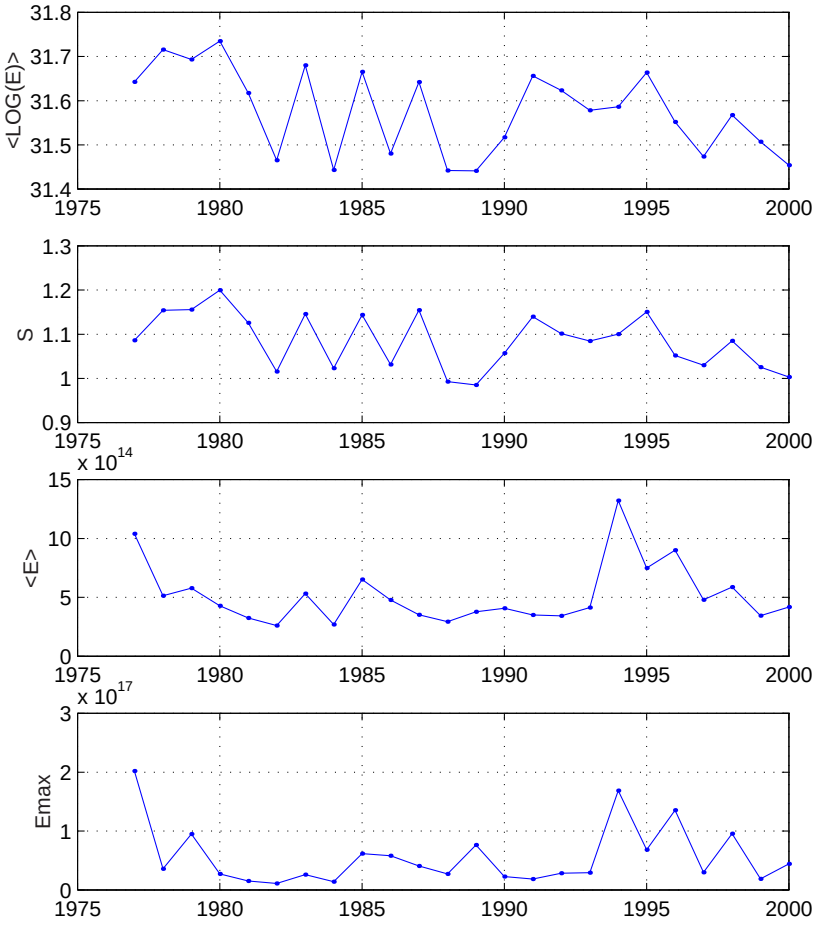

Figure 5.7: Plots of annual variations of thermodynamic parameters (top to bottom) $\langle \ln E \rangle$, S, $\langle E \rangle$ and E_{max} 1977-2000.

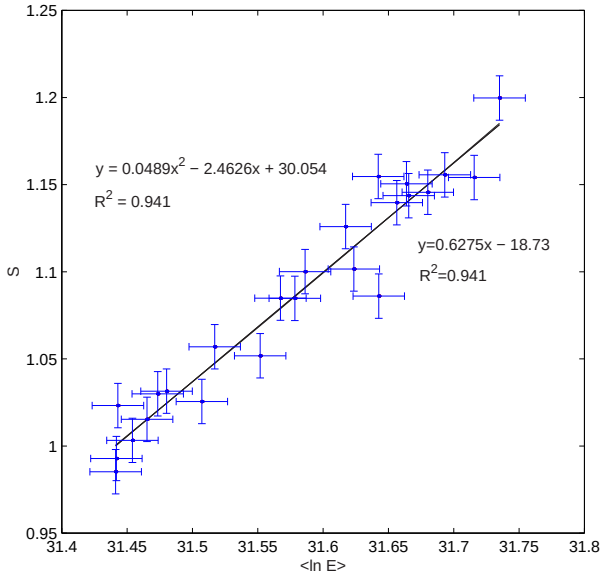

Figure 5.8: Plot of S against $\langle \ln E \rangle$ for temporal data for years 1977-2000. The black line(s) are linear and quadratic least squares fits that are indistinguishable. The error bars are calculated to one standard error.

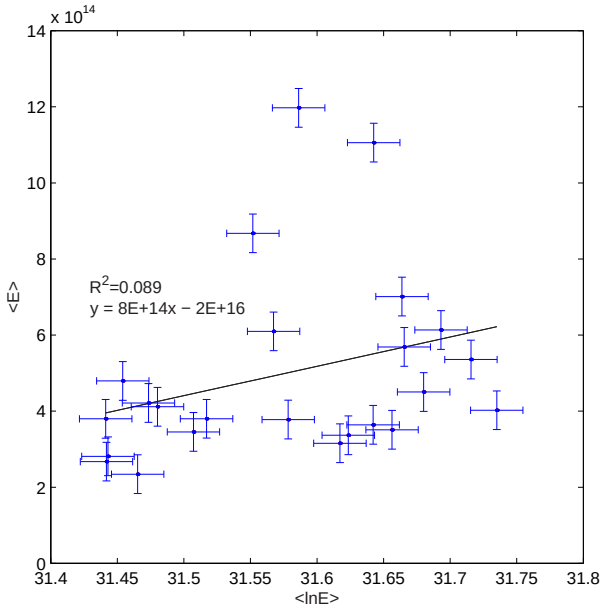

Figure 5.9: Plot of $\langle E \rangle$ against $\langle \ln E \rangle$ showing a negligible correlation ($R^2 = 0.09$).

5.4.2 'Tectonic' temperature T_T

Following the statistical definition of effective/tectonic temperature (denoted T_T here) (see section 4.7.3), I now measure T_T with time for the radiated energy. I also compare its temporal variation with the mean energy release $\langle E \rangle$. This is shown in figure 5.10a. It can be seen that there is a coupling between the tectonic temperature and the mean energy release. To further demonstrate this, I plot T_T against $\langle E \rangle$ in figure 5.10b. We can see from figure 5.10b that there is a good correlation between the two. This result is in agreement with that found for the numerical NBTW model (figure 4.17), suggesting that areas of higher mean energy release will be of higher 'temperature' and therefore less predictable. This is since higher temperatures are associated with larger more erratic fluctuations in energy.

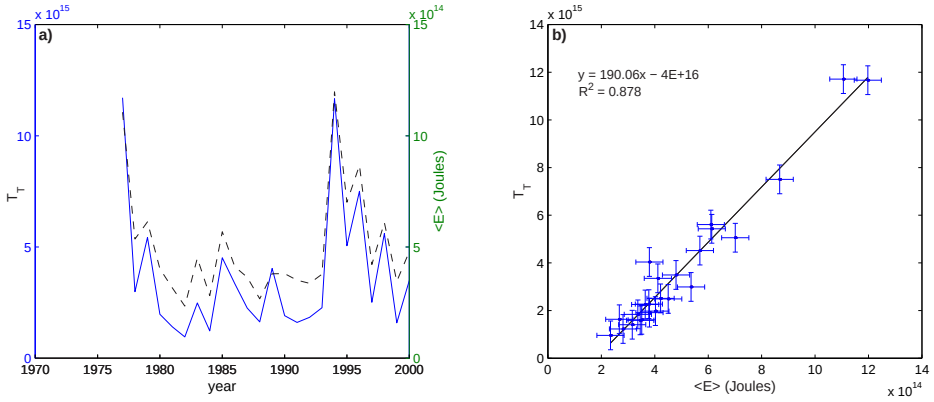

Figure 5.10: Plot of a) Temporal variation of energy $\langle E \rangle$ (dashed line) and temperature T_T (solid line) for period 1977-2000. b) T_T against $\langle E \rangle$ showing a positive correlation between the two.

5.4.3 Three scaling exponents

From the data, I now calculate the three scaling exponents B, b_1 and b_2, defined in section 5.3.3. I calculate B from the probability distribution of the energy release. This is shown in figure 5.11. The figure shows the very close to power-law nature of the annual data. The results of b_1 are given in table 5.1. I then calculate b_2 from the rank ordering of the magnitude data. This is shown in figure 5.12. A summary of the results of the scaling exponents with time is shown in figure 5.13. In chapter 3, it was shown that the scaling

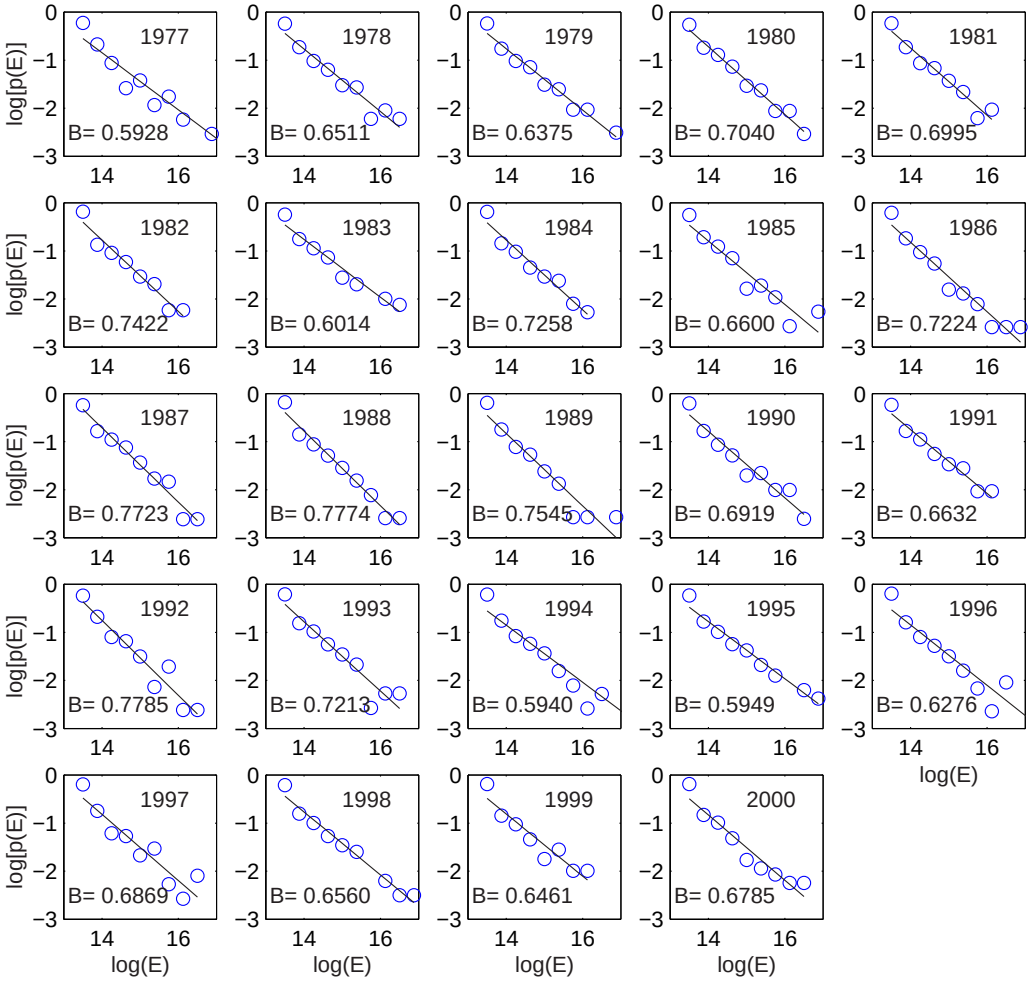

Figure 5.11: Plot of probability distributions for annual energy data 1977-2000 showing slopes of distributions B.

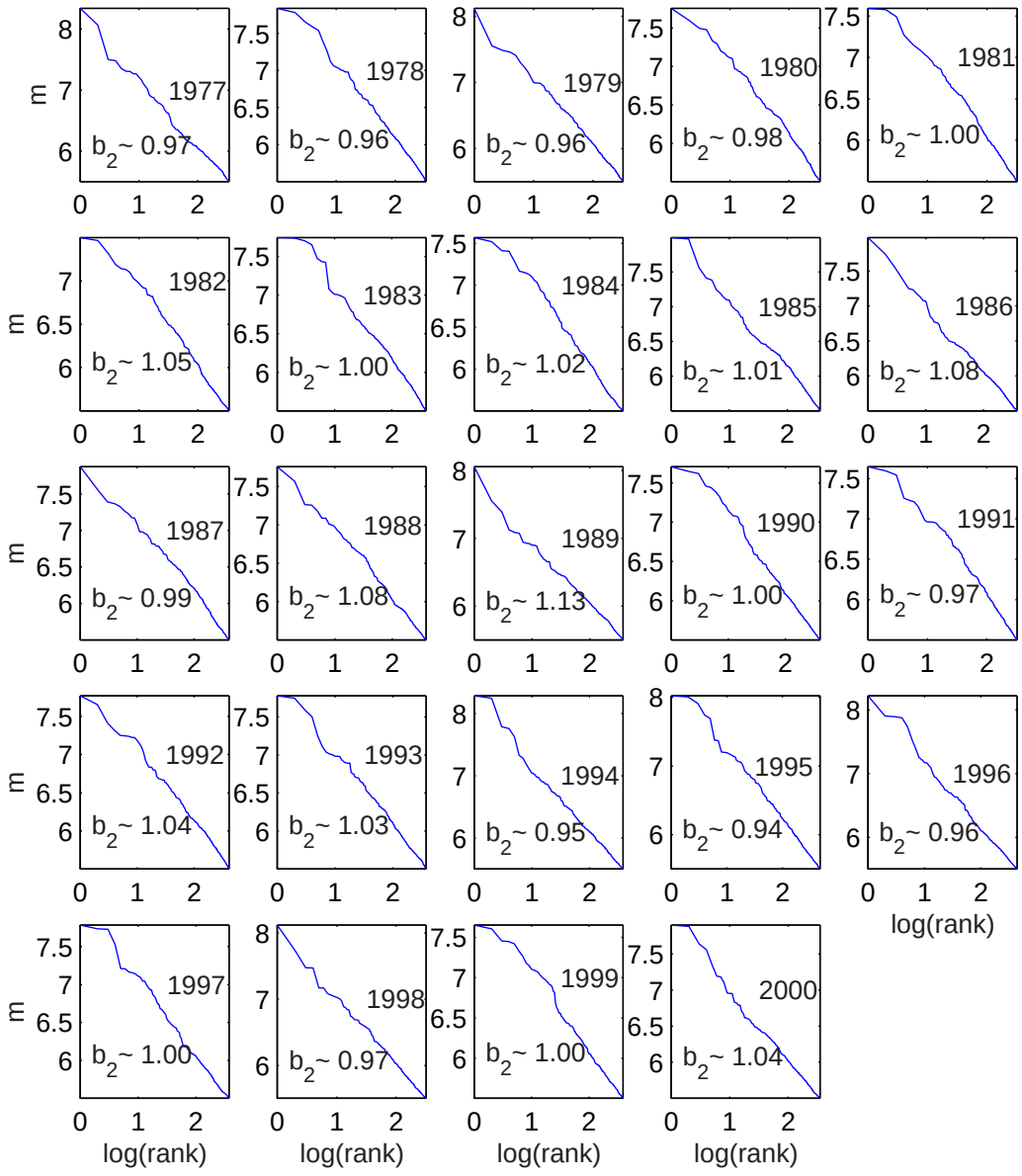

Figure 5.12: Rank ordering plots showing magnitude against rank for annual moment magnitude data and values of b_2.

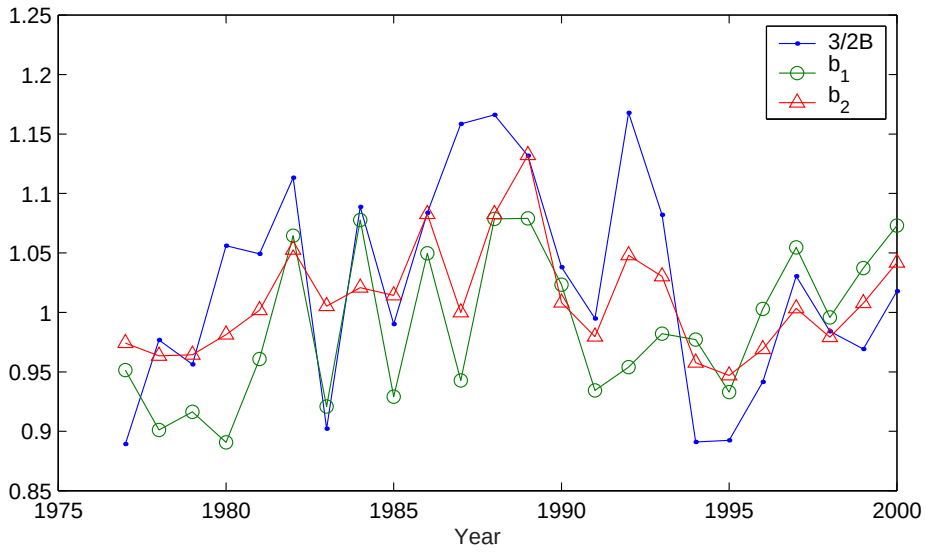

Figure 5.13: Plot of temporal variations of scaling exponents B, b_1 and b_2 1977-2000. The B exponent is rescaled for comparison with b_1 and b_2.

exponent can have an effect on the mean energy and entropy of a data set since it will be one of the parameters governing the *shape* of a distribution (section 3.6.1). I now investigate if there is any correlation between the three scaling exponents calculated and the main thermodynamic variables measured, namely, $\langle \ln E \rangle$, S and $\langle E \rangle$. These results are shown in figure 5.14. The results show in almost all cases there is at least a weak negative correlation between the thermodynamic variables and the scaling exponents measured. The most notable correlation is seen in figure 5.14*b*. We can see that there is a very distinct negative correlation between b_1 and $\langle \ln E \rangle$. This is not surprising because $m \sim \ln E$ (Kanamori and Anderson, 1975) and given b_1 depends on $\langle m \rangle$ (equation 5.5). However, there is no apparent correlation between B and $\langle \ln E \rangle$ in figure 5.14*a*. This would suggest that either the two are not related for real earthquake populations *or* that the B values are on average universal, therefore clustered around a particular value and not showing any obvious change with $\langle \ln E \rangle$.

5.4.4 Data check

In chapter 4, every run had the same number of data points. Here, the numbers vary annually as depicted by figure 5.3. I therefore plot the thermodynamic and scaling expo-

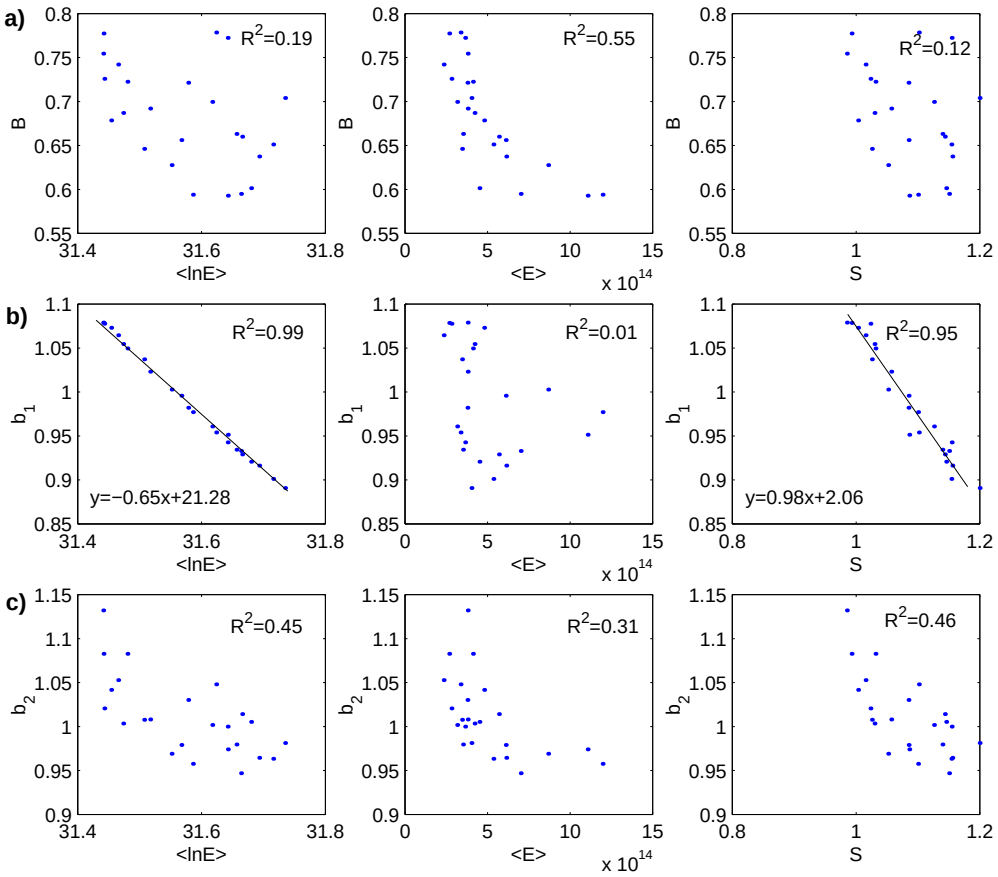

Figure 5.14: Plot of $\langle \ln E \rangle$, S and $\langle E \rangle$ against a) B, b) b_1 and c) b_2.

nent variables against their annual totals to see if there are any systematic dependencies on data numbers. This is shown in figure 5.15. The figure shows no obvious dependence of any of the variables on their numbers. This validates using the pre-1982 data since the number of points does not influence the results. This concludes the temporal study of the

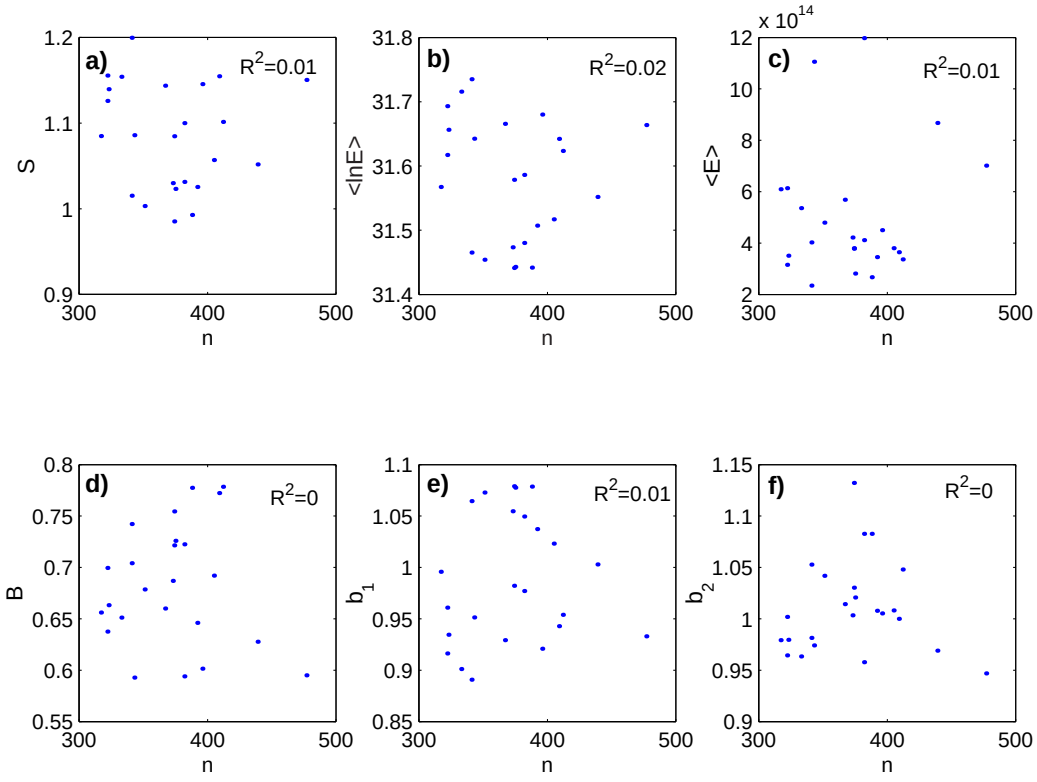

Figure 5.15: Plot of a) S on n b) $\langle \ln E \rangle$ on n c) $\langle E \rangle$ on n d) B on n e) b_1 on n f) b_2 on n for $1977 - 2000$ data.

CMT catalogue. The results of the temporal study are summarised in table 5.1.

5.5 The spatial (regional) study

5.5.1 Flinn-Engdahl regionalisation

Flinn and Engdahl (1974) developed a standard to subdivide the Earth based on geographic and geological constraints (referred to here as the FE regionalisation). Although the classification has several hundred subdivisions, it broadly divides the earth in to 50

year	n	$\langle \ln E \rangle$	$\langle E \rangle \times 10^{15}$	S	$T_T \times 10^{16}$	B	b_1	b_2
1977	343	31.64	1.11	1.09	1.17	0.59	0.95	0.97
1978	333	31.72	0.54	1.15	0.30	0.65	0.90	0.96
1979	322	31.69	0.61	1.16	0.54	0.64	0.92	0.96
1980	341	31.74	0.40	1.20	0.20	0.70	0.89	0.98
1981	322	31.62	0.32	1.13	0.14	0.70	0.96	1.00
1982	334	31.47	0.23	1.02	0.10	0.74	1.06	1.05
1983	396	31.68	0.45	1.15	0.25	0.60	0.92	1.01
1984	375	31.44	0.28	1.02	0.12	0.73	1.08	1.02
1985	367	31.67	0.57	1.14	0.45	0.66	0.93	1.01
1986	382	31.48	0.41	1.03	0.34	0.72	1.05	1.08
1987	409	31.64	0.36	1.15	0.23	0.77	0.94	1.00
1988	388	31.44	0.27	0.99	0.16	0.78	1.08	1.08
1989	374	31.44	0.38	0.99	0.40	0.75	1.08	1.13
1990	405	31.52	0.38	1.06	0.19	0.69	1.02	1.01
1991	323	31.66	0.35	1.14	0.16	0.66	0.93	0.98
1992	412	31.62	0.34	1.10	0.18	0.78	0.95	1.05
1993	374	31.58	0.38	1.08	0.23	0.72	0.98	1.03
1994	382	31.59	1.20	1.10	1.17	0.59	0.98	0.96
1995	477	31.66	0.70	1.15	0.51	0.60	0.93	0.95
1996	439	31.55	0.87	1.05	0.75	0.63	1.00	0.97
1997	373	31.47	0.42	1.03	0.25	0.69	1.05	1.00
1998	317	31.57	0.61	1.08	0.56	0.66	1.00	0.98
1999	392	31.51	0.35	1.03	0.16	0.65	1.04	1.01
2000	351	31.45	0.48	1.00	0.35	0.68	1.07	1.04
average	**8938**	31.58 (0.01)	0.50 (2.49)	1.09 (0.06)	0.37 (2.95)	0.68 (0.06)	0.99 (0.06)	1.01 (0.05)

Table 5.1: Summary of results for annual temporal study. The totals are given in bold and standard deviations are given in brackets.

tectonic regions numbered 1 to 50 (called the FE number). These are shown earthquake locations in figure 5.16. The FE coordinates used to construct figure 5.16 and to regionalise the CMT data in this study were obtained from the United States Geological Survey (ftp ghtftp.cr.usgs.gov). I then incorporated the FE data into a matlab code to analyse and subdivide the CMT earthquake data. The FE system predates the CMT catalogue. This means that there cannot be any spatial retrospective bias in the data selection by using it (Kagan, 1997; Al-Kindy and Main, 2003a). Also, because the FE classification is standardised, the results shown here can be reproduced, compared and checked against results of other authors using the same classification. I group the data into tectonic zones following Kagan's grouping in *Kagan* (1997). The four subgroups of Kagan[2] (1997) based on tectonic deformation style are as follows and are defined in accordance with Fowler (1990) and Kearey and Vine (1996):

1. **Subduction zones**: These are areas of tectonic plate destruction where oceanic lithosphere subducts under continental or oceanic lithosphere. This can generate earthquakes up to depths of 700 km. Subduction zones are characterised by high seismic activity, volcanic arcs and large earthquakes. In accordance with Kagan (1997) these are FE regions 1, 5, 6, 7, 8, 12, 13, 14, 15, 16, 18, 19, 20, 21, 22, 23, 24 and 46. Examples include Japan, the Caribbean Loop and Alaska-Aleutian Arc.
2. **Collision zones**: These are areas where continental crust collide. These areas are characterised by the formation of mountain belts. In accordance with Kagan (1997) these are FE regions 25, 26, 27, 28, 29, 30, 31, 41, 47 and 48 and include Northern India and Western and Eastern Asia.
3. **Intra-continental zones**: These are areas where the lithosphere is deformed under the influence of extensional forces and are found on continents of various settings. In accordance with Kagan (1997) these are FE regions 34, 35, 36, 37, 38, 42, and 49. The main example is the African Rift Valley.
4. **Mid-ocean ridges**: There are areas in the oceans where new oceanic lithisphere is constructed as new material rises from the mantle and the plates spread apart. They are characterised by shallow earthquakes and add to a total length of 60,000

[2]Kagan has a fifth grouping of 'others' which do not fit into any of the four categories given here. Although these are shown where possible, they are not used in the final spatial analysis.

Figure 5.16: World map showing Flinn-Engdahl regionalisation that subdivides the world into 50 regions. Earthquakes within regions are also shown.

km worldwide. Ridges play an important role in the dissipation of heat and are responsible for approximately 60% of global heat loss (Sclater et al., 1996). In accordance with Kagan (1997) these are FE regions 4, 32, 33, 40, 43, 44 and 45 that include the Mid-Atlantic and Indian Ocean ridges.

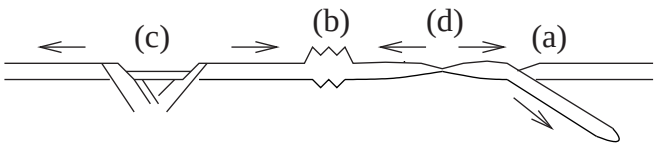

Figure 5.17: Schematic of the four deformation styles in the crust: a) Subduction zone, b) Collision zone, c) Intra-continental zone, d) Mid-ocean ridge.

It is important here to note from 5.16 that the regions are of different size and there may therefore be a more pronounced variation in the number of earthquakes within each area bin when compared with the yearly bins of the temporal study (figure 5.3). I demonstrate this in figure 5.18. We can see from figure 5.18 that the variation in number of events

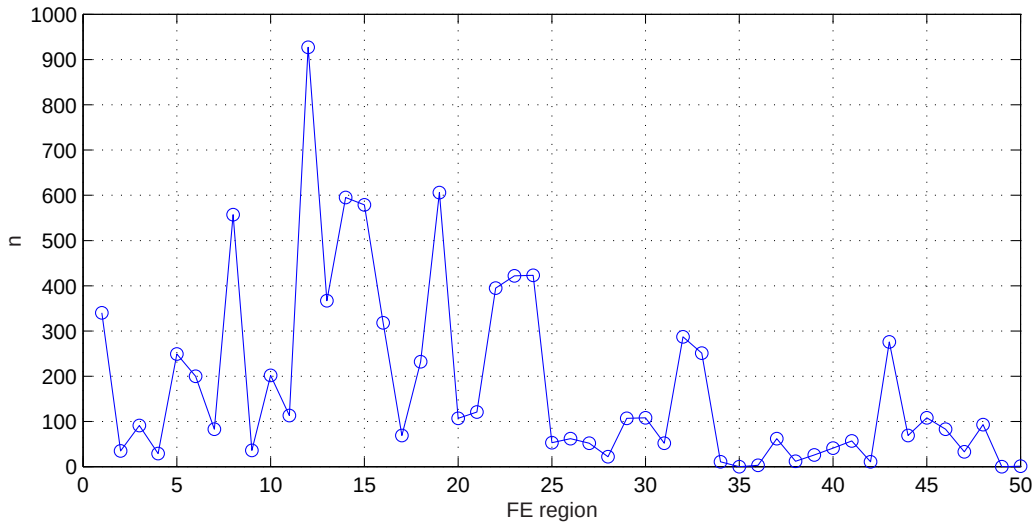

Figure 5.18: Plot of number of points n for FE regions 1-50.

per region is considerable. Therefore, the effect of data numbers on thermodynamic variables is checked in a similar way as the temporal study in figure 5.15. Because some regions contain no data or too few to calculate any of the thermodynamic variables

Zone type	Number of regions	Events
Subduction	17	6047
Collision	9	617
Intra-continental	1	62
Mid-ocean ridges	5	963
Total	**32**	**7689**

Table 5.2: Number of regions analysed per deformation zone and corresponding total number of events.

accurately, I remove any regions with $n < 30$ to ensure stable estimates of S and B etc. This leaves a total of 32 out of the 50 regions for analysis and a total of 7656 earthquake events in accordance with Al-Kindy and Main (2003). The quota for each zone style is shown in table 5.2.

5.5.2 Testing criticality

I now test criticality for the spatial ensemble as I did the temporal ensemble (5.8) by plotting S against $\langle \ln E \rangle$ for the regionalised data. This is shown in figure 5.19. In figure 5.19 I plot data for the 32 FE regions grouped by deformation type. The figure shows two things. Firstly, the difference between the linear and quadratic fits is more evident than the case for the temporal data in figure 5.8. This would suggest that in the spatial sense, the data are sub-critical since they deviate from equation 3.26. The curvature of the quadratic curve is also in the right sense as predicted analytically in chapter 3 (figure 3.13). Second, it can be noted that the mid-ocean ridges (mor) are at the lower end of the curve (lower S) whereas the subduction zones (sub) are scattered at the higher end of S. The significance of this curvature is addressed using Akaike Information Criterion (AIC) (Akaike, 1978).

5.5.3 Akaike information criterion (AIC)

Figure 5.19 shows both a linear and quadratic fit with R^2 values of 0.93 and 0.95 respectively. A better fit (smaller residual error or higher R^2) for a quadratic fit model is expected as it has an extra free parameter. We are therefore required to penalise for the extra

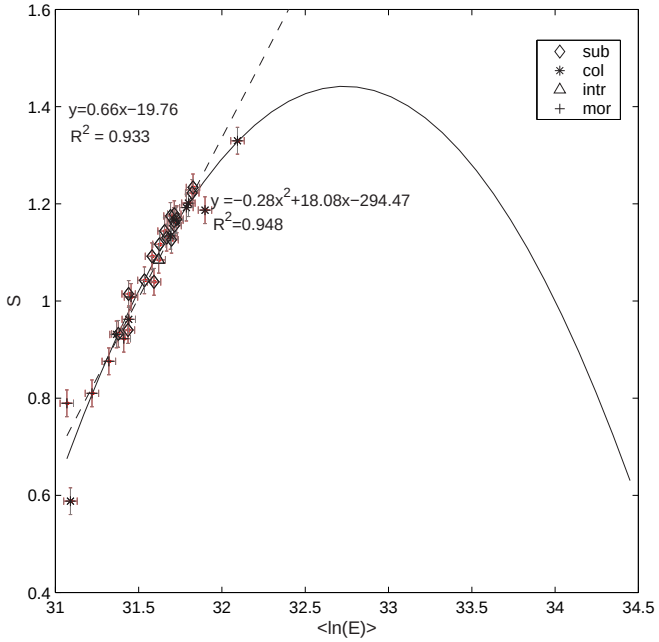

Figure 5.19: Entropy S against energy $\langle \ln E \rangle$ for regionalised data with linear (dashed line) and quadratic (solid line) fits (modified from Al-Kindy and Main, 2003). The different symbols correspond to 4 different deformation styles: 'sub'=subduction, 'col'=collision, 'intr'=intra-continental and 'mor'=mid-ocean ridge. Errors bars are calculated to one standard error.

free parameter in the quadratic fit in order to compare its fitness to a linear model. The penalization is done here using Akaike's Information Criterion (AIC) (Akaike, 1978; Draper and Smith, 1998; Main et al., 1999). If data points can be defined by

$$y_i = \gamma(x_i) + \epsilon_i \qquad (i = 1, 2, 3, ...n) \tag{5.6}$$

where γ is the theoretical model, ϵ is an error term and n is the number of points (here $n = 31$), the residual sum of squares RSS is then

$$RSS = \sum_{n}^{i=1} [y_i - \widehat{\gamma}(x_i)]^2 \tag{5.7}$$

with $\widehat{\gamma}$ the maximum likelihood model estimate and

$$L(y, x^*) = -\frac{n}{2} \ln(RSS) \tag{5.8}$$

The Akaike Information Criterion is then

$$AIC = L(Y) - q \tag{5.9}$$

where q is the number of free parameters. The simplest model consistent with the data has the highest AIC. I calculate this criterion on the 32 data points in figure 5.19 as shown in figure 5.20. Figure 5.20 shows that a quadratic fit (polynomial order =2) gives a higher value for AIC when compared to a linear fit (polynomial order =1) despite the penalty for the additional free parameter. The difference in AIC of 3.5 between the linear and quadratic fit is considered significant since $AIC_{q+1} - AIC_q > 1$. That is, by putting in an extra parameter, AIC decreases by 1, but the likelihood increases by 4.5, so the resultant gain of 3.5 is significant. It can be concluded from figure 5.20 that a quadratic fit statistically better describes the data than a linear fit and the distribution can be described as 'sub-critical'. This result is published in Al-Kindy and Main (2003).

5.5.4 Re-examination of Al-Kindy and Main (2003)

After the publication of Main and Al-Kindy (2003) and the submission of this thesis, it was noted that the curvature of S vs. $\langle \ln E \rangle$ in figure 5.19 will be influenced by the point corresponding to Flinn-Engdahl region 47. This is the lowest point on figure 5.19 on

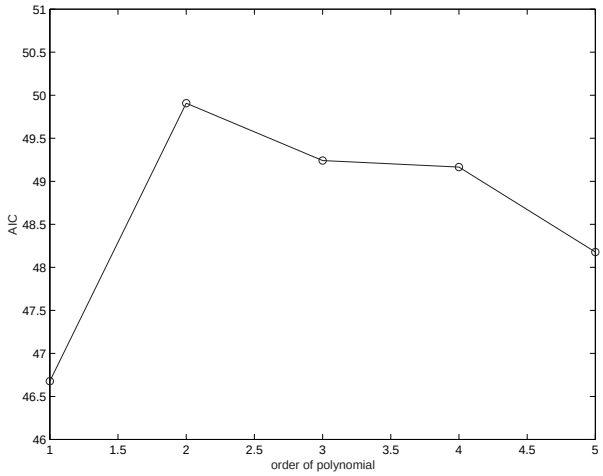

Figure 5.20: Plot of Akaike information criterion (AIC) for polynomials of different powers with a quadratic distribution (n=2) giving the best fit (from Al-Kindy and Main, 2003).

both the x and y axis. Therefore, a repetition of S vs. $\langle \ln E \rangle$ plot and the AIC analysis is done here excluding this point to assess its influence on the final results.

First I compare the difference in the linear and polynomial (quadratic) fits to the data with and without region 47 in figure 5.21. It can be seen from the dashed lines in figure 5.21 that there is a decrease in slope of the linear fit and the curvature of the polynomial fit when FE region 47 is excluded although the curvature is still in the right sense. Therefore, the inclusion of the point has a notable influence on the curvature. To further compare the results of the curved fit to the linear fit excluding region 47, I recalculate the AIC as shown in figure 5.22 and compare it with the AIC including region 47. It can be seen from the figure that although there was previously a significant difference in the AIC between the linear and quadratic fits ($AIC_{q+1} - AIC_q \approx 4.5$), this difference becomes insignificant when region 47 is removed ($AIC_{q+1} - AIC_q \approx 0.25$). The AIC results tell us that a linear relation is the simplest fit to the data when region 47 is excluded. This means that the data is closer to being 'critical' with region 47 removed similar to the temporal data (figure 5.8).

In summary, it has been found after the publication of the Al-Kindy and Main (2003) that FE region 47 will influence the curvature of the S vs. $\langle \ln E \rangle$ plot for regional data. The inclusion of this point suggests sub-criticality whereas its exclusion suggests criticality following the criterion of chapter 3. The curvature is also in the right sense. However,

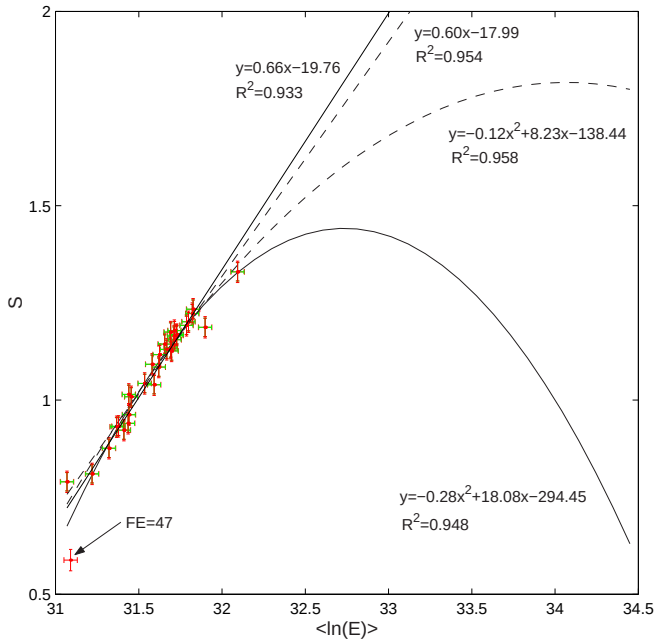

Figure 5.21: Plot of polynomial fits with (solid line) and without (dashed line) FE region 47 (arrow). The error bars are calculated to one standard error.

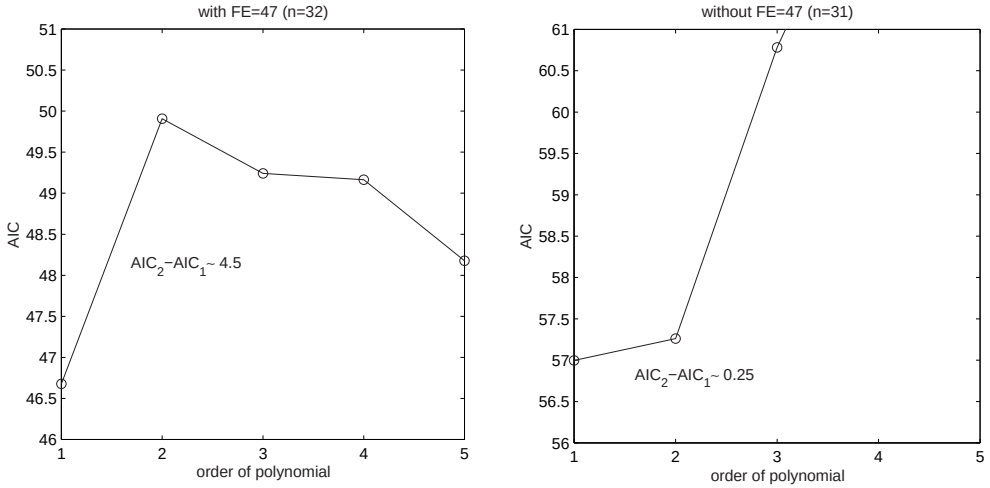

Figure 5.22: AIC plots with and without region 47.

this finding does not change the conclusion that the data analysed are more predictable in space than they are in time given the differences between different deformation zones as verified in section 5.5.7 below. In other words, we are more certain of the differences in space over a given time than we are of changes in time over a given space. All subsequent analyses in this chapter will exclude region 47 leaving a total of 7656 events over 31 regions. It can also be noted from figure 5.23 below that region 47 does not contain sufficient data to produce a reliable energy-probability plot.

5.5.5 Scaling exponents B, b_1 and b_2

It was shown in the temporal study that the scaling exponents B, b_1 and b_2 did vary somewhat annually as was summarised in table 5.1. Here I carry out the same analysis on the regional data to see if the change in scaling exponents is also present in the spatially divided data. First I calculate the values of B for all regions. This is shown in figure 5.23. I also calculate b_2 for all regions as shown in figure 5.24. Note that although I have included all 50 regions here, only regions with more that 40 recorded events are now used[3] in the final analysis. The values of b_1 are also calculated from the mean moment magnitude data for every region. A summary of the variation of the scaling exponents with region is shown in figure 5.25. It is clearly seen from figure 5.25 that there is a far better correlation between the scaling exponents with each other for the spatial case when compared to the temporal case (figure 5.13). This supports the claim that **regional variations are more amplified than temporal ones**. The deformation style will therefore have an influence on the general seismicity statistics.

Following from this, I now re-examine the question whether there is a more pronounced dependence of the thermodynamic variables on the scaling exponents in figure 5.26. The figure shows a good negative correlation between $\langle \ln E \rangle$, $\langle E \rangle$ and S and all three scaling exponents despite the different ways in which they are calculated. This suggests that these scaling exponents may be used as a measure of self-organisation since they are negatively correlated with S. This is particularly true for b_1 as was found for the temporal ensemble. This transpires that the higher the scaling exponent, the more the organisation (lower entropy). Also, the scaling exponents can be an indicator of what

[3] Kagan (1997) in his regional study uses regions with as few as 6 events.

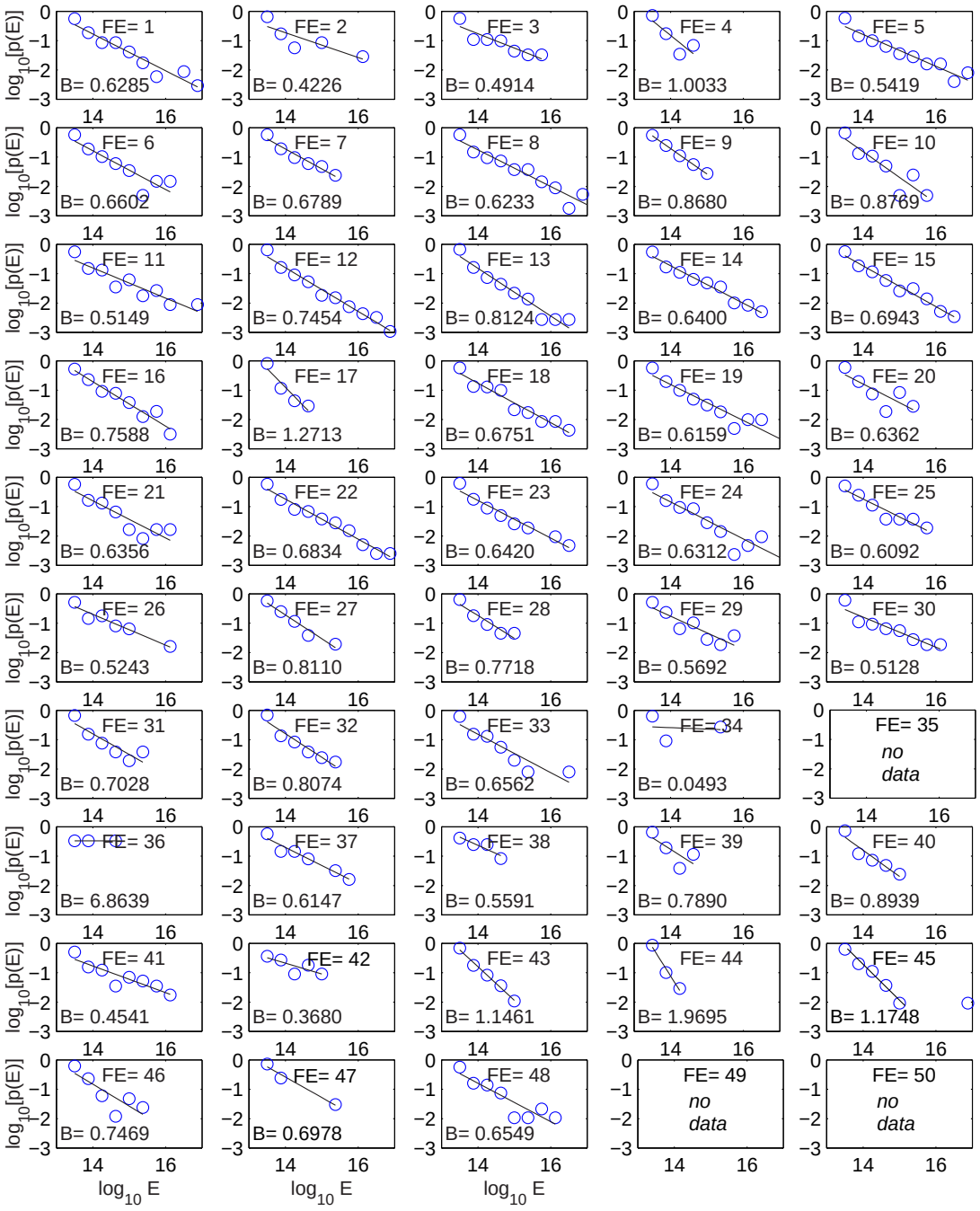

Figure 5.23: Plot of $\log[p(E)]$ against $\log E$ for FE regions 1-50 with corresponding values of B.

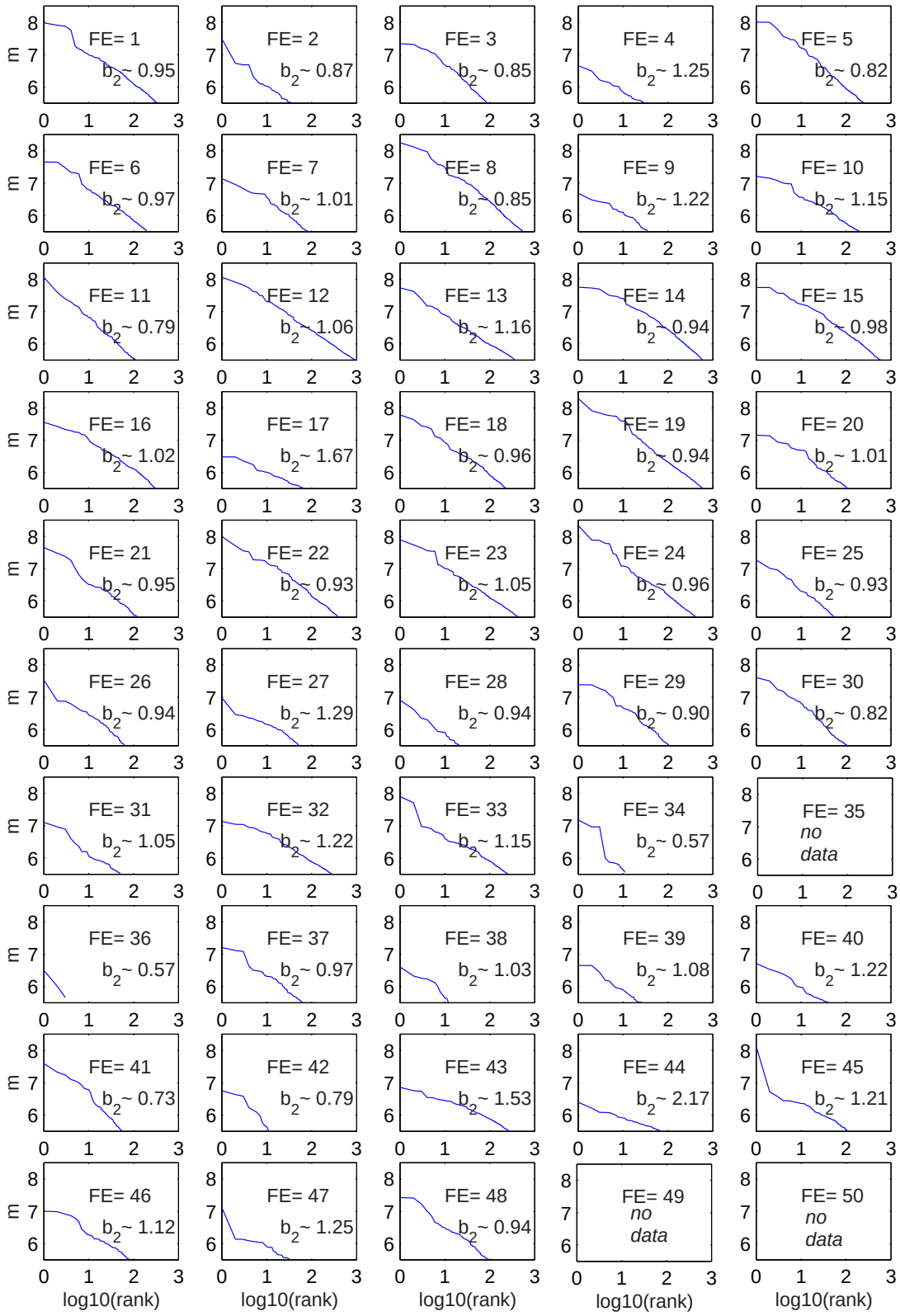

Figure 5.24: Plot of m against $\log(rank)$ for FE regions 1-50 with corresponding values of b_2.

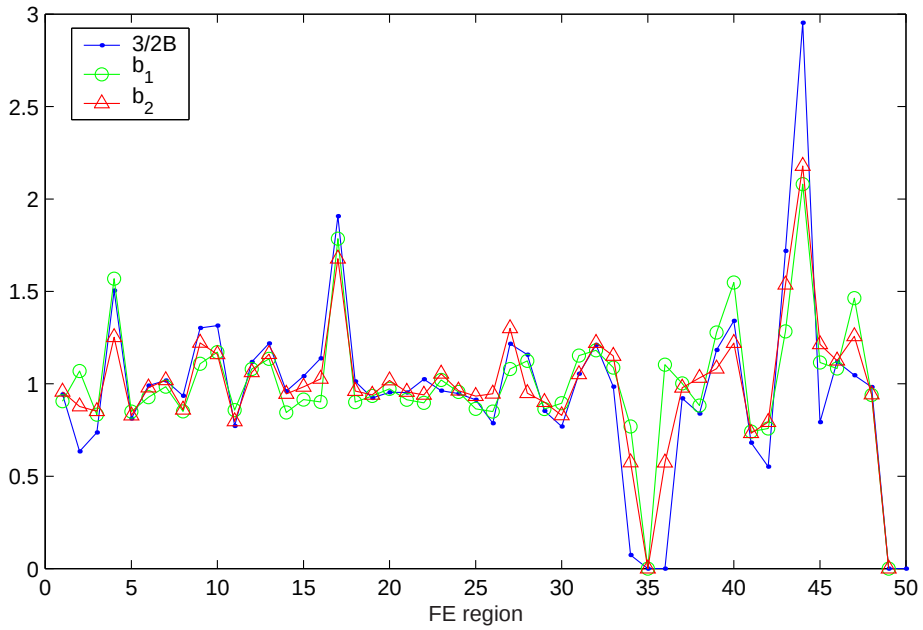

Figure 5.25: Plot of variation of scaling exponents B, b_1 and b_2 with FE region. The B value is rescaled for comparison with b_1 and b_2.

the expectation of the radiated energy is for a given region; the higher the exponents, the lower the mean energy as seen in figure 5.26. This is in agreement with Godano and Pingue (2000) who find a negative correlation between the maximum moment release and the scaling exponent B. The results here are also in agreement with models of seismicity (e.g. Olami et al., 1992; Main et al. 2000).

5.5.6 Data check

As I have demonstrated in figure 5.18, the number of events in each region varies considerably. A check is therefore performed to see if any of the variables measured are dependent on n as shown in figure 5.27. The figure shows that there is no obvious correlation between the parameters measured although the scatter decreases slightly with increasing n. Again, this justifies comparing data of different regions despite the difference in event numbers. This is done keeping in mind the exclusion of regions with $n < 40$ that could give scattered results.

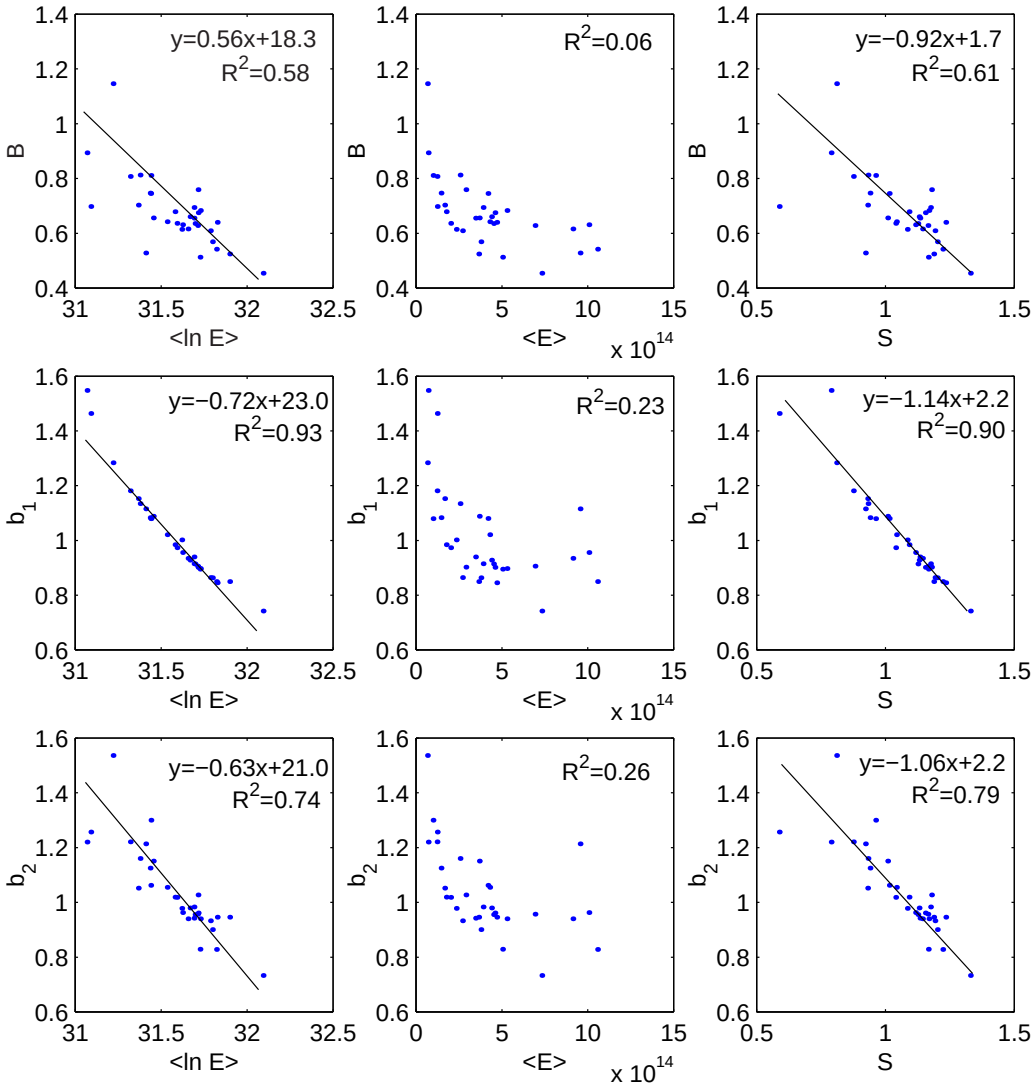

Figure 5.26: Plot of scaling exponents B, b_1 and b_2 against thermodynamic variables $\langle \ln E \rangle$, $\langle E \rangle$ and S.

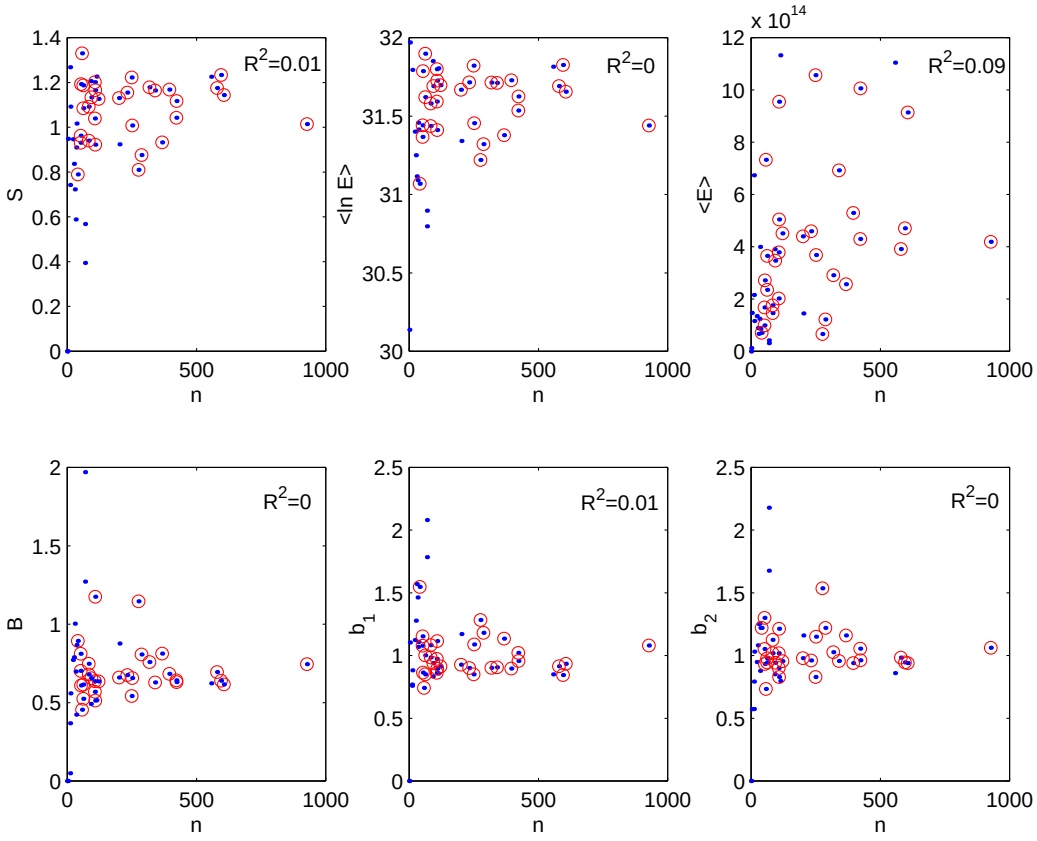

Figure 5.27: Plot of scaling exponents B, b_1 and b_2 against thermodynamic variables $\langle \ln E \rangle$, $\langle E \rangle$ and S. The circled points are those used in the final analysis. Other data not used due to insufficient number of events or because they do not fit into any of the four 'tectonic zone' categories.

5.5.7 Spatial study results

The results of the spatial study are summarised in table 5.3. It can be seen that there is a notable difference between the results of the subduction zones and the mid-ocean ridges. For example, all scaling exponents are higher for mid-ocean ridges ($B = 0.94$, $b_1 = 1.24$, $b_2 = 1.27$) relative to the subduction zones ($B = 0.67$, $b_1 = 0.95$, $b_2 = 0.96$). Kagan (1997) finds a similar result with $B = 0.92$ for mid-ocean ridges and $B = 0.63$ for subduction zones. Here, I confirm the result for a further two scaling exponents, b_1 and b_2. Kagan also bases his results on the cumulative frequency of events whereas I show results for incremental probability distributions. Variations of scaling exponents can be attributed to several factors including an increase in tectonic plate velocity (Cao and Gao, 2002) rheology (Lyakhovsky et al., 2001; Amitrano, 2003) and temperature (Wiens and Gilbert, 1996) both in space and time.

I also find that the entropy for the mid-ocean ridges is lower ($S = 0.88$) than for the subduction zones ($S = 1.11$). Although this entropy is measured on the 'dynamic' energy release, the result can be compared with that of Nicholson et al. (2000) who also find a lower 'spatial' entropy for mid-ocean ridges when compared to subduction zones. However, they do find that intra-continental zones have the highest spatial entropy. As I only have one zone representing intra-continental regions (FE=37), it is not possible to fully compare my results with theirs. Nonetheless, the results here, and those found by Kagan (1997) and Nicholson et al. (2000) all indicate a higher level of organisation in mid-ocean ridges relative to subduction zones. The results here for the collision zones are somewhat mixed as they are scattered between the two extremities of energy and entropy.

To confirm that the regional variations are real, I now conduct a check by randomising the data to see if the variations observed still remain. I do this by shuffling all magnitude data then repeating the analysis as I did above. I repeat this randomisation 20 times calculating the thermodynamic values for every region/zone. I then compare the mean of the randomised runs with the original un-shuffled results. These are shown in table 5.4. We can see from table 5.4 that the variations in mean values between different zones become less evident in the randomised data when compared to the 'real' data. For exam-

FE	n	$\langle \ln E \rangle$	$\langle E \rangle \times 10^{15}$	S	B	b_1	b_2
Subduction zones							
1	340	31.71	0.69	1.16	0.63	0.91	0.96
5	249	31.82	1.06	1.22	0.54	0.85	0.83
6	200	31.67	0.44	1.13	0.66	0.93	0.98
7	83	31.58	0.18	1.09	0.68	0.98	1.02
12	927	31.44	0.42	1.01	0.75	1.08	1.06
13	367	31.38	0.26	0.93	0.81	1.13	1.16
14	595	31.83	0.47	1.23	0.64	0.85	0.95
15	579	31.69	0.39	1.18	0.69	0.91	0.98
16	318	31.71	0.29	1.18	0.76	0.90	1.03
18	232	31.72	0.46	1.16	0.68	0.90	0.96
19	606	31.66	0.91	1.14	0.62	0.93	0.94
20	107	31.59	0.20	1.04	0.64	0.97	1.02
21	121	31.70	0.45	1.13	0.64	0.91	0.96
22	395	31.73	0.53	1.17	0.68	0.90	0.94
23	422	31.53	0.43	1.04	0.64	1.02	1.05
24	423	31.62	1.01	1.12	0.63	0.96	0.96
46	83	31.44	0.15	0.94	0.75	1.08	1.13
average	**6047**	31.64 (0.13)	0.49 (0.28)	1.11 (0.09)	0.67 (0.06)	0.95 (0.08)	0.96 (0.08)
collision zones							
25	53	31.79	0.27	1.19	0.61	0.86	0.93
26	62	31.90	0.36	1.19	0.52	0.85	0.95
27	52	31.44	0.10	0.96	0.81	1.08	1.30
29	107	31.80	0.38	1.20	0.57	0.86	0.90
30	108	31.73	0.50	1.17	0.51	0.90	0.83
31	52	31.37	0.17	0.93	0.70	1.15	1.05
41	57	32.09	0.73	1.33	0.45	0.74	0.73
47	*31*	*31.09*	*0.12*	*0.59*	*0.70*	*1.46*	*1.26*
48	93	31.69	0.35	1.13	0.66	0.94	0.94
average	**584**	31.73 (0.23)	0.39 (0.20)	1.14 (0.13)	0.60 (0.16)	0.92 (0.13)	0.95 (0.17)
intra-continental							
37	**62**	31.62	0.23	1.08	0.61	1.00	0.98
mid-ocean ridges							
32	287	31.32	0.12	0.88	0.81	1.18	1.22
33	251	31.45	0.37	1.01	0.66	1.09	1.15
40	41	31.07	0.07	0.79	0.89	1.55	1.22
43	276	31.22	0.07	0.81	1.15	1.28	1.54
45	108	31.41	0.96	0.92	1.17	1.12	1.21
average	**963**	31.29 (0.16)	0.32 (0.38)	0.88 (0.09)	0.94 (0.22)	1.24 (0.19)	1.27 (0.15)

Table 5.3: Summary of results for spatial study. The standard deviations are given in brackets and the total numbers of events per region are given in bold. Region 47 given in italics is not included in the calculation of the averages and n.

real	**subduction zones**	**collision zones**	**mid-ocean ridges**
$\langle \ln E \rangle$	31.64 (0.13)	31.73 (0.23)	31.29 (0.16)
S	1.11 (0.09)	1.14 (0.13)	0.88 (0.09)
B	0.67 (0.06)	0.60 (0.16)	0.94 (0.22)
b_1	0.95 (0.08)	0.92 (0.13)	1.24 (0.19)
b_2	0.99 (0.08)	0.95 (0.17)	1.27 (0.15)
randomised	**subduction zones**	**collision zones**	**mid-ocean ridges**
$\langle \ln E \rangle$	31.60 (0.10)	31.59 (0.17)	31.59 (0.09)
S	1.09 (0.07)	1.06 (0.04)	1.08 (0.04)
B	0.67 (0.09)	0.60 (0.13)	0.64 (0.08)
b_1	0.98 (0.01)	1.00 (0.04)	0.99 (0.04)
b_2	0.97 (0.02)	0.97 (0.05)	0.98 (0.04)

Table 5.4: Summary of mean results for real and randomised data sets. The standard deviations are given in brackets.

ple, note how all the scaling exponents for the randomised data become similar between zones. What is more interesting is that the results are closest to what is calculated for 'real' un-randomised subduction zones. Why is this happening? We can see from tables 5.2 and 5.3 that the largest number of data points are for subduction zones ($\sim 79\%$ of analysed data) compared to say mid-ocean ridges (13% of data). These therefore will overprint and smooth out the variations in the temporal data as well as the randomised data. In summary, the regional study shows systematic variations between deformation zones that are real. These are evident in the higher organisation (larger scaling exponents and lower S) and lower energy release for mid-ocean ridges when compared to subduction zones.

5.6 Comparison of results with theoretical phase diagrams

In chapter 3, I used analytical thermodynamic results to construct energy entropy phase diagrams that show how entropy varies with scaling exponent B, $\langle \ln E \rangle$ and $\langle E \rangle$ in the sub-critical, critical and super-critical regimes. I now make a direct comparison of both temporal and regional data with the theoretical curves to establish their state of criticality.

The phase diagrams are shown in figures 5.28 and 5.30 with zooms respectively in

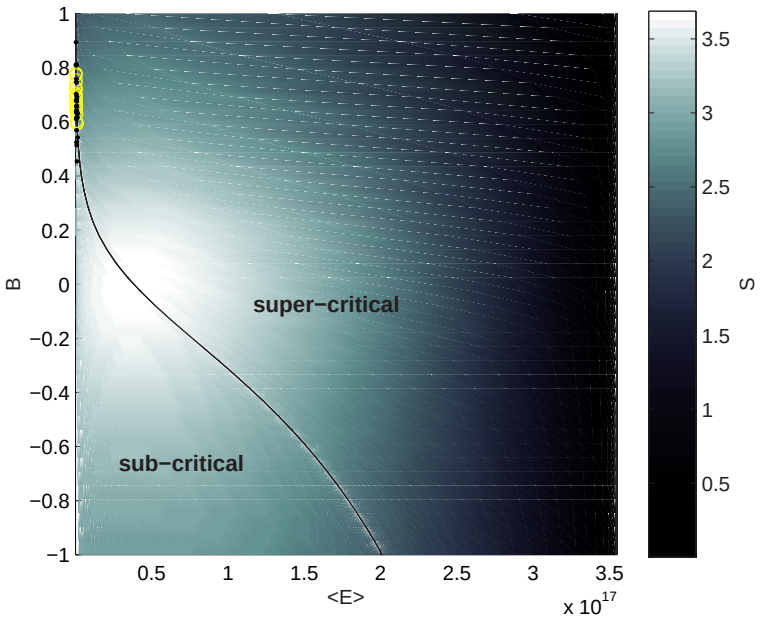

Figure 5.28: B vs $\langle E \rangle$ phase diagram with super-imposed results of temporal (circles) and spatial (dots) studies. Note the proximity of the data to the 'critical' solid curve.

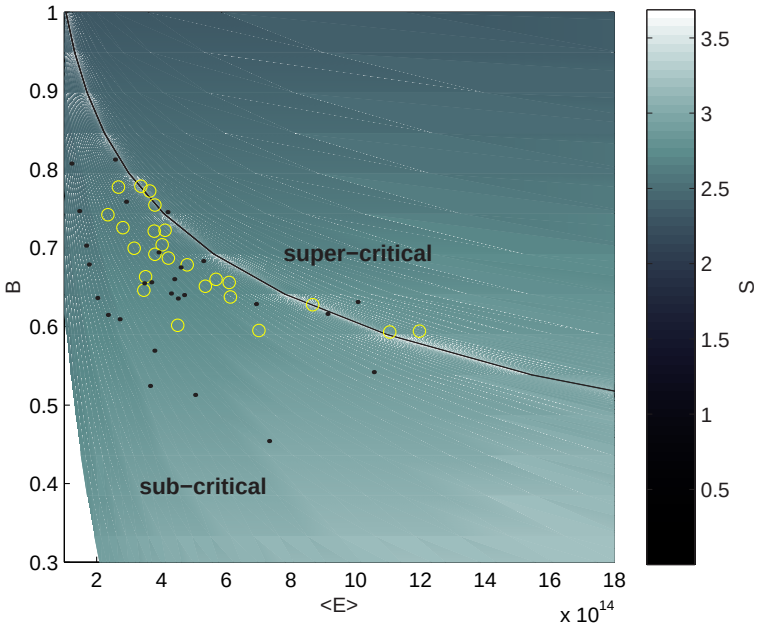

Figure 5.29: Close up B vs $\langle E \rangle$ phase diagram with super-imposed results of temporal (circles) and spatial (dots) studies.

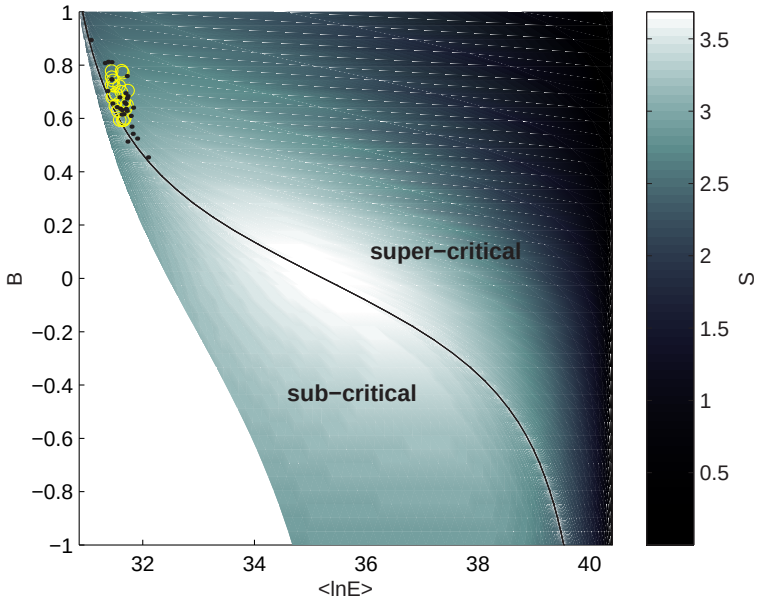

Figure 5.30: B vs $\langle \ln E \rangle$ phase diagram with super-imposed results of temporal (circles) and spatial (dots) studies. Note the proximity of the data to the 'critical' solid curve.

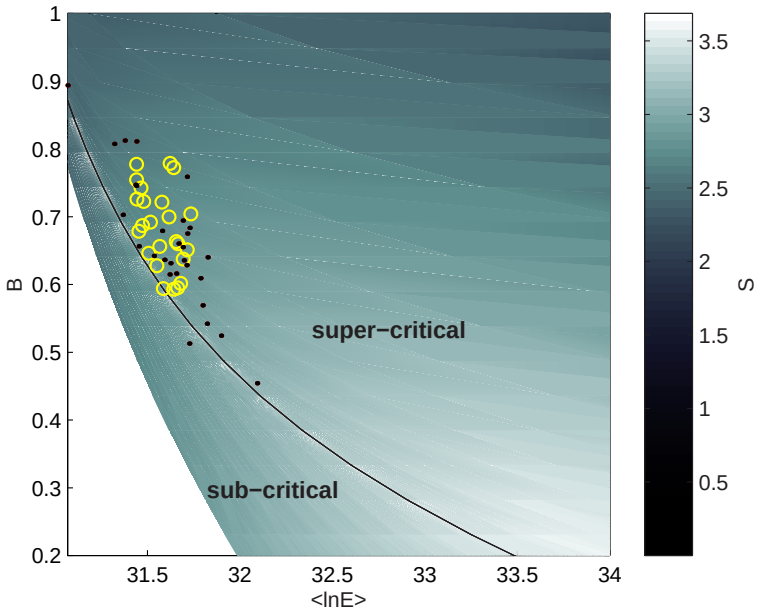

Figure 5.31: Close up of B vs $\langle \ln E \rangle$ phase diagram with super-imposed results of temporal (circles) and spatial (dots) studies.

figures 5.29 and 5.31. It can be seen from the four figures that the temporal data (circles) are clustered very close to the 'critical' line with the data mostly in the sub-critical regime for $\langle E \rangle$ (figure 5.29) and in the super-critical regime for the $\langle \ln E \rangle$ (figure 5.31). The spatial data (circles) are more scattered compared to the temporal data for both cases and lie in both the sub-critical and super-critical regimes. It is unclear to me why the $\langle \ln E \rangle$ data predominantly plot in the super-critical regime. However, they are with one standard deviation of the 'critical' line as shown by the error bars in figure 5.31. We know from the energy density distributions and the $\langle \ln E \rangle$ vs S plots (figures 5.8 and 5.19) that the data are critical to sub-critical. Nonetheless, it is reassuring that the data follow the trend of the critical line and are almost parallel to it for both $\langle E \rangle$ vs S and $\langle \ln E \rangle$ vs S plots. This further confirms that data (in theory) can maintain a criticality state (be it critical, sub-critical or super-critical) by varying the scaling exponent *and* mean energy. Therefore, universality can be violated without criticality necessarily being affected according to the thermodynamic definition outlined in this thesis.

5.7 Self-organised criticality?

In this brief second part, I look at the earthquake data in light of the results from the numerical model of chapter 4. Based on the results presented in this chapter, and the results deduced from the study of the numerical Bak et al. (1987) BTW model of self-organised criticality (SOC) (section 4.9), I now try establish if the Earth is indeed in a strict state of SOC. I have shown in the previous chapter that the conservative BTW model does show regional variations in the level of 'seismic' activity with it being most active away from the boundaries. Looking at figure 5.4, we see that the Earth too is more seismically active in some areas than others. Also demonstrated in the regional study of the BTW model was that we can get two different types of distributions, one of which was a power-law and the other a gamma distribution (figure 4.26), so any variations in distributions observed in figures 5.11 and 5.23 need not contradict SOC. However, there are two crucial contradictory factors:

1. The breakdown of universality: this was not seen in the BTW model but seen here for all three scaling exponents as summarised in tables 5.1 and 5.3. A regional vari-

property	SOC	data
spatial variability	yes	yes
conservative	yes	no
power-law and gamma	yes	yes
universality	yes	no
SOC	yes	**no**

Table 5.5: Comparison of model of SOC and results of earthquake data analysis.

ation in scaling suggests a form of correlation length and a variation in the system dynamics with space on a fundamental level (e.g. ocean-ridges vs. subduction-zones). **This vital difference suggests that the Earth cannot be best described by a pure state of self-organised criticality**.

2. The BTW model is internally conservative which allows for avalanche events to cascade to length-scales approaching the system size. We know however from the laws of thermodynamics and general observation that the Earth's lithosphere must be dissipative. Also, earthquake ruptures spanning the size of the entire crust have not been observed.

I summarise my findings in table 5.5. I hope this very briefly and hopefully conclusively ends the ongoing debate on whether Earth seismicity is a SOC process; it is not. The Earth's seismicity may be described as a process undergoing self-organised subcriticality or (SOSC) as proposed by Al-Kindy and Main (2003a). This is simply a dissipative SOC model in accordance with the NBTW model -or similar models- shown in chapter 4. An SOSC model can accommodate for all the aspects outlined in table 5.5 and because it is dissipative, it is more in tune with natural systems.

5.8 Entropy production and heat flow

There are two thermodynamic assumptions or predictions that can be made about driven dissipative structures. These, in accordance with Kondepudi and Prigogine (1998) (see chapter 2), are as follows:

1. Keeping everything constant, an increase in entropy will be accompanied by a decrease in entropy production.
2. Entropy production is related to heat flow

Based on this, I attempted to conduct a simplified study to see if areas of higher (lower) entropy will show lower (higher) heat flow. Following my viva examination, this study was subsequently removed from the main body of this thesis since it proved inconclusive and was not rigorous enough. However, to my best of knowledge, no such attempt at relating entropy as derived from seismic energy release (or self-organisation) to heat flow has ever been made. I have therefore included this study in the appendix of this thesis for the curious reader. On an encouraging note, it should be mentioned here that based on available evidence, mid-ocean ridges have a higher heat flow and, as shown in this chapter, lower entropy when compared to subduction zones and vice-versa.

5.9 Chapter summary

This chapter examined criticality and self-organised criticality in the crust through temporal and spatial analysis of data from the Harvard Centroid Moment Tensor catalogue. The regional study was also extended to The Global Heat Flow Database. The following results were found:

1. The gamma entropy equation derived in chapter 3 is found to be applicable and in agreement with real earthquake populations. The temporal study suggests that in a thermodynamic sense the Earth is critical or very close to critical. The spatial study on the other hand shows that the Earth is best described as a sub-critical system. This quantitatively shows that earthquakes are more predictable in space then they are in time. However, if we are to exclude FE region 47, the spatial data are then also best described as 'critical'. Overall however, the data show more variation spatially than temporally.
2. A study of three different scaling exponents B, b_1 and b_2 shows that scaling variability exists for a spatial ensemble of earthquake data. This contradicts the premise of universality for earthquake populations.

3. The weak to strong negative correlation between the scaling exponents and the thermodynamic variables suggests that scaling exponents can be used as a proxy for variables such as the entropy S and the mean energies $\langle E \rangle$ and $\langle \ln E \rangle$. This is in agreement with Godano and Pingue (2000) who find a negative correlation between the maximum cut-off seismic moment and the scaling exponent B.

4. The spatial study shows that mid-ocean ridges are more organised (lower entropy) than the continental subduction (and collision) zones. In accordance with the background presented in chapter 2 and the prediction of chapter 3, this might suggest that mid-ocean ridges should be of higher entropy production and therefore higher heat flow. This qualitative inference is found to be in agreement with studies of heat flow data (e.g. Pollack et al., 1993) that show higher heat flow for oceanic regions compared to continents. This study however proved inconclusive and is included in the appendix of this thesis.

5. In relation to SOC and point 2 above, the violation of universality as shown by the variations in regional measurements of three scaling exponents B, b_1 and b_2 contradicts self-organised criticality. This gives impetus to describe Earth seismicity using self-organised sub-criticality in accordance with the NBTW model described in chapter 4.

Chapter 6

Discussions and prospects

"The laws of thermodynamics have a different feel from most of the other laws of physics. There is something more palpably verbal about them - they smell of their human origin" -Percy W. Bridgman[1]

6.1 Introduction

In this thesis, it has been shown that the tools of equilibrium thermodynamics/statistical mechanics can be used to better understand self-organisation in dissipative out-of-equilibrium power-law systems. The systems I examined in this thesis were the conservative and non-conservative BTW numerical models and seismicity of real earthquake populations. I ended the previous main chapters with a discussion/summary of the their respective results. In this chapter, I discuss some issues and questions raised by the results from the previous chapters. I also attempt to give a 'bigger picture' discussion pointing out the relevance of the work done here with thermodynamics and self-organisation in general. I also make suggestions on directions particular areas could be built upon and further advanced. I try where possible to discuss the issues in the order they first appear in this thesis.

[1] Physics Nobel Prize winner, 1946. As quoted by Kirkaldy (1985).

6.2 The gamma entropy equation

6.2.1 Scaling exponent B

The gamma entropy equation derived in chapter 3 for logarithmic bins is given here once more for reference:

$$S \sim B\langle \ln E \rangle \tag{6.1}$$

The equation was successfully applied to both numerical model data in chapter 4 and temporal and spatial earthquake data in chapter 5. However, there are some questions that can be raised here. For example, why is S proportional to B? I have shown that the entropy is inversely proportional to B in the phase diagrams in chapter 3 (figure 3.11) and results of chapter 5 (figure 5.26). However, as it can be seen from figure 5.26, B is also inversely proportional to $\langle \ln E \rangle$ so if we take the extreme case of $B \to 0$, $\langle \ln E \rangle \to large$ compensating for the reduction of B. The gamma entropy for $B = 0$ reduces to a pure Boltzmann exponential. It is also stressed that the derivation of the gamma entropy equation was done integrating with respect to energy and not B. Nonetheless, it is interesting to have an equation that combines energy, entropy and a power-law scaling exponent all in one expression. What would be interesting if possible is to derive an expression with respect to B assuming a fixed energy.

6.2.2 Applicability

There has been debate in the literature on whether equilibrium statistical mechanics and thermodynamics can be applied to far-from-equilibrium systems (Bridgman, 1950, Sornette, 2000). A clear result from this thesis is that they are indeed applicable to a dynamic ensemble of synthetic and real earthquake data. The application of equilibrium thermodynamics and statistical mechanics to non-equilibrium systems is currently of great interest to many branches of physical and biological science. In relation to seismicity models, Rundle et al. (1995) suggest for a numerical model that *'Boltzmann fluctuations will be important in these systems, and that these may be the origin of extended spatial correlation observed in real earthquake fault systems'* conjuring that standard techniques of equilibrium statistics may be used in the interpretation of at least some far-from-

equilibrium dynamic systems. In addition, Rundle (1993) uses a statistical-mechanics approach to explain deviations from the Gutenberg-Richter law at lower magnitudes. This is done using a similar approach to Main and Burton (1984) as outlined in chapter 3.

Looking at a chaotic model, Egolf (2000) states that *'some far-from-equilibrium systems might be understood in terms of equilibrium statistical mechanics'*. Egolf continues to prove this statement for a far-from-equilibrium chaotic model. Similarly, Klimontovich (1999) shows theoretically the applicability of statistical mechanics and Shannon information theory to open biological and quantum systems. The applications of equilibrium thermodynamics and information theory have even been applied to power-law numeric 'sequences' that have been contaminated by noise (Freund et al., 1996). The use of equilibrium thermodynamics has also been applied to better understand self-organisation away from equilibrium in the laboratory. For example, statistical entropy has been successfully measured to quantify the level of chaos in a Bénard cell type experiment (Caputo and Atten, 1987), in quantifying transient spatial distribution of fractures in a rock physics experiment (Nanjo et al., 2000) and very recently to vibration-fluidised granular matter (D'Anna et al., 2003). Studies extending to dissipative climate models include Lorenz et al. (2001) and Ozawa et al. (2001).

Applications in the field include spatial entropy (configurational entropy) such as to distributions of earthquakes locations (Nicholson et al., 2000; Goltz and Böse, 2002). Although the application of entropy (information and statistical mechanical) to quantifying spatial distribution is common practice (e.g. Goltz, 1997), the application to open driven systems remains somewhat controversial since *'they appear to have little in common with equilibrium systems'* (Egolf, 2000). It is emphasised that in the majority of the examples outlined, a stationary steady-state is normally the underlying assumption to the application of equilibrium thermodynamics and statistical mechanics to these problems. In summary, although the application of equilibrium thermodynamics and statistical physics to far-from equilibrium is emerging in the literature (as outlined in the references above), this area of physics/thermodynamics is in its infancy leaving a lot of scope for further research. This thesis, to my best of knowledge, is a first formal attempt at applying such an approach to understand self-organisation in energy released from the Earth's crust in the

form of earthquakes. This is encouraging for further application to other natural systems (biology, ecology, hydrology etc.).

6.3 Lessons from SOC and numerical modelling

6.3.1 Dissipation

Regarding SOC, the reoccurring theme seems to be *'It is still fair to say that the appearance of large scale power-law scaling ranges in the dynamics of these [SOC] systems remains an important unexplained effect'* (Cross and Hohenberg, 1993). But, what can we learn from SOC based on the results presented in this thesis? I have shown through analysis of the conservative BTW numerical model that there is heterogeneity in the spatial occurrence of site failures with distance from the edges (figure 4.19). This is because dissipation is only allowed to occur at the edges in the BTW model. Once internal dissipation is introduced, the spatial heterogeneity disappears (figure 4.23). However, once internal dissipation is present, the pure power-law in the energy probability distribution also disappears and we are left with gamma type distributions (figure 4.7). So, dissipation at the edges in the BTW model is essential to achieve SOC whereby internal dissipation destroys pure SOC. This destruction of pure SOC is very sensitive to dissipation as exhibited by equation 4.26.

What can this tell us about real systems? Nicolis and Prigogine (1977) suggest dissipation is a primary cause behind symmetry breaking (defined in chapter 2) and the occurrence of spatial patterns: *'a symmetry-breaking instability induced by diffusion implies that that the primary pattern is necessarily a spatial dissipative structure'* (Nicolis and Prigogine, 1977, p.g 416). In that particular example, the process of dissipation was diffusion as opposed to say convection as in the Bénard cell experiment. It is therefore not only important how much a driven system is dissipative to self-organise, *where* and *how* it dissipates energy is also important. Therefore, dissipation may have a quantitative element (the percentage of energy lost say) as well as a qualitative one (where from the system it occurs say) which must be taken in to account. **This may be an underlying factor as to why different driven systems show different forms of organ-**

isation such as Bénard cells (Cakmur et al., 1997) power-laws (Bak et al., 1987) and periodic chemical reactions (Cross and Hohenberg[2], 1993; Kondepudi and Prigogine, 1998), biomolecular processes (Cavanagh and Akke, 2000) and ecological interaction (Visscher, 2003).

Qualitative dissipation could be an interesting and general area of further study that is beyond the scope of this thesis. For example, shallow earthquakes are closer to a dissipative boundary (the surface) than deeper ones. Following from the results of the BTW model, should one predict a difference in the statistical properties of deeper earthquakes compared to shallower ones? This is found to be the case (e.g. Ogata et al., 1991; Wiens and Gilbert, 1996) although many other factors must be taking into account such as temperature, pressure and chemical processes that vary with depth. Also for scope of further study, numerical models could be created with different modes of dissipation. These models could be set up with say a fixed level of dissipation but changing the mode of dissipation between different runs (changing geometry etc.). One may then establish the controlling factors on the level of self-organisation.

Generally speaking, I cannot think of any driven systems showing patterns that are *not* dissipative. The BTW model for example would produce an unobservable 'infinite' avalanche if no dissipation were present at the boundaries. In the Earth's lithosphere, there are several candidates for dissipation that are quantitatively and qualitatively different, both internally and external. These include seismic efficiency, heat flow, fluid convection, radioactivity and so on although the most significant of these are seismicity and heat flow (Keary and Vine, 1996; Scholz, 2000). Indeed, Kirkaldy (1985) simply looks at the issue of self-organisation as *'...a tendency for dissipative systems subject to strong driving forces to simultaneously seek saturation of the available energy source and an equilibrium with the heat sink'*. It is this path to equilibrium and hence the minimisation of free energy through dissipation that therefore probably distinguishes between the types of self-organisation in driven systems, power-law or otherwise as depicted in figure 6.1. Being able to predict the patterns a system would evolve to have by somehow solving for its level or mode of dissipation is a great challenge that even

[2]Cross and Hohenberg (1993) give a very extensive review of pattern formation away from equilibrium. However, only a scintilla of their review touches on power-law statistics.

Prigogine and colleagues had failed to achieve (Ball, 1999). This renders the issue of *dissipation mode* an interesting area for further study (see below).

6.3.2 Attractors

The main property that distinguishes SOC systems from critical point (CP) equilibrium systems as outlined in chapter 2 (section 2.7.2) is that power-law statistics only appear at the critical point in CP systems whereby they are an attractor state in SOC systems. What this means is that although CP system statistics are very susceptible to perturbations, SOC systems are not[3]. Sethna et al. (2001) study the 'crackling noise'[4] from various systems such as earthquakes, sand piles, magnets and paper crumbling and show that they all belong to a *universality class* of power-law systems regardless of the different microscopic properties governing them. There appears to be an underlying attractor state to all these systems. Sethna et al. (2001) also distinguish between criticality in self-organised critical systems and CP systems in the sense that the critical points in CP systems are normally phase-transitions whereby for SOC systems they are simply phases out of a possibility of many in a phase space. The noise element in a dynamic power-law systems allows it to *'meander through and explore the phase space of its variables'* (Ball, 1999).

From the results outlined in chapter 5, Earth seismicity as we see it 'meanders' the various functions, scaling exponents and energy states to an attractor state that is defined by a gamma type distribution as depicted in figure 6.2. Figure 6.2 is a simplification of the S vs $\langle \ln E \rangle$ phase diagrams shown in chapters 3 and 5. We can see in figure 6.2 that out of the myriad of possibilities, the data are circumambient about a relatively specific area alongside the 'critical' line. The mechanisms behind why and how earthquakes globally should all be attracted to this *phase* must be universal. The results outlined in chapter 5 show that subduction and ocean-ridges zones have different energy probability scaling exponents with $B = 0.67$ (subduction) and $B = 0.94$ (ridges) so strict universality is violated. However, both systems belong to the same generic *universality class* of power-

[3] Note that susceptibility here refers to the deviation from a state (such as a power-law) rather that the 'sensitivity' in SOC systems that refers to the possibility for a small fluctuation cascading in to a very large one.

[4] Sethna et al. (2001) use the term 'crackling noise' as a general term for power-law noise.

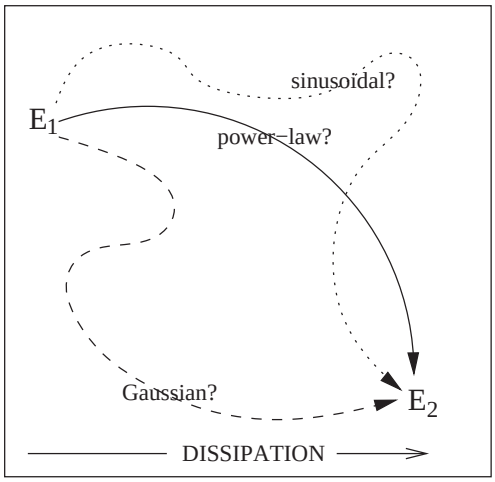

Figure 6.1: Schematic diagram of possible phase path ways systems can acquire to dissipate energy.

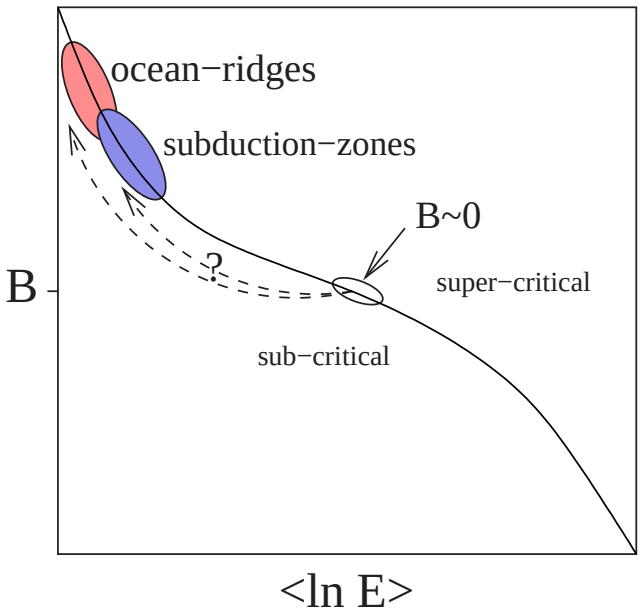

Figure 6.2: Schematic diagram illustrating possible phase evolution paths (dashed line) for subduction and ocean-ridge earthquake populations.

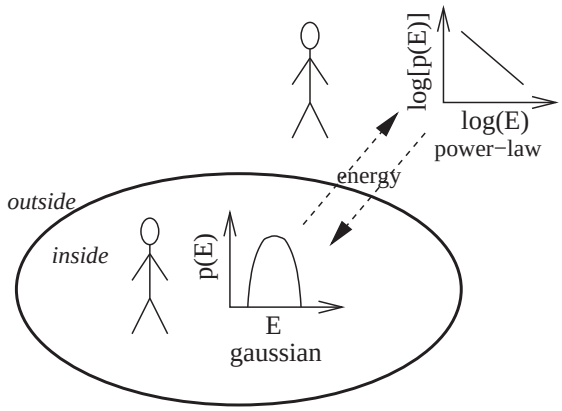

Figure 6.3: Internal and external observation of energy distributions.

law gamma type systems. That is, the data are all attracted to the upper end of the critical line in the B vs $\langle \ln E \rangle$ phase diagram.

6.3.3 Observer dependent criticality

One of the most interesting things learned from the modelling in chapter 4 is the difference between the external and internal energy probability distributions $p(E_e)$ and $p(E_i)$. While $p(E_e)$ was a power-law/gamma as observed for earthquakes, $p(E_i)$ was closer to an equilibrium normal or Gaussian distribution (figure 4.12) similar to what is seen for say a gas (Mandl, 1988). This occurs over all dissipation levels and despite there being a positive correlation between the internal and external energies measured. It may be difficult to test this for real systems such as the Earth's crust since measuring internal energy is not an easy or realistic task (Vitti et al., 2001). The results non-the-less are reminiscent of some recent laboratory experiments on granular media (D'Anna et al., 2003) showing both Guassian statistics and a Brownian noise signature (figure 4.11) in internal energy fluctuations away from equilibrium. Similar 'Boltzmann' fluctuations were also found in a simple slider-block model (Rundle et al., 1995). It would be interesting non-the-less to investigate other systems that may show bi-modal statistics in their internal and external energy probability distributions since **their criticality will depend on if the observer is 'inside' or 'outside' the system** as depicted in figure 6.3.

6.3.4 Defining SOC?

My examination of SOC through models and an extensive review of literature draws me to the belief that SOC is still not well defined. Perhaps the reason this is the case is because *'SOC is a phenomenological definition rather than a constructive one'* (Jensen, 1998). The definitions will therefore stem from observation rather than some underlying theory or formulism. Thus, for now, the very general definition of 'a slowly driven system-away-from equilibrium showing power-laws with no tuning from the outside' is the one likely to remain. To extend this definition to similar systems that show gamma type statistics and variations in the scaling exponent, I have proposed the term 'self-organised sub-critical' in chapter 4 (as in Al-Kindy and Main, 2003).

6.4 Summary

General:

- In this brief chapter, I first discussed the gamma entropy equation and some of the questions it raised. I also state how it adds to the newly emerging field of applying statistical mechanics and thermodynamics traditionally applied to equilibriums systems to far-from equilibrium systems.
- Several lessons have been learned from SOC and numerical modelling. First that not only is dissipation important in the level of self-organisation in a system, the method or *quality* in which this dissipation occurs is also important. This could be one explanation to why dissipative systems can show different patterns (power-law, sinusoidal, etc.). The modelling has also shown that the statistics of systems can be bi-modal. That is, have one energy probability distribution internally and another one as observed externally. This observer dependency may have implications on our assessment of the criticality of systems in nature

Prospects

- Testing the application of the gamma entropy equation to other power-law gamma type systems.

– A formal study of dissipation specifically. This can be done both on the quantitative and qualitative aspects on real and numerical systems. Cellular automata models similar to those outlined and used in chapter 4 can be used to investigate the *dissipation mode*. For example, how does allowing dissipation at only one edge, two edges etc affect the energy probability distributions and level of organisation. Experimentation with different geometrical dissipation sinks within the models could be tested such as braded, periodic and random modes of dissipation and the influences they might have.

  On a biological level, what modes of dissipation give rise to what patterns observed such as 3, and 5 and 6 fold symmetries observed in some micro-organisms and flora and spiral and sinusoidal geometries found in DNA and cells (see examples in Nicolis and Prigogine, 1977 and Ball, 1999). That is, what is the energy exchange mechanisms between the *inside* and *outside* of these systems and are there any systematic dependencies between these mechanisms and the resulting patterns?

Chapter 7

Conclusions

> *'Begin at the beginning' the King said, very gravely, 'and go on till you come to the end: then stop.*' - From Lewis Carroll's *Alice's Adventures in Wonderland*.

The primary aim of this thesis was to study the Earth's crust as a self-organising dissipative structure. This was done to examine its level of self-organisation, proximity to criticality and to test Prigogine and colleague's prediction on self-organisation and entropy production. The investigations were carried out with reference to analytical statistical mechanics and thermodynamics, numerical models and earthquake data from the Harvard Centroid Moment Tensor Catalogue. The secondary aim was to further probe the concept of Self-Organised Criticality and its applicability to Earth seismicity.

The following main conclusions were drawn from my investigations:

Although equilibrium systems at the critical point and non-equilibrium self-organised critical systems share a power-law, they are different. For equilibriums systems, the critical point is fixed whereby for driven self-organising systems, it is an attractor state.

The gamma entropy equation for the gamma distribution is derived in the form $S \sim B\langle \ln E \rangle$. This equation is indicative of a system very near to or at a critical state. The equation was found to be in general agreement with numerical as well as temporal and spatial earthquake data. This successful application of concepts developed from equilibrium statistical mechanics to a non-equilibrium steady-state system shows parallels

with recent studies of other physical systems (e.g. fluidised granular media). Criticality phase diagrams are also found to agree with the regional and temporal earthquake data in general. The phase diagrams suggest that criticality can be maintained if there is a change in the scaling exponent B provided there is also a corresponding change in the mean energy release.

It is known that the critical point is at the state of global maximum entropy for equilibrium systems ($B = 0$), this is not the case for power-law gamma systems. This is because the critical point for gamma systems occurs below the state of maximum entropy for a sub-critical system and beyond the maximum entropy point for a super-critical system. This distinction should also be taken in to account when comparing equilibrium and non-equilibrium systems.

For the locally driven, dissipative BTW numerical model, the internal properties show two characteristics that are indicative of an equilibrium system: Gaussian type statistics in its internal energy distribution, and Brownian noise in its internal energy fluctuation signature. In contrast, the radiated energy follows power-law gamma type statistics. Although simple, the questions these results raise are important because they suggest that our definition of 'criticality' may be observer dependant. If the observer -or observation tool- is *in* the system or *out* of it will vary our assessment of criticality. The model also shows that the organisation occurs at the expense of increasing entropy production (dissipation) globally. The model is more organised externally (low entropy) and more disorganised internally (high entropy) with increasing dissipation. Also, a locally driven NBTW model shows the relation between mean radiated energy $\langle E \rangle$ and dissipation to be $\langle E \rangle \sim (1 - \alpha)^{-0.975}$ where α is the conservation factor. This relation demonstrates the non-linear sensitivity of a self-organising system to the level of dissipation.

The BTW model does show spatial heterogeneity in contrast to the original notion of SOC. In the regional study, a gamma distribution does not contradict the BTW model and therefore is included within the framework of SOC. Also, the model shows universality (a global constant scaling exponent) despite the edge effect of dissipation at the boundaries. This final finding contradicts what was found for real earthquake populations that showed regional variations in the scaling exponent B. This is the main factor in concluding that earthquake seismicity is not SOC but what I describe as self-organised sub-critical

(SOSC). SOSC is a looser form of SOC that allows for variations in the scaling exponent and internal dissipation, more in tune with natural systems. The BTW model also shows no spatial correlation between the point of origin of an avalanche and its relative size.

Earthquake populations are more predictable spatially than they are temporally. The spatial variations are mainly evident in the differences between ocean-ridges and subduction zones. The lower entropy of the mid-ocean ridges when compared to subduction zones is in agreement with the studies of earthquake spatial organisation (configurational entropy). The scaling exponents vary systematically in space with ocean-ridges having relatively higher exponents. The variations were confirmed for three different scaling exponents using a least-squares fit (B), Aki's maximum likelihood method (b_1) and using rank-order statistics (b_2). This variation in scaling strongly question 'universality' in earthquake seismicity.

The scaling exponent B, b_1 and b_2 are negatively correlated with entropy and hence the level of self-organisation of power-law gamma type systems. This is highlighted in the constructed phase-diagrams and in the analysis of real earthquake populations. This suggests that scaling exponents could be used as a proxy for the level of self-organisation in power-law gamma type systems.

To conclude, the results of this thesis are hopefully a step forward in our quest to understand self-organisation in dissipative structures. However, many questions remain. For example, is heat flow in the crust the best proxy for entropy production? What are the underlying dissipation mechanisms driving the Earth or other similar systems to a power-law gamma type attractor state as opposed to any other? What other examples in nature are there of observer dependent criticality? Is there a related underlying cause for B varying globally? There is therefore a plethora of scope for further investigation into this emerging and fascinating field of physics. This chapter may be the end of this thesis, but it is refreshingly by no means "*the end*".

Fahad Al-Kindy,

University of Edinburgh,

September 2003.

Bibliography

Abercrombie, R. (1995). Earthquake source scaling relationships for -1 to 5 ml using seismograms recorded at 2.5 kn depth. *J. Geophysica Res.*, **100**, 24,015–24,036.

Abercrombie, R. & Leary, P. (1993). Source parameters of small earthquakes recorded at 2 km depth, Cajon Pass, Calafornia: implications for earthquake scaling. *Geophys. Res. Lett.*, **20**, 1511–1514.

Akaike, H. (1978). A bayesian analysis of the minimum aic procedure. *Annals of the Institute of Statistical Mathematics*, **30:A**, 9–14.

Aki, K. (1965). Maximum likelihood estimate of b in the formula $\log n = a - bm$. *Bull. Earthq. Res. Inst,. Univ.of Tokyo*, **59**, 237–239.

Al-Kindy, F.H. (1999). *Broad-band (cm-Km) power-law scaling heterogeneity in the Earth's crust: Evidence from fractal analysis of geophysical borehole logs*. MRes thesis, University of Edinburgh.

Al-Kindy, F.H. & Main, I.G. (0000). Internal and external thermodynamics of a non-conservative cellular automata model. *2003*, 0000, in preparation.

Al-Kindy, F.H. & Main, I.G. (2003). Testing self-organized criticality in the crust using entropy: a regional study of global earthquake population. *J. Geophs. Res.*, **in press**.

Amitrano, D. (2003). Brittle-ductile trasition and associated seismicity: Experimental and numerical studies and relationship with the b value. *J. Geophys. Res.*, **108**, 19(1–15).

Angulo-Brown, F. & Muñoz-Diosdado, A. (1999). Further seismic properties of a spring-block earthquake mode;. *Geophys. J. Int.*, **139**, 410–418.

Bak, P. (1997). *How Nature Works*. Oxford University Press.

Bak, P. & Flyvbjerg, H. (1992). Self-organization of cellular magnetic-domain patterns. *Phys. Rev. A*, **45**, 2192–2200.

Bak, P. & Tang, C. (1989). Earthquakes as a self-organized critical phenomena. *J. Geophys. Res.*, **94**, 15,635– 15,637.

Bak, P., Tang, C. & Wiesenfeld, K. (1987). Self-organized criticality: An explanation of $1/f$ noise. *Phys. Rev. Lett.*, **59**, 381–384.

Ball, P. (1999). *The Self-Made Tapestry: pattern formation in nature*. Oxford University Press.

Bean, C.J. (1996). On the cause of $1/f$-power spectra scaling in borehole sonic logs. *Geophys. Res. Lett.*, **23**, 3119–3122.

Ben-Jacob, E. & Levine, H. (2001). The artistry of nature. *Nature*, **409**, 985–986.

Ben-Zion, Y., Dahmen, K., Lyakhovsky, V., Eratas, D. & Agnon, A. (1999). Self-driven mode switching of earthquake activity on a fault system. *Earth. Plan. Sci. Lett.*, **172**, 11–21.

Bender, B. (1983). Maximum likelihood estimation of b values for magnitude grouped data. *Bull. Seism. Soc. Am.*, **73**, 831–851.

Bird, P., Kagan, Y.Y. & Jackson, D.D. (2002). *Plate Boundary Zones, Geodynamics Series 30*, chap. plate tectonics and earthquake potential of spreading ridges and ocean transform faults, 203–218. American Geophysical Union.

Bonnet, E., Bour, O., Odling, N.E., Davy, P., Main, I.G., Cowie, P. & Berkowitz, B. (2001). Scaling of fracture systems in geological media. *Rev. Geophys.*, **39**, 347–383.

Bowman, D.D., Ouillon, G., Sammis, C.G., Sornette, A. & Sornette, D. (1998). An observational test for the critical earthquake concept. *J. Geophys. Res.*, **372**, 24,359–24,372.

Bridgman, P.W. (1950). The thermodynamics of plastic deformation and generalized entropy. *Rev. Mod. Phys.*, **22**, 56–63.

Bruce, A. & Wallace, D. (1989). *The New Physics*, chap. Critical point phenomena: Universal physics at large length scales, 236–267. Cambridge University Press.

Bufe, C.G. & VArnes, D.J. (1993). Predictive modeling of the San Francisco Bay region. *J. Geophs. res.*, **98**, 9871–9883.

Burridge, R. & Knopoff, L. (1967). Model and theoretical seismicity. *Bull. Seism. Soc. Am.*, **57**, 341–371.

Burroughs, S.M. & Tebbens, S.F. (2002). The upper-truncated power-law applied to earthquake cumulative frequency-magnitude distributions: Evidence from a time-independent scaling parameter. *Bull. Seism. Soc. Am.*, **92**, 2983–2993.

c. Chen, C. & Chang, C.L. (2004). Comment on "Entropy, energy, and proximity to criticality in global earthquake populations". *Geophys. Res. Lett.*, **31**, 2003GL019008.

Cakmur, R.V., Egolf, D.A., Plapp, B.B. & Bodenschatz, E. (1997). Bistability and competition of spatiotemporal chaotic and fixed point attractors in Rayleigh-Bènard convection. *Phys. Rev. Lett.*, **79**, 1853–1856.

Callen, H.B. (1957). Principle of minimum entropy production. *Phys Rev.*, **105,**, 360–365.

Cao, A. & Gao, S. (2002). Temporal variations of seismic b-values beneath Northeastern Japan island arc. *Geophys. Res. Lett.*, **29**, 48 (1–3).

Caputo, J.G. & Atten, P. (1987). Metric entropy: An experimental means of characterizing and quantifying chaos. *Phys. Rev. A.*, **35**, 1311–1316.

Cavanagh, J. & Akke, M. (2000). May the driving force be with you - whatever that is. *Nature*, **7**, 11–13.

Ceva, H. (1995). Influence of defects in a coupled map lattice modelling earthquakes. *Phys. Rev. E*, **52**, 154–158.

Chapman, S. & Watkins, N. (2001). Avalanching and self-organised criticality, a paradigm for geomagnetic activity? *Space Sci. Rev.*, **95**, 293–307.

Christensen, K. & Olami, Z. (1992). Scaling, phase transitions, and nonuniversality in a self-organized critical cellular automaton model. *Phys. Rev. A*, **46**, 1829–181838.

Christensen, K. & Olami, Z. (1993). Sandpile models with and without an underlying spatial structure. *Phys. Rev. E*, **48**, 3361–3372.

Christensen, K., Olami, Z. & Bak, P. (1992). Deterministic $1/f$ noise in nonconcervative models of self-organized criticality. *Phys. Rev. Lett.*, **68**, 2417–2420.

Cowie, P.A., Sornette, D. & Vanneste, C. (1995). Multifractal scaling proerties of a growing fault population. *Geophys. J. Int.*, **122**, 457–469.

Crampin, S. (1994). The fracture criticality of crustal rocks. *Geophys. J. Int.*, **118**, 428–438.

Crampin, S., Volti, T. & Stefánsson, R. (1999). A successfully stress-forecast earthquake. *Geophys. J. Int.*, **138**, F1–F5.

Cross, M.C. & Hohenberg, P.C. (1993). Pattern formation outside equilibrium. *Rev. Mod. Phys.*, **65**, 851–1112.

Dahmen, K., Ertas, D. & Ben-Zion, Y. (1998). Gutenberg-Richter and charecteristic earthquake behaviour in simple mean-field models of heterogeneous faults. *Phys. Rev. E*, **58**, 1494–1501.

D'Anna, G., Mayor, P., Barrat, A., Loreto, V. & Nori, F. (2003). Observing brownian motion in vibration-fluidized granular media. *Nature*, **424**, 909–912.

Davies, G.F. (1980). Review of oceanic and global heat flow estimates. *Rev. Geophys. Space. Phys.*, **18**, 718–722.

de Carvalho, J.X. & Prado, C.P.C. (2000). Self-organized criticality in the Olami-Feder-Christensen model. *Phys. Rev. Lett.*, **84**, 4006–4009.

Dewar, R. (2003). Information theory explaination of the fluctuation theorem, maximum entropy production and self-organized criticality in non-equilibrium stationary states. *J. Phys. A: Math. Gen.*, **36**, 631–641.

Dobrovol'skiy, I.P. (1994). Seismic efficiency of the tectonic earthquake. *Phys. Soc. Earth. Russian Edition (english translation)*, **30**, 462–465.

Draper, N.R. & Smith, H. (1998). *Applied Regression Analysis*. John Wiley & Sons.

Dubois, J. (1998). *Non-linear Dynamics in Geophysics*. John Wiley & Sons Ltd.

Dugdale, J.S. (1998). *Entropy and its Physical Meaning*. Taylor Francis Ltd.

Egolf, D.A. (2000). Equilibrium regained: From nonequilibrium chaos to statistical mechanics. *Science*, **287**, 101–104.

Feder, J. (1988). *Fractals*. Plenum, New York.

Fowler, C.M.R. (1990). *The Solid Earth, An Introduction to Global Geophysics*. Cambridge University Press.

Frette, V., Christensen, K., Malthe-S, A., Feder, J., J, T. & Meakin, P. (1996). Avalanche dynamics in a pile of rice. *Nature*, **379**, 49–54.

Freund, J., Ebeling, W. & Rateitschak, K. (1996). Self-similar sequences and universal scaling of dynamical entropies. *Phys. Rev. E.*, **54**, 5561–5566.

Frollich, C. & Davis, S.D. (1993). Teleseismic b values; or, much to do about 1.0. *J. Geophys. Res.*, **98**, 631–644.

Geller, R.J. (1997). Earthquake prediction: a critical review. *Geophys. J. Int.*, **131**, 425–450.

Ghaffari, P., Lise, S. & Jensen, H. (1997). Nonconservative sandpile models. *Phys. Rev. E*, **56**, 6702–6709.

Gilbert, T., Dorfman, J.R. & Gaspard, P. (2000). Entropy production, fractals and relaxation to equilibrium. *Phys. Rev. Lett.*, **85**, 1606–1609.

Godano, C. & Pingue, F. (2000). Is the seismic moment-frequency relation universal? *Geophys. J. int.*, **142**, 193–198.

Goltz, C. (1997). *Fractal and Chaotic Properties of Earthquakes, Lecture notes in earth sciences*. Springer-Verlag Berlin Heidelberg.

Goltz, C. & Böse, M. (2002). Configurational entropy of critical earthquake populations. *Geophys. Res. Lett.*, **29**, 51–1 – 51–4.

Grassberger, P. (1994). Efficient large-scale simulations of a uniformly driven system. *Phys. Rev. E*, **49**, 2436–2443.

Grasso, J.R. & Sornette, D. (1998). Testing self-organized criticality by induced seismicity. *J. Geophys. Res.*, **103**, 29965–29987.

Gutenberg, B. & Richter, C.F. (1954). *Seismicity in the Earth and Associated Phenomena*. Princeton University Press, Princeton, N.J., second edition edn.

Helander, P., Chapman, S.C., Dendy, R.O., Rowlands, G. & Watkins, N.W. (1999). Exactly solvable sandpile with fractal avalanching. *Phys. Rev. E*, **59**, 6356–6360.

Henderson, J. (1992). *Fracture Mechanics and the Evolution of Seismicity in an Intra-Plate Setting*. Phd thesis, University of Edinburgh, Scotland.

Henderson, J., Main, I.G., Pearce, R.G. & Takeya, M. (1994). Seismicity in Northeast Brazil: fratcal clustering and the evolution of the b value. *Geophys. J. Int.*, **116**, 217–226.

Hergarten, S. (2002). *Self-Organized Criticality in Earth Systems*. Springer-Verlag.

Jánosi, I.M. & Kertész, J. (1993). Self-organized criticality with and without conservation. *Physica A*, **200**, 179–188.

Jaynes, E.T. (1957). Information theory and statistical mechanics. *Phys. Rev.*, **106**, 620–630.

Jensen, J.H. (1998). *Self-Organized Criticality: Emergent Complex Behavior in Physical and Biological Systems*. Cambridge University Press.

Kagan, Y.Y. (1993). Statistics of characteristic earthquakes. *Bull. Seism. Soc. Am.*, **83**, 7–24.

Kagan, Y.Y. (1994). Observational evidence for earthquakes as a nonlinear dynamic process. *Physica D*, **77**, 160–192.

Kagan, Y.Y. (1997). Seismic moment-frequency relation for shallow earthquakes: Regional comparison. *J. Geophys. Res.*, **102**, 2835–2852.

Kagan, Y.Y. (1999). Universality of the seismic moment-frequency relation. *Pure Appl. Geoph. (PAGEOPH)*, **155**, 537–573.

Kagan, Y.Y. (2002). Seismic moment distribution revisited: Ii. moment conservation principle. *Geophys. J. Int.*, **149**, 731–754.

Kanamori, H. & Anderson, D.L. (1975). Theoretical basis for some empirical relations in seismology. *Bull. Seism. Soc. Am.*, **65**, 1073–1095.

Katz, J.I. (1986). A model of propergating brittle failiure in heterogeneous media. *J. Geophys. Res.*, **91**, 10,412–10,420.

Kay, J. (1984). *Self-Organization in Living Systems*. Ph.d. thesis, University of Waterloo, Waterloo, Ontario, Canada.

Kearey, P. & Vine, F.J. (1996). *Global Tectonics*. Blackwell Science Ltd., 2nd edn.

Kirkaldy, J.S. (1985). Pattern formation, logistics, and maximum path probability. *Phys. Rev A.*, **31**, 3376–3390.

Klimontovich, Y.L. (1999). Entropy and information of open systems. *Physics-Uspekhi*, **42**, 375–384.

Kondepudi, D. & Prigogine, I. (1998). *Modern Thermodynamics*. John Wiley & Sons.

Koravos, G.C., Main, I.G., Tsapanos, T.M. & Musson, R.M. (2003). Maximum earthquake magnitudes in the aegean are constrained by tectonic moment release rates. *Geophys. J. Int.*, **152**, 94–112.

Kumagai, H., Fukao, Y., Watanabe, S. & Baba, Y. (1999). A self-organized model of earthquakes with constant stress drop and the b-value of 1. *Geophys. Res. Lett.*, **26**, 2817–2820.

Lauritsen, K.B., Zapperi, S. & Stanley, H.E. (1996). Self-organized branching process: Avalanche models with dissipation. *Phys. Rev E*, **54**, 2483–2488.

Leary, P.C. (1991). Deep borehole log evidence for fractal distribution of fractures in crystaline rock. *Geophys. j. Int.*, **107**, 615–627.

Leary, P.C. & Al-Kindy, F.H. (2002). Power-law scaling of spatially correlated porosity and log (permeability) sequences from north-central north sea brae oilfield well core. *Geophys. J. Int.*, **148**, 402–425.

Leonard, T., Papasouliotis, O. & Main, I.G. (2001). A poisson model for identifying characteristic size effects in frequency data: Application to frequency-size distributions for global earthquake, "starquakes", and fault lengths. *J. Geophys. Res.*, **106**, 13,473–13,484.

Leung, K., Müller, J. & Andersen, J. (1997). Generalization of a two-dimensioal burridge-knopoff model of earthquakes. *J. Phys. France*, **7**, 423–429.

Lipkin, B.S. (1999). *LaTeX for Linux*. Springer-Verlag, New York, Inc.

Lise, S. & Jensen, H. (1996). transitions in nonconserving models of self-organized criticality. *Phys. Rev. Lett.*, **76**, 2326–2329.

Lise, S. & Paczuski, M. (2001a). Scaling in a nonconservative earthquake model of self-organized criticality. *Phys. Rev. E*, **64**, 046111(1–5).

Lise, S. & Paczuski, M. (2001b). Self-organized criticality and universality in a nonconcervative earthquake model. *Phys. Rev. E*, **63**, 036111(1–5).

Lise, S. & Paczuski, M. (2002). Nonconcervative earthquake model of self-organized criticality on a random graph. *Phys. Rev. Lett.*, **88**, 228301 (1–4).

Lise, S. & Stella, A.L. (1998). Boundary effects in a random neighbor model of earthquakes. *Phys. Rev. E*, **57**, 2622–3636.

Lomnitz-Adler, J. (1993). Automaton models of seismic fracture: Constraints inposed by the magnitude-frequency relation. *J. Geophys. Res.*, **98**, 17,745–17,756.

Lorenz, R. (2003). Full steam ahead - probably. *Science*, **299**, 837–838.

Lorenz, R.D., Lunine, J.I., Withers, P.G. & McKay, C.P. (2001). Titan, Mars and Earth: Entropy production by latitudinal heat transport. *Geophys. Res. Lett.*, **28**, 415–418.

Lu, C., Takayasu, H., Tretyakov, A., Takayasu, M. & Yumoto, S. (1998). Self-organized criticality in a block lattice model of the brittle crust. *Phys. Lett. A*, **242**, 349–354.

Lyakhovsky, V., Ben-Zion, Y. & Agnon, A. (2001). Earthquake cycle, fault zones, and seismicity patterns in a rheologically layered lithosphere. *J. Geophs. Res.*, **106**, 4103–4120.

Main, I.G. (1987). A charactersitic earthquake model of seismicity preceding the eruption of Mount St. Helens on 18 May 1980. *Phys. Earth Planet Int.*, **49**, 283–293.

Main, I.G. (1995). Earthquakes as a critical phenomena: Implications for probabilistic seismic hazard analysis. *Bull. Seism. Soc. Am.*, **85**, 1299–1308.

Main, I.G. (1996). Statistical physics, seismogenisis, and seismic hazard. *Rev. Geophys.*, **34**, 433–462.

Main, I.G. (2000). Apparent breaks in scaling in earthquake cumulative frequency-magnitude distribution: Fact or artifact. *Bull. Seism. Soc. Am.*, **90**, 86–97.

Main, I.G. & Al-Kindy, F.H. (2002). Entropy, energy, and proximity to criticality in global earthquake populations. *Geophys. Res. Lett.*, **29**.

Main, I.G. & Al-Kindy, F.H. (2004). Reply to comment by Chien-chih Chen and Chun-Ling Chang on “Entropy, energy and proximity to criticality in global earthquake populations”. *Geophys. Res Lett.*, **31**, 2004GL019497.

Main, I.G. & Burton, P.W. (1984). Information theory and the earthquake frequency-magnitude distribution. *Bull. seism. Soc. Am.*, **74**, 1409–1426.

Main, I.G. & Burton, P.W. (1989). Seismotectonics and the earthquake frequency-magnitude distribution in the aegean area. *Geophs. J.*, **98**, 575–586.

Main, I.G., Henderson, J.R., Meredith, P.G. & Sammonds, P.R. (1994). Self-organized criticality in fluid-rock interactions in the britle field. *PAGEOPH*, **142**, 529–543.

Main, I.G., Leonard, T., Papasouliotis, O., Hatton, C.G. & Meredith, P.G. (1999). One slope or two? detecting statistically significant breaks of slope in geophysics data, with application to fracture scaling relationships. *J. Geophys. Res.*, **26**, 801–2804.

Main, I.G., O'Brian, G. & Henderson, J.R. (2000). Statistical physics of earthquakes: Comparison of distribution exponents of source area and potential energy and the dynamic emergence of log-periodic energy quanta. *J. Geophys. Res.*, **105**, 6105–6126.

Malamud, B.D. & Turcotte, D.L. (1999). Self-organized criticality applied to natural hazards. *Journal of the International Society for the Prevention and Mitigation of Natural Hazards*, **20**, 93–116.

Mandl, F. (1988). *Statistical Physics*. John Wiley & Sons Ltd., 2nd edn.

Manna, S.S., Chakrabarti, A.D. & Cafiero, R. (1999). Critical states in a dissipative sandpile model. *Phys. Rev. E*, **60**, R5005–R5008.

Mantegna, R.N., Buldyrev, S.V., Goldberger, A.L., Havlin, S., Peng, C.K., Simons, M. & Stanley, H.E. (1994). Systematic analysis of coding and noncoding dna sequences using methods of statitical linguistics. *Phys. Rev. E.*, **52**, 2939–2050.

Marsan, D., Bean, C.J., Steacy, S. & McClosky, J. (2000). Observation of diffusion processes, and implications for the predictibility of seismicity systems. *J. Geophys. Res.*, **105**, 28081–28094.

Middleton, A.A. & Tang, C. (1995). Self-organized criticality in nonconcerved systems. *Phys. Rev. Lett.*, **74**, 742–745.

Mousseau, N. (1996). Synchronization by disorder in coupled systems. *Phys. Rev. Lett.*, **77**, 968–971.

Mulargia, F. (2001). Retrospective selection bias (or the benifit of hindsight). *Geophys. J. Int.*, **146**, 489–496.

Nagahama, H. (1992). Maximum entropy and shear strain of shear zone. *Math. Geol.*, **24**, 947–955.

Nanjo, K., Nagahama, H. & Yodogawa, E. (2000). Symmetry properties of spatial distribution of microfracturing in rock. *Forma*, **15**, 95–101.

Nicholson, T., Sambridge, M. & Gudmundsson, O. (2000). On entropy and clustering in earthquake hypocentre distributions. *Geophys. J. Int.*, **142**, 37–51.

Nicolis, G. (1989). *The New Physics*, chap. Physics of far from equilibrium systems and self-organisation, 316–347. Cambridge University Press.

Nicolis, G. & Prigogine, I. (1977). *Self-Organization in Nonequilibrium Systems - From Dissipative Structures to Order Through Fluctuations.*. John Wiley & Sons, Inc.

Ogata, Y., Imoto, M. & Katsura, K. (1991). 3-d spatial variation of b-values of magnitude-frequency distributions beneath the Kanto District, Japan. *Geophys. J. Int.*, **104**, 135–146.

Ohmura, H. & Ozuma, A. (1997). Thermodynamics of a global-mean state of the atmosphere: A state of maximum entropy increase. *J. Climate*, 441–445.

Olami, Z., Feder, H.J.S. & Christensen, K. (1992). Self-organized criticality in a contiuous, nonconcervative cellular automaton modeling earthquakes. *Phys. Rev. Lett.*, **68**, 1244–1247.

Öncel, A.O., Wilson, T.H. & Nishizawa, O. (2001). Size scaling relationships in the active fault networks of japan and their correlation with the Gutenberg-Richter b value. *J. Geophys. Res.*, **106**, 21,827–21,841.

Onsager, L. & Mechlap, S. (1953). Fluctuations and irreversable processed. *Phys. Rev.*, **91**, 1505–1512.

Ozawa, H., Shimokawa, S. & Sakuma, H. (2001). Thermodynamics of fluid turbulence: A unified approach to the maximum transport properties. *Phys. Rev. E.*, 26303:1–8.

Ozawa, H., Ohmura, A., Lorenz, R.D. & Pujol, T. (2003). The second law of thermodynamics and the global climate system: A review of the maximum entropy production principle. *Rev. Geophys.*, **41**, 2002RG000113.

Pacheto, F.J., Scholz, C.H. & Skies, L.R. (1992). Change in the frequency-size relationship from small to large earthquakes. *Nature*, 71–73.

Perrot, P. (1998). *A to Z of Thermodynamics*. Open University Press.

Pollack, H.N., Hurter, S.J. & Johnson, J.R. (1993). Heat flow from the earth's interior: Analysis of the global data set. *Rev. Geophys.*, **31**, 267–280.

Posadas, A., Hitara, T. & Vital, F. (2002). Information theory to characterize spatiotemporal patterns of seismicity in the Kanto Region. *Bull. Seism. Soc. Am.*, **92**, 600–610.

Pride, S.R. & Toussaint, R. (2002). Thermodynamics of fiber bundles. *Physica A*, **312**, 159–174.

Reiter, L. (1990). *Earthquake Hazard Analysis*. Colombia University Press, New York.

Rice, J.R. (1993). Spatio-temporal complexity of slip on a fault. *J. Geophys. res.*, **98**, 9885–9907.

Rinaldo, A., Maritan, A., Colaiori, F., Flammini, A., Rigon, R., Rodriguez-Iturbe, I. & Banavar, J. (1996). Thermodynamics of fractals networks. *Phys. Rev. Lett.*, **76**, 3364–3367.

Robinson, R. (2000). A test of the precursory accelerating moment release model on some recent New Zealand earthquakes. *Geophys. J. int.*, **140**, 568–576.

Ruelle, D. (2001). A departure from equilibrium. *Nature*, **414**, 263–264.

Rundle, J.B. (1993). Magnitude-frequency relation for earthquakes using a statistical mechanical approach. *J. Geophys. Res.*, **98**, 21,943–21,949.

Rundle, J.B., Klein, W., Gross, S. & Turcotte, D.L. (1995). Boltzmann fluctuations in numerical simulations of nonequilibrium lattice threshold systems. *Phys. Rev. Lett.*, **75**, 1658–1661.

Sammonds, P.R., Meredith, P.G. & Main, I.G. (1992). Role of pore fluids in the generation of seismic precursors to shear stress. *Nature*, **359**, 228–230.

Scholz, C.H. (1977). Size distribution for large and small earthquakes. *Bull. Seism. Soc. Am.*, **87**, 1074–1077.

Scholz, C.H. (2002). *The Mechanics of Earthquakes and Faulting*. Cambdridge University Press, 2nd edn.

Schroeder, M.R. (1991). *Fractals, Chaos, Power Laws: Minutes from an Infinite Paradise*. W. H. Freeman and Company, New York.

Schwarz, D.P. & Coppersmith, K.J. (1984). Fault behaviour and characteristic earthquakes: examples from Wasatch and San Andreas fault zones. *J. Geophys. Res.*, **89**, 5681–5698.

Sclater, J.G., Jaupart, C. & Galson, D. (1980). The heat flow through the oceanic and continental crust and heat loss of the Earth. *Rev. Geophys.*, **18**, 269–311.

Sethna, J.P., Dahmen, K.A. & Myers, C.R. (2001). Crackling noise. *Nature*, **410**, 242–250.

Shannon, C.E. (1948). A mathematical theory of communications. *Bell System Technical Journal*, **27**, 379–423 and 623–656.

Shen, P.Y. & Mansinha, L. (1983). On the principle of maximum entropy and the earthquake frequency-magnitude relation. *Geophys. J. Astr. Soc.*, **74**, 777–785.

Sibson, R.H. (1982). Fault zone models, heat flow, and the depth distribution of earthquakes in the continental crust of the United States. *Bull. Seismol. Soc. Am.*, **72**, 151–163.

Smethurst, D.P. & Williamns, H.C. (2001). Are hospital waiting lists self regulating. *Nature*, **410**, 652–653.

Smith, W.D. (1981). The b-value as an earthquake precursor. *Nature*, **289**, 136–139.

Sornette, D. (2000). *Critical Phenomena in Natural Sciences: Chaos, Fractals, Self-organization and Disorder: Conceptsand Tools*. Springer-Verlag.

Sornette, D. & Pisarenko, V. (2003). Fractal plate tectonics. *Geophys. Res. Lett.*, **30**, 5(1–4).

Sornette, D., Davy, P. & Sornette, A. (1990). Structuration of the Lithosphere in plate tectonics as a self-organized critical phenomenon. *J. Geophys. Res.*, **95**, 17,353–17,361.

Sornette, D., Knopoff, L., Kagan, Y. & Vanneste, C. (1996). Rank-ordering statsitics of extreme events: Application to the distribution of large earthquakes. *J. Geophys. Res.*, **101**, 13,883–13,893.

Stauffer, D. & Aharony, A. (1994). *Introduction to Percolation Theory*. Taylor and Francis Ltd., revised second edition edn.

Stein, S. & Wysession, M. (2003). *An Introduction to Seismology, Earthquakes, and Earth Structure*. Blackwell Publishing Ltd.

Toussaint, R. & Pride, S. (2002a). Fracture of disordered solids in compression as a critical phenomenon: II. model hamiltonian for a population of interacting cracks. *Phys. Rev. E.*, art. 036136.

Toussaint, R. & Pride, S.R. (2002b). Fracture of disordered solids in compression as a critical phenomenon: III. analysis of the localization transition. *Phys. Rev. E.*, **66**, art. 036137.

Turcotte, D.L. (1997). *Fractals and Chaos in Geology and Geophysics*. Cambridge University Press, second edition edn.

Turcotte, D.L. & Schubert, G. (2002). *Geodynamics*. Cambridge University Press, 2nd edn.

Utsu, T., Ogata, Y. & Matsu'ura, R.S. (1995). The centenary of the Omori formula for a decay law of aftershock activity. *J. Phys. Earth.*, 1–33.

Vere-Jones, D. (1976). A branching model for crack propagation. *Pure. Appl. Geoph. (PAGEOPH)*, **29**.

Vere-Jones, D., Robinson, R. & Yang, W. (2001). Remarks on the accelerated moment relese model: problems of model formulation, simulation and estimation. *Geophys. J. Int.*, **144**, 517–531.

Viti, M., Albarello, D. & Mantovani, E. (2001). Classification of seismic strain estimates in the mediterranean region from a 'bootstrap' approach. *Geophys. J. Int.*, **146**, 399–415.

Von-Herzen, R., Ruppel, C., Molnar, P., Nettles, M., Nagihara, S. & Ekström, G. (2001). A constraint on the shear stress at the pacific-australian plate boundary from heat flow and seismicity at the Kermadec forearc. *J. Geophys. Res.*, **106**, 6817–6833.

Wiens, D.A. & Gilbert, H.J. (1996). Effect of slab temperature on deep-earthquake aftershock productivity and magnitude-frequency relations. *Nature*, **384**, 153–156.

Wolfram, S. (1986). *Theory and Applications of Cellular Automata*. World Scientific Publishing Co. Pte. Ltd.

Wyant, P.H., Mongroo, A. & Hameed, S. (1988). Determination of the heat-transport coefficient in energy-balance climate models. *J. Atmos. Sci.*, **45**, 189–193.

Wyss, M. & Wiemer, S. (2000). Change in the probability for earthquakes in Southern Calafornia due to the Landers magnitude 7.3 earthquake. *Science*, **290**, 13341338.

Zöller, G. & Hainzl, S. (2001). Detecting premonitory seismicity patterns based on critical point dynamics. *Natural Hazards and Earth System Sciences*, **1**, 93–98.

Zöller, G., Hainzl, S. & Kurths, J. (2001). Obseervation of growing correlation length as an indicator for critical point behavior prior to large earthquakes. *J. Geophys. Res.*, **106**, 2167–2175.

Derivation of Shannon entropy H

The following derivation of Shannon entropy H is given by inference to the appendices of Shannon (1948) and Jaynes (1957) :

Derivation of $H = -\sum p_i \log pi$:

H is a continuous function of probability p_i. For equal probabilities p_i,

$$H(\frac{1}{n}, \frac{1}{n}, ..., \frac{1}{n}) = A(n) \tag{1}$$

and is a monotonically increasing function of n. A choice of s^m equally likely possibilities can be decomposed into a series of m choices from s equally likely possibilities to give

$$As^m = mAs \tag{2}$$

and similarly for another choice

$$At^n = nAt \tag{3}$$

n is made large and m is chosen to satisfy:

$$s^m \leq t^n < s^{m+1} \tag{4}$$

Taking logarithms and dividing by $n \log s$:

$$\frac{m}{n} \leq \frac{\log t}{\log s} < \frac{m+1}{n} \tag{5}$$

or

$$\left| \frac{\log t}{\log s} - \frac{m}{n} \right| < \frac{1}{n} \tag{6}$$

Now given $s^m = mA(s)$, $A(t^n) = nA(t)$ and $A(s^{m+1}) = (m+1)A(s)$ we can write 4 as:

$$mA(s) \leq nA(t) < (m+1)A(s) \tag{7}$$

Dividing by $nA(s)$ we have:

$$\frac{m}{n} \leq \frac{A(t)}{A(s)} < \frac{m+1}{n} \tag{8}$$

or

$$\left| \frac{A(t)}{A(s)} - \frac{m}{n} \right| < \frac{1}{n} \tag{9}$$

From 6 and 9 we get

$$\left| \frac{\log t}{\log s} - \frac{A(t)}{A(s)} \right| < \frac{2}{n} \tag{10}$$

For large n we have

$$A(S) = K \log S \tag{11}$$

Now, we put $p_i = \frac{n_i}{\sum n_i}$. We can break this down to a choice of m symbols subdivided in to a choice of n symbols. So for $H = H(s_1, s_2, ..., s_m)$ we have:

$$K \log \sum n_i = H + K \sum p_i \log n_i \tag{12}$$

hence

$$H = K \left[\sum p_i \log \sum n_i - \sum p_i \log n_i \right] \tag{13}$$

and given $\sum p_i = 1$

$$H = -K \left[\sum p_i \log \frac{n_i}{\sum n_i} \right] \tag{14}$$

giving the Shannon entropy:

$$-K \sum_{i=1}^{m} p_i \log p_i \tag{15}$$

Entropy and heat flow

During the course of this thesis, I attempted to investigate the relationship between heat flow and seismicity. The rational behind this was that because entropy is related to entropy production (chapter 2) and entropy production to heat flow, one would expect there perhaps to be a correlation between the level of self-organization S as measured from seismicity and the corresponding heat flow Q. However it was noted that the analysis I carried out was on the total heat rather than the heat due to seismic activity and the results subsequently removed. Nonetheless, because the analysis uses the Flinn-Engdahl regionalisation on global heat flow data, these results may be of some interests and are therefore included here.

I use the Global Heat Flow Database described by Pollack et al. (1993) that contains over 24,774 observations of heat flow worldwide. The database is provided by the International Heat Flow Commission whose website is maintained by the University of North Dakota (http://www.heatflow.und.edu/index2.html). In accordance with Pollack et al. (1993), I only include data with $Q \leq 250 mW m^{-2}$ since data above this value are considered spurious. The locations of data measurements are shown in figure 1. I then use the same code I wrote to perform Flinn-Engdhal regionalisation used for earthquakes to calculate the average heat flow $\langle Q \rangle$ for each FE region. My results are summarised in table 1. I also plot the thermodynamic variables and scaling exponents calculated from the radiated seismic energy against the heat flow data Q in figures 2 and 3 respectivly showing no correlation.

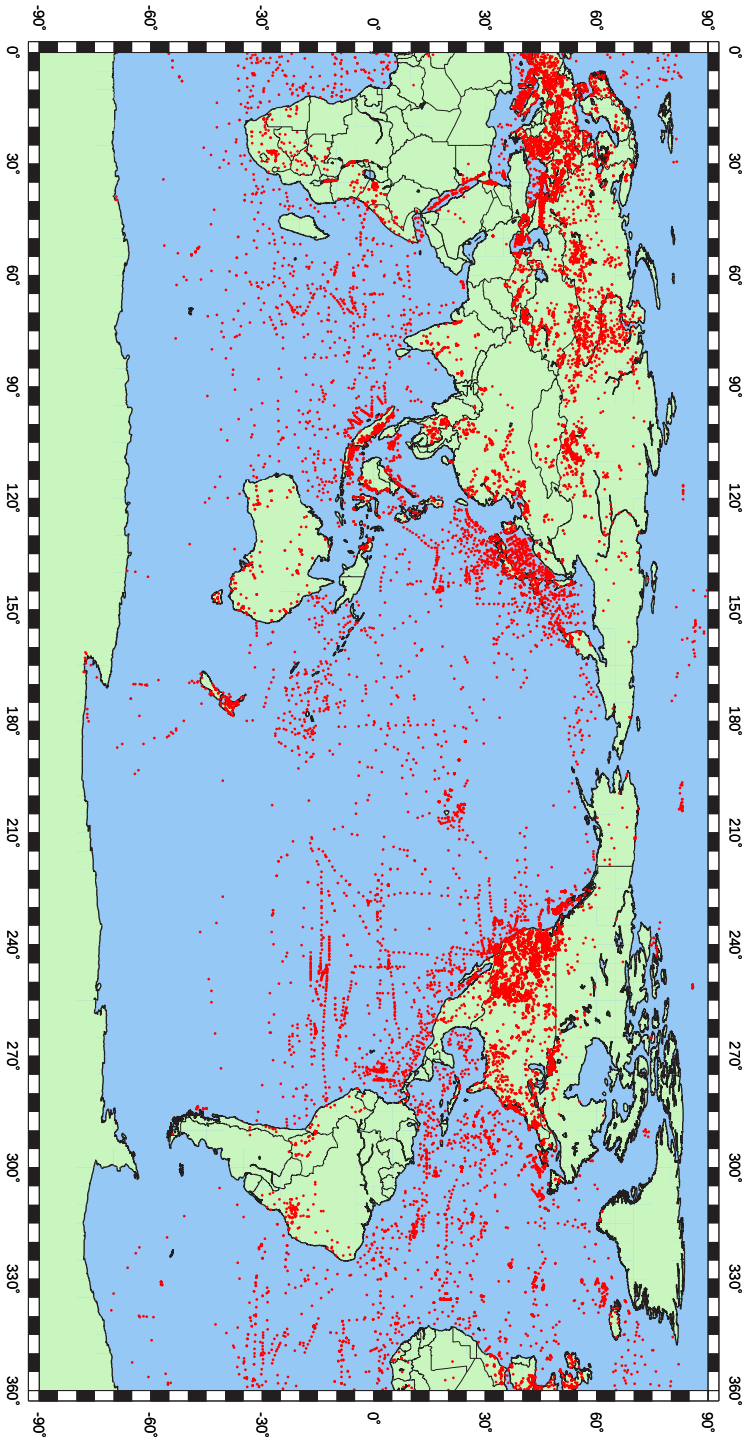

Figure 1: Map of Global Heat Flow Database data

FE no.	$\langle Q \rangle$	n
subduction zones		
1	74.92	60
5	100.04	157
6	76.84	121
7	68.51	151
12	57.37	37
13	84.38	48
14	84.22	48
15	60.23	40
16	81.12	55
18	65.39	126
19	85.88	572
20	74.19	255
21	77.83	47
22	61.56	45
23	66.55	114
24	77.11	287
46	118.39	267
average	77.32 (15.16)	**243**
collision zones		
25	73.35	241
26	76.43	244
27	61.00	25
29	49.56	829
30	57.21	1523
31	87.32	740
41	73.36	654
48	56.56	259
average	66.85 (12.69)	**4515**
intra-continental		
37	63.48	611
mid-ocean ridges		
32	62.51	1755
33	62.16	507
40	87.51	222
43	80.62	128
45	74.60	8
average	73.48 (11.16)	**2620**

Table 1: Summary of results for regional study of the Global Heat Flow Database. The standard deviations are given in brackets and the totals in bold.

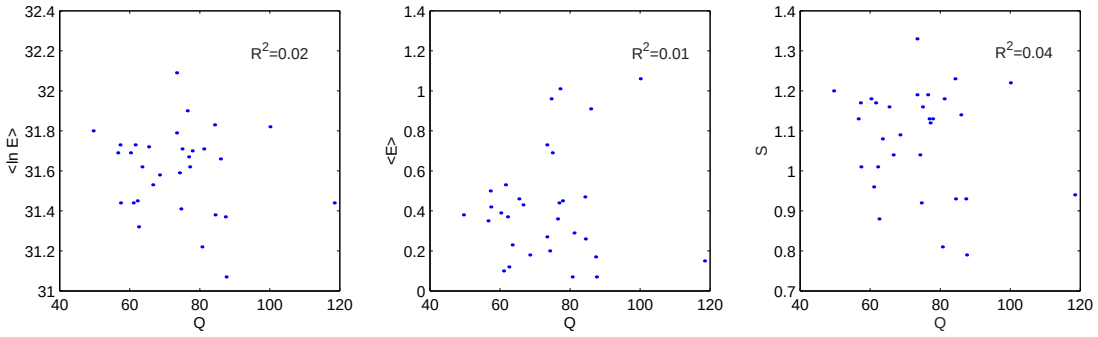

Figure 2: Plot of thermodynamic variables $\langle \ln E \rangle$, $\langle E \rangle$ and S against heat flow Q showing no correlation.

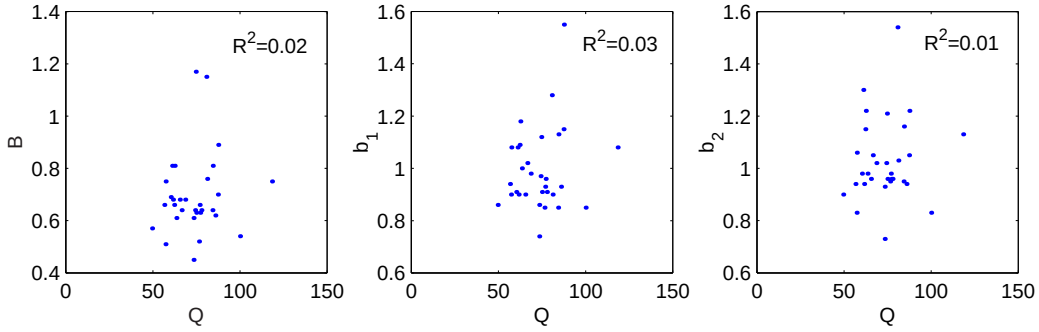

Figure 3: Plot of heat flow Q against scaling exponents B, b_1 and b_2 showing no correlation.

List of Symbols

A	Cluster/fault area
b	Seismic b-value (Gutenberg and Richter)
b_1	Magnitude power-law scaling exponent (Aki's method)
b_2	Rank-order statistics scaling exponent
B	Energy-probability power-paw scaling exponent
B_S	Inferred B from gamma entropy equation
D	Fractal dimension
E	Energy
$\overline{E}$	Mean energy (model)
$\langle E \rangle$	Energy expectation
$\langle \ln E \rangle$	Logarithmic energy expectation
E_e	External energy (model)
E_i	Internal energy (model)
E_S	Seismic energy release
f	Frequency
F	Free energy
g	Degeneracy term
H	Configurational entropy
J	Joules (measure of energy)
k	Bolzmann's constant ($1.38066 \times 10^{-23} J/K$) and thermal conductivity
K	Kelvin
m	Earthquake (moment) magnitude

M_O	Seismic moment
M_S	Surface wave magnitude
Nm	Newton.meter (Measure of seismic moment)
p	Probability
p_C	Percolation threshold
P	Pressure
Q	Heat (flow)
Q_Σ	Total heat
S	Entropy
S_e	External entropy (model)
S_i	Internal entropy (model)
S_γ	Gamma entropy (theoretical)
t	Time
t_C	Critical time
T	Temperature
T_C	Critical temperature
T_e	External temperature (model)
T_i	Internal temperature (model)
T_T	Tectonic/effective/statistical temperature
u	Slip
W	Work
W_f	Tectonic work
Z	Partition function
α	Conservation parameter (model)
α_C	Critical conservation parameter (model)
β	Temperature parameter (thermodynamics)
η	Seismic efficiency
θ	Temperature parameter (gamma distribution)

θ_C Critical ‘temperature’

σ Stress

σ_C Critical stress

ξ Correlation length

Publications

Main I.G. and F.H. Al-Kindy (2002). Entropy, energy and proximity to criticality in global earthquake populations. *Geophys. Res. Lett.*, **29**, 4.

Al-Kindy, F. H. and I .G. Main (2003). Testing Self-Organized Criticality in the crust using entropy: A regionalized study of the CMT global earthquake catalogue. *J. Geophys. Res.*, **108**, B11.

Main I.G. and F.H. Al-Kindy (2004). Reply to comment by Chien-chih Chen and Chun-Ling Chang on "Entropy, energy and proximity to criticality in global earthquake populations". *Geophys. Res. Lett.*, **31**, 2004GL019497.